INVESTIGATION OF PRIMARY PRODUCTION AND NUTRIENT CYCLES IN THE CILICIAN BASIN

A THESIS SUBMITTED TO
THE GRADUATE SCHOOL OF INSTITUTE OF MARINE SCIENCES
OF
MIDDLE EAST TECHNICAL UNIVERSITY

BY

VELİ ÇAĞLAR YUMRUKTEPE

IN PARTIAL FULFILLMENT OF THE REQUIREMENTS
FOR
THE DEGREE OF MASTER OF SCIENCE
IN
PHYSICAL OCEANOGRAPHY

FEBRUARY 2011

Approval of the thesis:

INVESTIGATION OF PRIMARY PRODUCTION AND NUTRIENT CYCLES IN THE CILICIAN BASIN

submitted by **VELİ ÇAĞLAR YUMRUKTEPE** in partial fulfillment of the requirements for the degree of
Master of Science in Physical Oceanography Department, Middle East Technical University by,

Prof. Dr. Ferit Bingel
Dean, Graduate School of **Marine Sciences** _____

Prof. Dr. Emin Özsoy
Head of Department, **Physical Oceanography** _____

Assoc. Prof. Dr. Barış Salihoğlu
Supervisor, **Marine Sciences, METU** _____

Examining Committee Members:

Assoc. Prof. Dr. Bettina Fach Salihoğlu
Marine Sciences, METU _____

Assoc. Prof. Dr. Barış Salihoğlu
Marine Sciences, METU _____

Prof. Dr. Süleyman Tuğrul
Marine Sciences, METU _____

Date: _____

I hereby declare that all information in this document has been obtained and presented in accordance with academic rules and ethical conduct. I also declare that, as required by these rules and conduct, I have fully cited and referenced all material and results that are not original to this work.

Name, Last Name: VELİ ÇAĞLAR YUMRUKTEPE

Signature :

ABSTRACT

INVESTIGATION OF PRIMARY PRODUCTION AND NUTRIENT CYCLES IN THE CILICIAN BASIN

Yumruktepe, Veli Çağlar

M.S., Department of Physical Oceanography

Supervisor : Assoc. Prof. Dr. Barış Salihoğlu

February 2011, 94 pages

This study aims at investigating the limiting nutrient(s) in Mersin Bay to determine appropriate water treatment procedures for the cessation of eutrophication. In-situ physics, chemistry and biology data were collected on the continental shelf of Mersin Bay from 2008 to 2010. To test the influence of river discharges and define the limiting nutrient(s), the Delft3D coupled ecosystem model was used. The model is forced by boundary conditions derived from CYCOFOS forecast data, ERA-INTERIM climatic forcing, river discharges and remotely sensed wind patterns, while the collected data were used to calibrate the simulations. Sensitivity analyses suggest that phosphorus is the limiting nutrient. Vertical mixing and stratification due to seasonal temperature variations play an important role in controlling phosphate concentrations and distributions and therefore influence the dominant algal distribution in the water column. The coastal and offshore waters of Mersin Bay show different ecosystem characteristics. Coastal waters are influenced by river discharge and offshore waters are influenced by the general circulation of the Cilician Basin, which suggests that coastal waters remain trapped near the coast by the offshore general circulation. Analyses also show the influence of atmospheric deposition on primary production, especially during periods of strong stratification by 25 % increase in production where there is reduced vertical supply of phosphorus from below the seasonal thermocline.

Keywords: nutrient limitation, primary production, 3D coupled ecosystem modelling, Cilician Basin, river discharge

ÖZ

KİLİKYA BASENİNDE BİRİNCİL ÜRETİMİN VE BESİN DÖNGÜSÜNÜN İNCELENMESİ

Yumruktepe, Veli Çağlar
Yüksek Lisans, Fiziksel Oşinografi
Tez Yöneticisi : Assoc. Prof. Dr. Barış Salihoğlu

Şubat 2011, 94 sayfa

Bu çalışma, ötrofikasyon olgusunu engellemeyi ve su arıtımı yöntemlerini belirlemede kullanılacak olan sınırlayıcı besin elementlerini belirlemeyi amaçlamaktadır. 2008 ile 2010 yılları arasında, Mersin Körfezi kıta sahanlığı içerisinde detaylı fiziksel, kimyasal ve biyolojik ölçümler yapılmıştır. Nehir girdilerinin etkisinin ve sınırlayıcı besin elementlerinin belirlenmesi için, Delft3D bağlı hidrodinamik ve ekosistem modeli kullanılmıştır. Model, sınır koşulları için CYCOFOS öngörü verileri, iklimsel değişimler için ERA-INTERIM model sonuçları, nehir girdisi ve uzaktan algılanan rüzgar düzenleri kullanılarak yönetilmiş olup, sahada toplanan veriler ile kalibre edilmiştir. Hassasiyet analizleri, fosfor elementinin sınırlayıcı besin elementi olduğunu göstermektedir. Fosfor elementinin konsantrasyonu ve dağılımı, dikeyde karışıma ve tabakalaşma olgularına neden olan yıllık sıcaklık değişimlerinden etkilendiği gibi, bu yapı su kolonundaki baskın tür dağılımını etkilemektedir. Kıyı ve açık Mersin Körfezi suları farklı ekosistem özellikleri göstermektedirler. Kıyı suları büyük ölçüde nehirlerden ve açık sular ise Kilikya Baseni genel akıntısından etkilenmektedir. Bu olgu, kıyı sularının, açık bölge su akımları tarafından kıyıda hapsedildiğini önermektedir. Analizler aynı zamanda, tabakalaşmanın yoğun olduğu ve mevsimsel termoklinin altından forfor beslenmesinin azaldığı dönemlerde, birincil üretime atmosfer girdilerinin de katkısının olduğunu göstermektedir.

Anahtar Kelimeler: sınırlayıcı besin elementi, birincil üretim, 3D ekosistem modeli, Kilikya Baseni,

nehir girdisi

To my family

ACKNOWLEDGMENTS

I would like to begin by thanking my supervisor Dr. Barış Salihoğlu for his supervision, encouragement and support through the course of this work.

I am also thankful for the suggestions and advice of Dr. Temel Oğuz , Dr. Süleyman Tuğrul and Dr. Bettina Fach Salihoğlu. Their help was priceless for the progress of this study.

Special thanks to Dr. Heather Anne Cannaby for giving an endless courage, guidance and support for this study and much more.

I would like to extend my gratitute to Dr. Meinte Blass and Dr. Firmijn Zijl of Deltares for their consult throughout this study. With their experience and invaluable support, this study progressed much more smoothly.

Many thanks to all my colleagues past and present, in particular the ecosystem modelers group for their help one way or the other throughout my short past in IMS. Times I have spent in Setüstü were much more valuable with my dear friends and family in IMS.

Also, I would like to thank all of the IMS members for their kind welcome from the first day I arrived here.

Finally, endless gratitudes to my mother, father and sister for everything. I couldn't have achieved anything without their kind and warm support they have given me all my life.

TABLE OF CONTENTS

LIST OF TABLES

TABLES

LIST OF FIGURES

FIGURES

CHAPTER 1

INTRODUCTION

1.1 Background Information

1.1.1 Geometry and Topography of the Study Area, Mersin Bay and Cilician Basin

The Cilician Basin, lies in the northeastern corner of the Mediterranean Sea between Cyprus and the southern coast of Turkey. Together with the onshore extension of the Adana Basin, they form the combined Cilician-Adana Basin (Shaw and Bush, 1978), positioned between the longitudes 33.5 and 35.5. The basin has a water volume of approximately 9.5 million km^3 and has a basin area of 19000 km^2 (Toker, 2003). The shelf bordering the north of the Cilician Basin is narrow (Figure 1.1). The distance between the coast and the shelf break, which corresponds to 200 m depth, is less than 15 km wide. In the regions where the deposits of Seyhan and Berdan Rivers are settled, the shelf is 40 km wide (Ediger et.al., 2002). The deepest parts of the Cilician Basin are on average 1000 m deep (Evans et.al., 1978). The overall pattern of topography of the basin is asymmetric, the deepest part is located in the southwestern corner, and the bottom topography gradually increases towards the northeastern corner. There are relatively steep slopes offshore from the Göksu Delta, 2.38^o to 5.7^o being the maximum slope . As mentioned, the northeastern part has more gradual slope of 0.19^o, between the shores of the city of Mersin and Seyhan River (Toker, 2003; Ediger et.al., 1997).

Mersin Bay is located in the northeastern part of the Cilicia Basin connecting with the main basin along the 100 m contour. The bay covers an area of nearly 1150 km^2 within the continental shelf off southeastern Turkey, between Göksu and Seyhan deltas. The continental shelf of Mersin Bay forms the northwestern margin of the Adana-Cilician Basin; it extends from the Göksu delta (in the southwest) to the Seyhan-Tarsus-Ceyhan delta (in the northeast) and is narrower and steeper in the southwest than in the northeast (Ediger et.al., 1997).

The main area of concern in this study is Mersin Bay, because the bay is subjected to both high

anthropogenic and natural influence from the major city Mersin and major rivers Seyhan and Berdan.

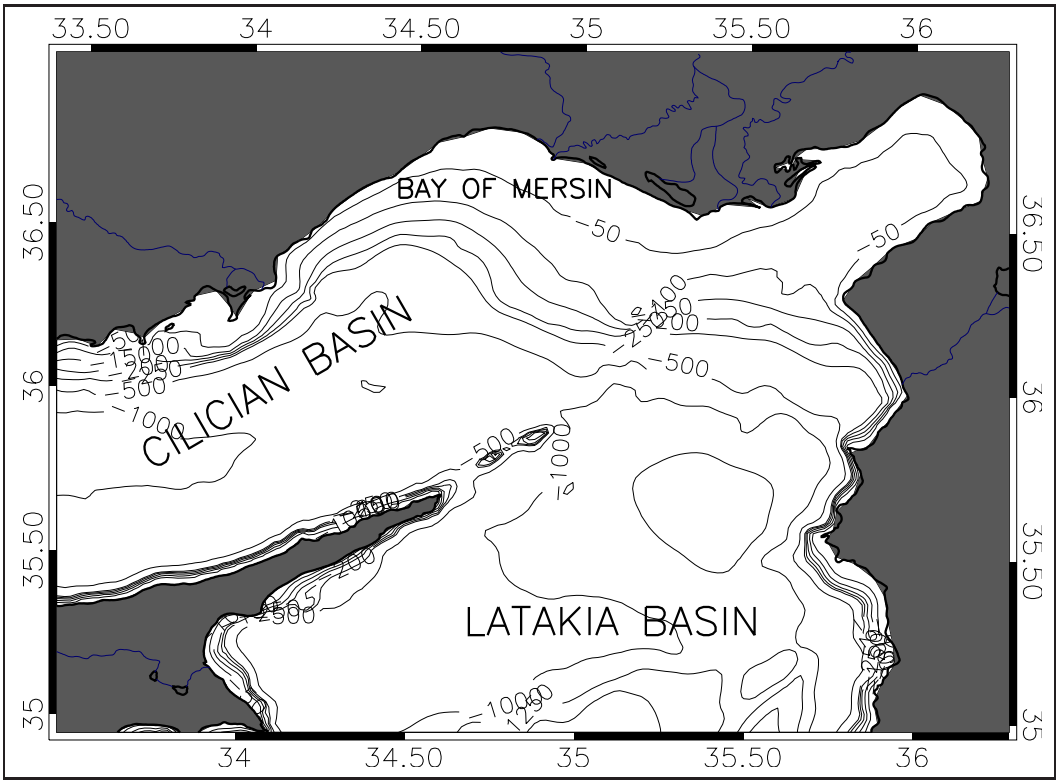

Figure 1.1: General topography of the Cilicia Basin (GEBCO)

1.1.2 Physical Characteristics

1.1.2.1 Water Masses

The most important water masses in the Eastern Mediterranean from top to bottom are modified Atlantic Water (MAW), Levantine Intermediate Water (LIW) and Eastern Mediterranean Deep Water (EMDW) (Özsoy *et. al.*, 1989; Alhammoud *et. al.* ,2005). In this section, water masses and their interactions with the southern coasts of Turkey will be briefly described with a special focus on the Cilician Basin.

Due to the imbalance between the evaporation and precipitation flux in the Mediterranean Sea, there is a continuous intrusion of Atlantic Surface Water from the Strait of Gibraltar. As the evaporative flux is much larger than the precipitation flux, in spring and summer months, this penetration tends to increase, resulting in an intrusion of less saline surface waters into the Mediterranean. At the very western parts of the Mediterranean, this water mass can be traced as deep as 150-200 m, with a

salinity range of 36.15-37.15 ppt. As Atlantic Water (AW) travels to the east along the North African Coast, mixing with the surrounding waters, it loses its low salinity characteristics, and therefore is sometimes called the modified Atlantic Water. It can be traced with a salinity range of 38.5-39 ppt between depths 20-100 m. MAW can also be traced, especially in summer and fall months below the homogeneous high saline and temperature mixed surface layer. The surface waters in these months, with respect to evaporation and heating, trap the MAW below. In winter months, due to high mixing in the water column, the thickness of the MAW is reduced (Özsoy *et. al.*, 1987).

The Levantine Intermediate Water is formed mainly in the Northeastern Mediterranean, south of the Turkish Coast, in the depth range of 200-600 m, and eventually flows out of the Mediterranean to the Atlantic Ocean (Malanotte-Rizzoli *et. al.*, 1999). In their study Özsoy and Ünlüata, 1983, state that the LIW is formed along the southern coast of Turkey, due to cold outbreaks in winter, excess of evaporation over precipitation and runoff in winter. These events usually occur near Rhodes, the Gulf of Antalya and North of Cyprus. Özturgut (1976) describes the source of LIW, east of Rhodes and the Bay of Antalya, with temperature 16.4^{o}C and salinity 39.15 ppt in Antalya and temperature 16.2^{o}C and salinity 39.12 ppt in east of Rhodes (Figure 1.2). In view of these studies, there have been more theories on the reason for the formation of LIW. Ovchinnikov and Plakhin, 1984, state that inside the cyclones, density domes are formed, and due to winds and evaporation, dense waters convect down to deeper layers from the sides of the dome. They also proved that this event may happen with a numerical model. Özsoy *et. al.*, 1987, further agree that throughout the Northern Levantine Basin, several cyclonic and anticyclonic gyres are present, so the formation of LIW can be traced throughout the whole Northern Levantine Basin.

In the deepest layers of the Levantine Basin, Eastern Mediterranean Deep Water (EMDW) is present. Though not much is known about this water mass, the common idea is that it is formed by strong cooling in the northern part of the eastern basin, in the Adriatic and the Aegean. It can be traced with temperature nearly 13.6^{o}C, salinty 38.7 ppt and density higher than 1029.05 kg/m^{3} (Figure 1.2). Also in addition to these three major water masses, in summer months at the surface above the MAW, a thin layer of high temperature and salinity is present called the Levantine Surface Water (LSW). It is believed that this water mass plays an important role in the formation of LIW (Alhammoud *et. al.*, 2005).

Özsoy and Ünlüata (1983) state that because of the cold winters and wind regimes, the local winds and winter conditions in Cilician Basin, Göksu Valley and Bay of Iskenderun can create favorable conditions for formation of the intermediate waters in Eastern Coast of Turkey. Low temperatures

and high density in surface waters in February are close to the characteristics of LIW stated by authors.

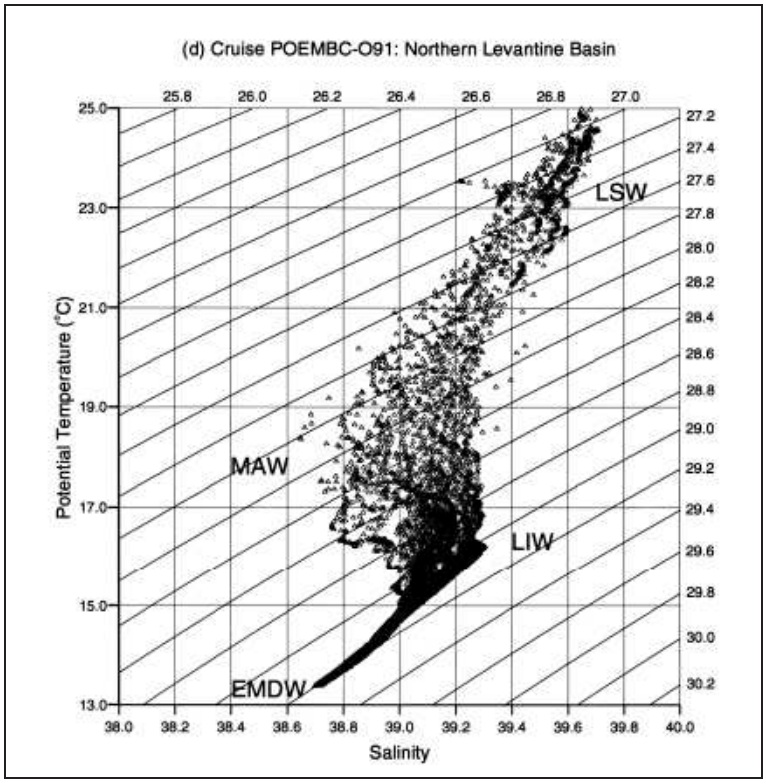

Figure 1.2: Water Mass Characteristics of Northern Levantine Basin from POEM Experiments (after Malanotte et.al., 1999)

1.1.2.2 Circulation

The Mediterranean general circulation patterns have been focus of studies by many scientist since the beginning of the 20th century. The first ones recorded were the studies conducted by Nielsen, 1912, and Schott, 1915, who presented a general cyclonic circulation system in the Mediterranean. Later, this study has been supported by observations and modelling studies (Özsoy *et. al.*, 1987).

Ovchinnikov, 1966, states that surface water of Atlantic origin is carried along the coast by the North African Current, in the Levantine Basin changes its course toward the northeast to Crete. This water mass spreads into two different currents, one heads west back again and the other heads southeast to the Egyptian coasts. This current splits into two different currents, one heads north into the Rhodes Gyre which covers an area between Rhodes Island and central parts of the Levantine Basin. The east flowing current, reaches the coasts of Israel, and heads north along the coasts of Lebanon and Syria. Eventually, this current enters the Cilician Basin, and flows out of the basin along the Turkish Coasts towards the Rhodes Gyre. The magnitude of the surface currents in winter months is on av-

erage 10-25 cm/s, decreasing by half in summer months. Ovchinnikov further stated that the current system is not strongly affected by seasonal changes and that throughout the year general circulation patterns do not vary. Wind patterns are the dominant factors in forming these patterns, along with the small effect of the horizontal density gradients.

In contrast to the results of Ovchinnikov, Özsoy, 1989, states that the circulation is mainly cyclonic at all depths, not just the surface, and concluded that the thermohaline gradients were the main driving forces for the circulation. Data to define the circulation patterns in EMED have been collected during the international POEM program. The results of this program revealed a different circulation pattern from the traditional picture (Alhammoud *et. al.*, 2005). The circulation system is composed of two systems of sub-basin gyres. These are Mersa-Matruh and Shikmona anticyclonic systems in south, and cyclonic Rhodes Gyre in the north regions of Eastern Mediterranean. Between the gyres Mersa-Matruh and Rhodes, there is a strong 40 cm/s jet called the Central Levantine Basin Current (CLBC) by Özsoy, 1989, and Mid-Mediterranean Jet (MMJ) by Robinson *et. al.*, (1991) (Figure 1.3). This jet bifurcates and one of the branches flows northward around the Rhodes Gyre, eventually merging with the Aegean Sea and Cretan Passage. The other branch flows eastward and bifurcates again, one branch flows towards the west of Cyprus and the other to the south of Cyprus. In contradiction with the results from Neilsen, 1912 and Ovchinnikov, 1966, where most of the transport is counter-clockwise around Cyprus, but within the POEM observations around the Shikmona Gyre, the flow is southward and permanent.

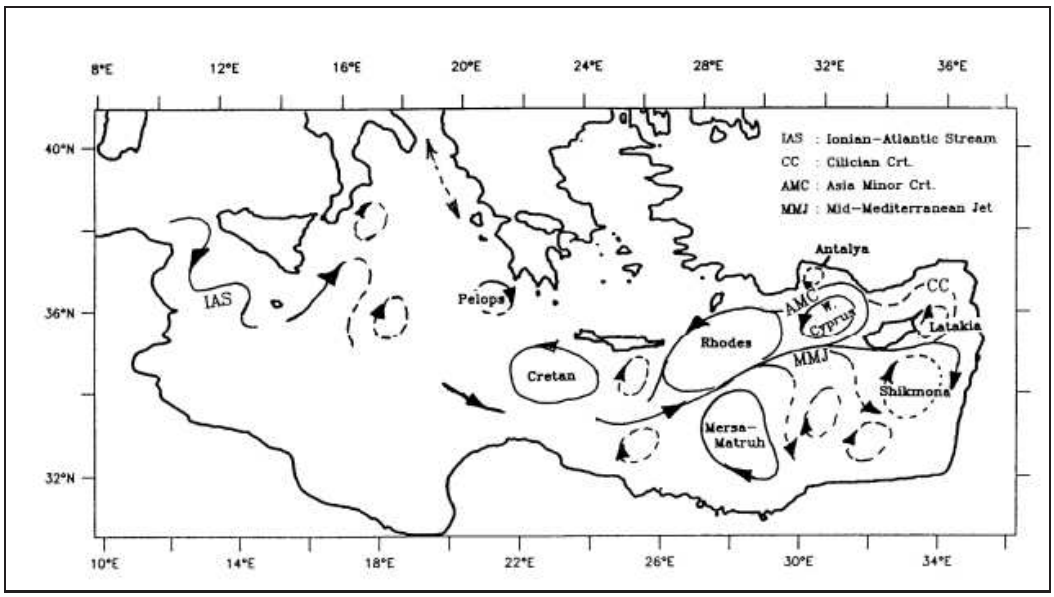

Figure 1.3: General Circulation Patterns of Levantine Basin (after Robinson et.al., 1991)

Cyclonic circulation dominates the northeastern corner of the Mediterranean (Özsoy *et. al.*, 1987; Özsoy and Ünlüata, 1983; Collins and Banner, 1979). The persistent surface current along the coasts of Israel, Lebanon and Syria turns westward and flows out of the Cilician Basin following the southern coasts of Turkey. Flowing between the series of cyclonic and anticyclonic mesoscale gyres, this current is called the Asia Minor Current (AMC). Two weak mesoscale gyres at the sides of the AMC, a cyclonic eddy attached to the eastern coast of Cyprus and an anticyclonic eddy near the Turkish-Syrian coast that extend north toward the Bay of Mersin complete the general mean circulation in the Cilician Basin. These patterns are also supported by the study of Collins and Banner (1979) conducted who combined satellite images, computed geostrophic fields and the measured secchi depths to picture the detailed flow patterns in the Cilician Basin (Figure 1.4). A detailed study of the coastal current systems of the south of Turkey has been conducted by Ünlüata *et. al.* (1983), who also confirmed the existence of a mean westerly flow averaging 10 cm/s. They also stated that a blocking effect of the coastline causes fluctuations in the flow patterns.

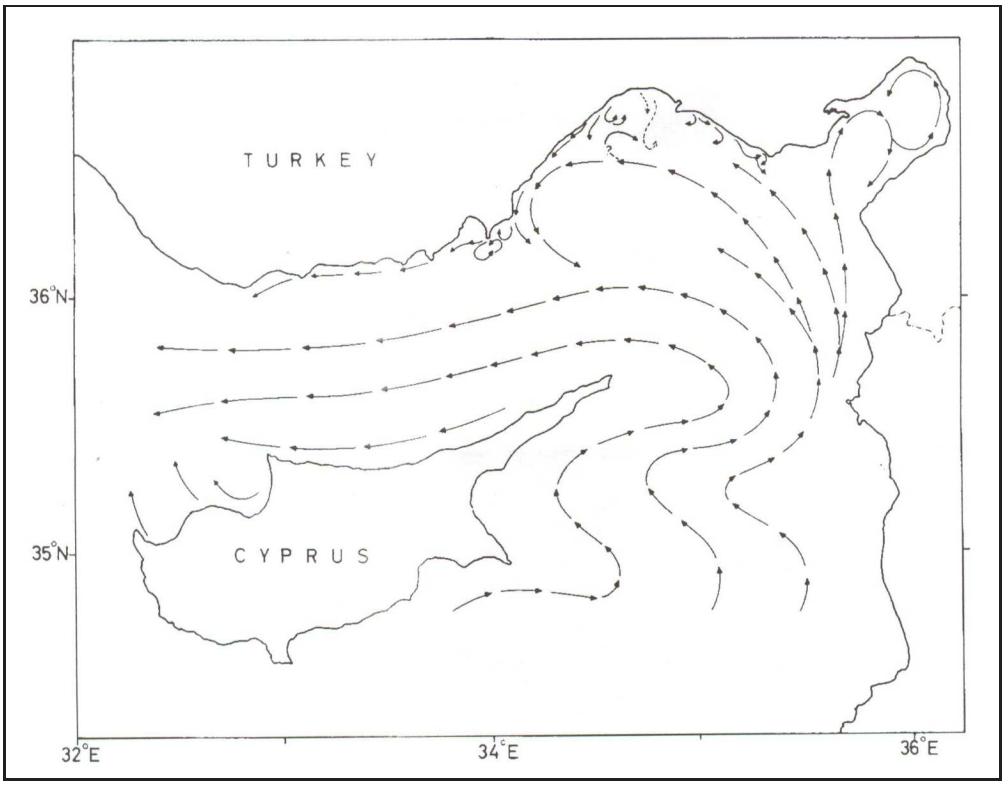

Figure 1.4: General Circulation Patterns of the Cilician Basin (after Collins and Banner, 1979)

1.1.2.3 Atmospheric Setting

Özsoy and Ünlüata (1983) and Ataktürk (1980), pictured the general characteristics of the regional wind patterns. In winter and spring, the area is under influence of extratropical cyclones. In summer

and fall, mid-latitude westerlies play a major role, combined with the local wind systems. Due to the existence of river valleys and gaps in the mountainous areas of the south Turkish Coast; Gulf of Antalya, Göksu Valley and Gulf of İskenderun, local winds are triggered and strengthened by cold outbreaks in winter, and winds of katabatic origin in summer are observed. Locally this wind character with a northwestern path is known as Poyraz in Turkey. Poyraz carries cold and dry air masses towards the coasts, which in turn as stated in previous sections play a role in the formation of LIW.

1.1.3 Ecosystem Dynamics of the Mediterranean Sea

1.1.3.1 Sources and Settings of Nutrients

Historical studies (Bethoux, 1989; Azov, 1991; Bethoux et.al., 1992; Yılmaz and Tuğrul, 1998; Bethoux et.al., 1998; Ediger et.al., 2005; Krom et.al., 2005;) in the Mediterranean Sea show that, it is one of the nutrient-poorest, oligotrophic water masses in the world. This characteristic is a result of low nutrient input from both lower layers (upwelling) and external sources, geophysical and arid climatic conditions. Primary production rates decreases towards the Eastern Mediterranean compared to the Western Mediterranean. Therefore the Eastern Mediterranean is considered to be an ultra-oligotrophic marine environment with the lowest deep water nutrient concentrations found in the world, and surface water nutrients below detection limit. One of the reason for this event is that, nutrient-depleted Atlantic surface water enters the basin from Gibraltar and Sicily, and intermediate waters with relatively higher dissolved organic nutrients are exported towards the Western and North Atlantic.

The sources of nutrients in the Mediterranean Sea are the inflow of low nutrient surface waters, from Gibraltar, atmospheric and riverine discharges. Although throughout the year there is inflow from the North Atlantic to the basin, providing a source of nutrients, this accounts for only 20 % of total input (Bethoux, 1989). The rest originates from riverine and atmospheric inputs. The major rivers in the western basin are the Ebro, Rhone and Po, which in total have $10^{11} m^3$ discharge per year. The effect of these nutrient rich discharges are only local and seasonal. Their effects can be spotted in coastal areas, where as the Mediterranean has an arid climate, due to higher evaporation than precipitation, the constant inflow of 32000 km^3 surface waters of Atlantic carries nutrient poor waters into the basin. As for the Eastern Mediterranean, the major river discharge was the River Nile with approximately $43x10^9 m^3$per year before the Aswan Dam, and now $4\text{-}5x10^9 m^3$ per year (Azov, 1991).

Extensive studies have been carried out to estimate nutrient inputs to the Mediterranean Sea. Krom *et. al.* (2004), referenced several authors who stated that, Po river inputs consist of 50 percent of nutrient source with dissolved nitrogen 20.2×10^9 mol per year and dissolved phosphate 0.9×10^9 mol per year. Calculated N and P inputs throughout the basin with a model yielded 28.9×10^9 mol N per year and 1.09×10^9 P per year. The dissolved nitrogen input from the River Nile is 0.48×10^9 mol per year and dissolved phosphorus 0.1×10^9 mol per year (Nixon, 2003).

The Mediterranean, being enclosed by continental masses, is strongly influenced by the atmospheric nutrient inputs. The Eastern Mediterranean receives air masses from Central and Eastern Europe throughout the year. The attenuation of nutrients from the atmosphere occurs through wet and dry deposition. Therefore, the regions with high precipitation receive higher wet deposition, mainly the Western Mediterranean (Krom et.al., 2004). They estimate the wet deposition flux in the Eastern Mediterranean as, 20.5 μmol nitrogen and 280 μmol phosphorus m^2/y. In parallel to the wet deposition, the dry deposition of nutrients is particularly important in Eastern Mediterranean, due to masses of dust transport. On average their estimate of dry deposition in the Eastern Mediterranean is 54 μmol nitrogen and 350 μmol phosphorus m^2/y.

The observed mean concentrations of dissolved and particulate nutrients also differ throughout the basin. In the western basin, nitrate ranges between 8.53-8.94 μM, phosphate ranges between 0.4-0.411 μM and silicate ranges between 7.98-8.59 μM in the water column, based on data collected at 8 stations during 1994 and nitrogen, phosphate and silicate had reported values of 4.5, 0.19 and 6 10^{-6} moles in Ionian Sea (Bethoux et.al., 1992). In the same study, a comparison has been carried out with the historical data. Nitrate data ranges between 6.32 and 8.68, phosphate data ranges between 0.34 and 0.404 and silicate data ranges between 7.43-8.38 μM for the upper 400 m within years 1962-1994. In Eastern Basin, the nutrient distributions compared to the western basin are relatively low. Especially in surface waters of the Rhodes Gyre, Antalya Basin and the Cilician Basin, the nutrients are nearly depleted throughout the year. Nitrate concentration range between 0.11 and 4.66 μM and phosphate data ranges between 0.02-0.16 μM in surface waters between 1991 and 1994. Nitrate concentration ranges between 4.6-5.84 μM and phosphate ranges between 0.16-0.22 μM. It should be stated that the least amounts of nutrients observed are in the anticyclonic Cilician Basin surface waters, phosphate being 0.02 μM most of the time. The nutrient blooms are observed in spring seasons (Ediger et.al., 2005; Yılmaz and Tuğrul, 1998). For the Southeast Mediterranean, the study of Krom et.al., 1991 yielded a similar picture. The study has been conducted in 1989 and surface waters of Southeast Cyprus are depleted in nutrients. Nitrate data ranges between 0.3-0.7 μM and phosphate was below detection limit (0.01μM). The deep waters consist of nearly constant

values of nitrate 5.5 μM and phosphate 0.24 μM.

A detailed study has been conducted in the Cilician Basin by Yılmaz and Tuğrul, 1998. The results were similar compared to historical studies for the basin. Using this study, a comparison of the coastal and offshore waters of Cilician Basin can be done. Especially in spring months (March-April), in coastal areas due to river discharges, relatively higher concentrations of nitrate and silicate has been observed with nitrate concentration ranging from 0.5 to 2.1 μM. On the contrary, the offshore surface water nitrate ranges between 0.05-0.1 μM. In January the same year, the effect of river discharge was not significant. Although, the surface waters of Cilician Basin are poor in nutrients, the layers below the euphotic zone show high nutrient characteristics, with nitrate concentrations of 6.5 μM at a depth of 400m. In agreement with the historical results, phosphate concentrations were as low as 0.02-0.04 μM for surface waters and 0.2 μM for deeper layers. Again in surface waters, silicate concentrations ranges between 1-2 μM, and can be as high as 9-10 μM in deeper layers.

Recent observations of atmospheric and riverine nutrient input to Mersin Bay (Koçak et.al., 2010) have provided estimations of nutrient inputs into the basin including comparisons of atmospheric and riverine sources between 1999 and 2007. In total nitrate, ammonium, phosphate and silicate inputs were 8, 3.2, 0.1 and 1.7 10^9 mol km^{-2} y^{-1} respectively. The dramatic picture of these results were that 90% of DIN and 60% of PO_4 sources from atmosphere, whereas 90% of silicate was of river origin.

1.1.3.2 Nutrient Limitations and Production

The Mediterranean Sea, and the Eastern Mediterranean in particular, is one of the largest water mass that is thought to be phosphorus limited because of high molar nitrate:phosphate ratio. When surface waters are excluded considering the variations in ratio due to production, the deeper layers show a relatively constant ratio of 29:1 (Krom et.al., 1991; Krom et.al., 2005), 28:1 (Yılmaz and Tuğrul, 1998). These results are higher compared to the Western Mediterranean (23:1) and North Atlantic (16:1). In the upper layers of the Eastern Mediterranean, the ratio varies from 5-25:1 in the euphotic zone and with values up to 120:1 at the top of the nutricline (Figure 1.5). The reason for the higher ratios of 120:1 in depths between 150-300m is the discrepancy of concentration increasing depths of N and P (Yılmaz and Tuğrul, 1998). After the winter mixing in water column, there is a winter phytoplankton bloom, and this bloom ceases when the stratification is significant and surface waters run out of phosphate. Krom et.al. (2004) concluded that, because the sources of nutrients in the Mediterranean Sea have an excess ratio of Redfield (N:P > 16:1), the whole Mediterranean has a

shortage of phophorus. Also, Yılmaz and Tuğrul, 1998, state that the most probable reason of the formation of phophorus-poor deep waters is the labile, dissolved organic and inorganic nitrogen rich sinking water.

Koçak et.al. (2010) suggests recent molar ratio of nutrients from rivers were on average 28 and 1.3 for N/P and Si/N respectively. The atmospheric N/P ratio is 10 times the river and riverine Si/N ratio is 100 times higher than the atmospheric ratio. These ratios further propagate phosphate limited environments into the basin. He further suggests that the silicate outcomes of these results can cause a switch from diatom dominated population to non-silicious species in coastal areas, especially in the bloom season, where recent studies show that diatoms are the dominant phytoplankton population (Uysal and Köksalan, 2010). The limitation of silicate over nitrogen can be important in this manner.

Production in the Mediterranean Sea varies with respect to the availability of nutrients. Bethoux et.al., 1998, state that the production in the Eastern Mediterranean and whole Mediterranean with respect to phosphate budgets are 5.5 and 8.2 gC m^2y^{-1} and with respect to nitrate budget 8 and 11 gC m^2y^{-1} accordingly. The gap between the results are due to the anomaly in N/P ratio. The satellite imagery study of Antoine *et. al.* (1995), states that the total production in the Eastern Mediterranean was 110 gCm^2y^{-1}, and 130 gC m^2y^{-1} for the whole Mediterranean. The production levels are in accordance with the nutrient-poor environment of the Eastern Mediterranean. In the North Eastern Levatine, the daily depth-integrated production ranges between 38.5 and 457 mgC m^2d^{-1}. For the anticyclonic Cilician Basin, daily depth integrated carbon uptake values were on average 250 mgC m^2d^{-1} with a yearly range of chlorophyll-a of 0.02 to 0.27 μg/L (Ediger et.al., 2005). Production in the Cilician Basin can be observed in Figure 1.5.

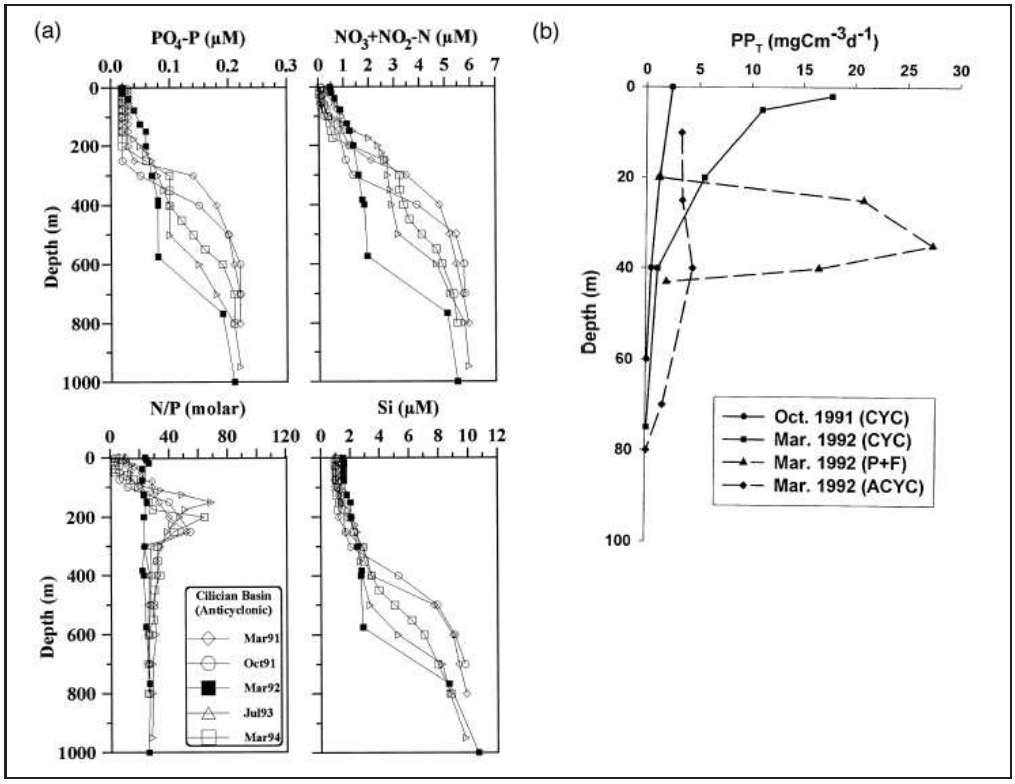

Figure 1.5: a) Vertical profiles of dissolved nutrients and N/P ratio in Cilician Basin for March 1991 - March 1994 (After Yılmaz and Tuğrul, 1998) - b) Vertical profiles of primary production in Rhodes Gyre (CYC), Peripheral and Frontal Area (P+F) and Cilician Basin (ACYC) for October 1991 and March 1992 (After Ediger et.al, 2005)

1.2 Aims and Objectives

The principal objectives of this study were:

- To investigate the dominant circulation patterns, transport and cycling of nutrients, and resulting primary production in Cilician Basin via modelling, where the inner domain shows eutrophic and the outer domain shows highly oligotrophic characteristics.
- To apply changing scenarios of domestic wastewater and river discharges into the model domain to investigate the eutrophication phenomena in the coastal zones and interactions with circulation patterns and nutrient transport.

Within the scope of these broad objectives, the following aims were identified for particular attention:

1. To model the circulation with respect to changing heat fluxes, wind pressures, and river discharges.
2. To model the primary production levels with respect to atmospheric and riverine nutrient in-

puts, lateral and vertical transport of nutrients and regionally specific parameterization of rates.

3. To assess the impact of different characteristics of the inner and outer domain on primary production and nutrient cycling.
4. To assess the effect of summer stratification and winter mixing on primary production.
5. To determine regionally specific limiting nutrients and test relevant discharge scenarios to deduce the effect of riverine and wastewater discharges on eutrophication phenomena for the coastal regions of the domain.

CHAPTER 2

DELFT3D: CONCEPTUAL DESCRIPTION

2.1 Modelling in Delft3D

Delft3D is a 2D/3D modelling system designed for application to hydrodynamics, sediment transport and morphology and water quality problems in fluvial, estuarine and coastal environments. Delft3D comprises of integrated modules that simulate the hydrodynamics and ecosystem dynamics of the area of concern. The heart of the modelling system in Delft3D is the Delft3D-FLOW module, which is a multi-dimensional (2D or 3D) hydrodynamic (and transport) simulation program which calculates non-steady flow and transport phenomena resulting from tidal and meteorological forcing on a curvilinear, boundary fitted grid. The ecosystem dynamics module for detailed chemistry simulations is Delft3D-WAQ and the specie specific phytoplankton growth module is Delft3D-ECO. Although the ECO module includes detailed phytoplankton growth equations, which are called BLOOM, as a substructure it interacts with WAQ equations for nutrient cycle dynamics. Besides the computation considerations, Delft3D also has built-in grid and sample generation tools, RGFGRID and QUICKIN.
In this study, for circulation simulations FLOW module, and for ecosystem simulations ECO modules are used. Brief descriptions of modules and their equations are provided in the following sections.

2.1.1 Delft3D-FLOW

Delft3D-FLOW solves the unsteady shallow water equations in two (depth-averaged) or in three dimensions. The equations consist of horizontal equations of motion, the continuity equation and transport equations for conservative constituents. In simulations, the flow can be forced by tides, current and total discharge forcing fields at the open boundaries, and wind stress at the surface, pressure gradients due to free surface gradients. Discharge and withdrawal of water can be included at certain selected locations in the grid. Also the heat budget can be modelled with several different

heat flux models built-in. For turbulence closure considerations, the four options k-epsilon, k-L, algebraic and constant model are included.

2.1.1.1 Hydrodynamic Equations and Assumptions

In Delft3D-FLOW the 2D (depth-averaged) or 3D non-linear shallow water equations are solved. These equations are derived from the three dimensional Navier Stokes equations for incompressible free surface flow, so that vertical accelerations are reduced to hydrostatic pressure relation due to shallow water approach. In addition to that, the varying density fields are taken into account in pressure term, hence the Boussinesq Assumption. In the σ-coordinate system, the immediate effect of bouyancy on the vertical flow is not considered. In Delft3D-FLOW vertical density differences are taken into account in the horizontal pressure gradients and in the vertical turbulent exchange coefficients. The vertical velocities are computed from the continuity equation. The set of partial differential equations in combination with an appropriate set of initial and boundary conditions are solved on a finite difference grid. The governing equations are given in the subsequent sections. Further details are referenced to Delft3D-FLOW manual.

Continuity Equation:

$$\frac{\partial \zeta}{\partial t} + \frac{1}{\sqrt{G_{\xi\xi}}\sqrt{G_{\eta\eta}}}\frac{\partial\left[(d+\zeta)u\sqrt{G_{\eta\eta}}\right]}{\partial \xi} + \frac{1}{\sqrt{G_{\xi\xi}}\sqrt{G_{\eta\eta}}}\frac{\partial\left[(d+\zeta)v\sqrt{G_{\xi\xi}}\right]}{\partial \eta} = Q,$$

$$Q = H\int_{-1}^{0}(q_{in} - q_{out})d\sigma + P - E$$

With q_{in} and q_{out}, local sources and sinks of water per unit volume (1/s), P, the non-local source term of precipitation and E non-local sink term due to evaporation.

Momentum Equation in Horizontal Direction:

$$\frac{\partial u}{\partial t} + \frac{u}{\sqrt{G_{\xi\xi}}}\frac{\partial u}{\partial \xi} + \frac{v}{\sqrt{G_{\eta\eta}}}\frac{\partial u}{\partial \eta} + \frac{\omega}{d+\zeta}\frac{\partial u}{\partial \sigma} - \frac{v^2}{\sqrt{G_{\xi\xi}}\sqrt{G_{\eta\eta}}}\frac{\partial \sqrt{G_{\eta\eta}}}{\partial \xi} + \frac{uv}{\sqrt{G_{\xi\xi}}\sqrt{G_{\eta\eta}}}\frac{\partial \sqrt{G_{\xi\xi}}}{\partial \eta} - fv =$$
$$-\frac{1}{\rho_0\sqrt{G_{\xi\xi}}}P_\xi + F_\xi + \frac{1}{(d+\zeta)^2}\frac{\partial}{\partial \sigma}(\nu_V\frac{\partial u}{\partial \sigma}) + M_\xi,$$

$$\frac{\partial v}{\partial t} + \frac{u}{\sqrt{G_{\xi\xi}}}\frac{\partial v}{\partial \xi} + \frac{v}{\sqrt{G_{\eta\eta}}}\frac{\partial v}{\partial \eta} + \frac{\omega}{d+\zeta}\frac{\partial v}{\partial \sigma} - \frac{uv}{\sqrt{G_{\xi\xi}}\sqrt{G_{\eta\eta}}}\frac{\partial \sqrt{G_{\eta\eta}}}{\partial \xi} + \frac{u^2}{\sqrt{G_{\xi\xi}}\sqrt{G_{\eta\eta}}}\frac{\partial \sqrt{G_{\xi\xi}}}{\partial \eta} - fv =$$
$$-\frac{1}{\rho_0\sqrt{G_{\eta\eta}}}P_\eta + F_\eta + \frac{1}{(d+\zeta)^2}\frac{\partial}{\partial \sigma}(\nu_V\frac{\partial v}{\partial \sigma}) + M_\eta$$

The vertical velocity , ω, is calculated from the continuity equation:

$$\frac{\partial \zeta}{\partial t} + \frac{1}{\sqrt{G_{\xi\xi}}\sqrt{G_{\eta\eta}}}\frac{\partial\left[(d+\zeta)u\sqrt{G_{\eta\eta}}\right]}{\partial \xi} + \frac{1}{\sqrt{G_{\xi\xi}}\sqrt{G_{\eta\eta}}}\frac{\partial\left[(d+\zeta)v\sqrt{G_{\xi\xi}}\right]}{\partial \eta} + \frac{\partial \omega}{\partial \sigma} = H(q_{in} - q_{out})$$

The vertical velocity ω is determined at the iso σ-surfaces. ω is the vertical velocity relative to the moving σ-plane.

Hydrostatic Pressure Assumption for the σ-grid approach:

$\frac{\partial P}{\partial \sigma} = -g\rho H$ hence integrated as: $P = P_{atm} + gH\int_{\sigma}^{0}\rho(\xi, \eta, \sigma', t)d\sigma'$

With the approach of non-uniform density fields, the local densities vary with the effect of temperature and salinity with respect to equation of state, so the hydrostatic equation becomes:

$$\frac{1}{\rho 0\sqrt{G_{\xi\xi}}}P_{\xi} = \frac{g}{\sqrt{G_{\xi\xi}}}\frac{\partial \zeta}{\partial \xi} + g\frac{d+\zeta}{\rho 0\sqrt{G_{\xi\xi}}}\int_{\sigma}^{0}(\frac{\partial \rho}{\partial \xi} + \frac{\partial \rho}{\partial \sigma}\frac{\partial \sigma}{\partial \xi})d\sigma' \text{ and}$$

$$\frac{1}{\rho 0\sqrt{G_{\eta\eta}}}P_{\eta} = \frac{g}{\sqrt{G_{\eta\eta}}}\frac{\partial \zeta}{\partial \eta} + g\frac{d+\zeta}{\rho 0\sqrt{G_{\eta\eta}}}\int_{\sigma}^{0}(\frac{\partial \rho}{\partial \eta} + \frac{\partial \rho}{\partial \sigma}\frac{\partial \sigma}{\partial \eta})d\sigma'$$

The first term in these equations represent the barotrophic pressure gradient (without atmospheric pressure) and the second term represents the baroclinic pressure terms.

2.1.1.2 Transport Equations and Assumptions

The flow in rivers, estuaries, and coastal seas often transport dissolved substances, salinity and/or heat. In Delft3D-FLOW, the transport of matter and heat is modelled by an advection-diffusion equation in three coordinate directions. Source and sink terms are included to simulate discharges and withdrawals. The transport equation here is formulated in a conservative form in orthogonal curvilinear coordinates in the horizontal direction and σ-coordinates in the vertical.

$$\frac{\partial (d+\zeta)c}{\partial t} + \frac{1}{\sqrt{G_{\xi\xi}}\sqrt{G_{\eta\eta}}}\{\frac{\partial[\sqrt{G_{\eta\eta}}(d+\zeta)uc]}{\partial \xi} + \frac{\partial[\sqrt{G_{\xi\xi}}(d+\zeta)vc]}{\partial \eta}\} + \frac{\partial \omega c}{\partial \sigma} =$$

$$\frac{d+\zeta}{\sqrt{G_{\xi\xi}}\sqrt{G_{\eta\eta}}}\{\frac{\partial}{\partial \xi}[\frac{D_H}{\sigma_{c0}}\frac{\sqrt{G_{\eta\eta}}}{\sqrt{G_{\xi\xi}}}\frac{\partial c}{\partial \xi}] + \frac{\partial}{\partial \eta}[\frac{D_H}{\sigma_{c0}}\frac{\sqrt{G_{\xi\xi}}}{\sqrt{G_{\eta\eta}}}\frac{\partial c}{\partial \eta}]\} + \frac{1}{d+\zeta}\frac{\partial}{\partial \sigma}[\frac{\nu_{mol}}{\sigma_{mol}} + max(\frac{\nu_{3D}}{\sigma_c}, D_V^{back})\frac{\partial c}{\partial \sigma}] - \lambda(d+\zeta)c + S$$

where,

$$S = (d+\zeta)(q_{in}c_{in} - q_{out}c) + Q_{tot}$$

Equation of State:

The default equation of state formulation in Delft3D-FLOW, is the UNESCO approach. Which is;

In the range: $0 < t < 40^oC; 0.5 < S < 43$ ppt

$$A = 8.24493 * 10^{-1} - 4.0899 * 10^{-3}t + 7.6438 * 10^{-5}t^2 - 8.2467 * 10^{-7}t^3 + 5.3875 * 10^{-9}t^4$$

$$B = -5.72466 * 10^{-3} + 1.0227 * 10^{-4}t - 1.6546 * 10^{-6}t^2$$

$$C = 4.8314 * 10^{-4}$$

$$\rho_0 = 999.842594 + 6.793952 * 10^{-2}t - 9.095290 * 10^{-3}t^2 + 1.001685 * 10^{-4}t^3 - 1.120083 * 10^{-6}t^4 + 6.536332 * 10^{-9}t^5$$

$$\rho = \rho_0 + AS + BS^{\frac{3}{2}} + CS^2$$

2.1.1.3 Heat Balance Equations:

Delft3D-FLOW model simulates the heat balance with different user-defined heat flux models. Some options require prescribing solar radiation and some require prescribing excess heat due to the atmospheric interaction, in which they both require further specific data input. All of these options were considered to be used in this study, but the most reasonable option to use was the OCEAN HEAT FLUX MODEL. The advantage of this option is that the model simulates the excess heat with atmospheric data, rather than solar radiation input. This configuration eliminates the instabilities of heat flux due to radiation in surface layers. The user has to define air temperature, relative humidity and percentage of cloud for the ocean heat flux model. Within the simulation process, the model defines its own surface net solar radiation with respect to the latitude of the domain. The general equation of heat balance can be seen below and for further details of the equations, the reader is referred to DELFT3D-FLOW manual.

$$Q_{tot} = Q_{sn} + Q_{an} - Q_{br} - Q_{ev} - Q_{co}$$

where;

Q_{sn} : net incident solar radiation (short wave)

Q_{an} : net incident atmospheric radiation (long wave)

Q_{br} : back radiation (long wave)

Q_{ev} : evaporative heat flux (latent heat)

Q_{co} : convective heat flux (sensible heat)

2.1.1.4 Time Integration:

In Delft3D-FLOW simulations, ADI (alternating direction implicit) time integration method is used for the shallow water equations. The ADI-method splits one time step into two stages. Each stage consists of half a time step. In both stages, all the terms of the model equations are solved in a consistent way with at least second order accuracy in space.

For the spatial discretization of the horizontal advection for momentum equation terms, three options are available for simulations; WAQUA, cyclic and flooding. The first two use higher-order dissipative approximations of the advection terms. The time integration is based on the ADI-method. For the water level gradient and the advection terms, the time levels are alternating; if in one stage a term is taken implicitly in time, this term will be taken explicitly in time in the other stage. The advection terms are integrated implicitly in the stage of the ADI-method in which the free surface gradient is at the old time level. In the stage in which the free surface gradient is integrated implicitly the advection terms are at the old time level. For stability the vertical terms are integrated implicitly in both stages. To ensure that the total mass is conserved the transport equation in Delft3D-FLOW is discretized with a mass conserving Finite Volume approach (flux form). For the spatial discretization of the horizontal advection terms, two options are available in Delft3D-FLOW. The first (and default) option is a finite difference scheme that conserves large gradients without generating spurious oscillations and is based on the ADI-method. This scheme is denoted as the Cyclic method. For both momentum and transport equations, cyclic method is used in this study.

$$\text{Courant Number}=2\Delta t\sqrt{gH}\sqrt{\frac{1}{\Delta x^2}+\frac{1}{\Delta y^2}}<4\sqrt{2};$$

is adviced for the choice of a time step in Delft3D-FLOW with respect to ADI time integration method.

The symbols used in the equations can be seen in Table 2.1

Table 2.1: List of Delft3D-FLOW Equation Symbols

Symbol	Units	Meaning
ξ	-	horizontal curvilinear coordinate, x
η	-	horizontal curvilinear coordinate, y
υ	m/s	fluid velocity in ξ direction

Symbol	Units	Meaning (continued)
v	m/s	fluid velocity in η direction
ω	m/s	velocity in the s-direction in the σ-coordinate system
U	m/s	depth averaged velocity in ξ direction
V	m/s	depth averaged velocity in η direction
σ	-	scaled vertical coordinate; $\sigma = \frac{z-\zeta}{d+\zeta}$; (surface = 0; $\sigma = -1$)
ζ	m	water level above some horizontal plane of reference (datum)
d	m	depth below some horizontal plane of reference (datum)
H	m	total water depth; H = d + ζ
$\sqrt{G_{\xi\xi}}$	m	coefficient used to transform curvilinear to rectangular co-ordinates
$\sqrt{G_{\eta\eta}}$	m	coefficient used to transform curvilinear to rectangular co-ordinates
ρ	kg/m^3	density of water
ρ_0	kg/m^3	reference density of water
P	kg/ms^2	hydrostatic water pressure
P	m/s	precipitation
P_ξ	kg/m^{2}s^2	gradient hydrostatic pressure in ξ direction
P_η	kg/m^{2}s^2	gradient hydrostatic pressure in η direction
F_ξ	m/s^2	turbulent momentum flux in ξ direction
F_η	m/s^2	turbulent momentum flux in η direction
f	1/s	Coriolis parameter (inertial frequency)
M_ξ	m/s^2	source or sink of momentum in ξ direction
M_η	m/s^2	source or sink of momentum in η direction
Q	m/s	global source or sink per unit area
q_{in}	1/s	local source per unit volume
q_{out}	1/s	local sink per unit volume
g	m/s^2	acceleration due to gravity
S	ppt	salinity
E	m/s	evaporation
c	kg/m^3	mass concentration
λ	deg	longitude co-ordinate in spherical co-ordinates
ν_{mol}	m^2/s	kinematic viscosity (molecular) coefficient
σ_{mol}	-	Prandtl-Schmidt number for molecular mixing (700 for salt, 6.7 for heat)
σ_{c0}	-	Prandtl-Schmidt number for constituent (0.7)

2.1.2 Delft3D-ECO:BLOOM Module

BLOOM is a generic ecological modelling tool that can be applied to fresh/marine waters to simulate the transport, dispersion, and ecological processes. The transport and dispersion of nutrients and phytoplankton species are offline coupled with the FLOW module results. The ecological processes can be summarized as follows;

- phytoplankton processes: primary production, respiration and mortality
- extinction of light
- decomposition of organic matter in water column and sediment layers
- nitrification and denitrification
- reaeration
- settling
- burial
- grazing, excretion and respiration

Further summarizing, the two main tasks of BLOOM module is to simulate

- transport of state variables in water column as a function of advective and dispersive transport
- simulation of water quality and ecological processes that determine the concentration of state variables. These processes are included as source and sink terms in advection and diffusion equations.

The advection-dispersion formulation can be seen below:

$$\frac{\partial C}{\partial t} = -\frac{\partial Cu}{\partial x} - \frac{\partial Cv}{\partial v} - \frac{\partial Cw}{\partial z} + \frac{\partial}{\partial x}(D_x \frac{\partial C}{\partial x}) + \frac{\partial}{\partial y}(D_y \frac{\partial C}{\partial y}) + \frac{\partial}{\partial z}(D_z \frac{\partial C}{\partial z}) + S(x, y, z)$$

where:

C : concentration (kg m^{-3})

u, v, w : components of the velocity vector (m s^{-1})

D_x, D_y, D_z : components of the dispersion tensor (m^2 s^{-1})

x, y, z : coordinates in three spatial dimensions (m)

S : source or sink of mass due to physical, chemical and biological processes (kg m^{-3} s^{-1})

For the simulation of competition between species, several phytoplankton groups are included as state variables in the formulation of BLOOM. In addition to the competition, the intergroup adaptation of species to different environments are also formulated with including subgroups as state variables. The legacy ecological models simulate the environment with restricting the growth of species due to the resource limitation. The availability of resources determine the competiton between species, so the growth is controlled by single but different parameter configuration, but in reality the growth may be suppressed by different factors, such as seasonal or diurnal changes of temperature, light or food availability. The dependence of species towards resources not only changes among different types but also interspecific as well. BLOOM formulation acts to consider the potential growth rates of each type on a seasonal basis, not just determining a constant in this manner.

In theory, BLOOM defines two parameters, potential net growth rate (Pn_k) and requirement for resources (n_{ik}). The model then consideres Pn_k/n_{ik} ratio to determine which specie will dominate within the next time step of simulation. The idea behind this approach is, if at the beginning of a time step the biomass of a specie is relatively low compared to its equilibrium, BLOOM will limits its growth by potential net growth rate, and if at the beginning of a time step, the biomass of a specie is close enough to its equilibrium, BLOOM will limit its growth by the availability of resources, which can be nutrient or light availability. The determination of potential net growth rates and resource limitation will be explained in following sections.

The observations show that most of the phytoplankton species adapt to varying environmental conditions rapidly. This results in different options in the model to be taken into account for better representation of the environment. Rather than defining different stochiometry, growth, mortality rates ,etc. BLOOM adopts an optimization technique to represent the interspecific adaptation capacity of species. The species are collected in different pools of state variables to define groups, and these groups are subdivided into types that are adopted to different limiting environments. Energy, nitrogen and phosphorus types make up a larger group of species. With the optimization technique, for each time step BLOOM cosideres which of the types would dominate the next time step with the results of resources from previous.

With all the limitation and optimization techniques, BLOOM configuration, Los (Los, 2009) states," *selects the best adopted combination of phytoplankton types at a certain moment and at a certain*

location consistent with the available resources, the existing biomass levels at the beginning of a time interval and the potential rates of change of each type."

2.1.2.1 Environmental Constraints

Nutrient Balance:

The model formulation for each time step, determines the concentration of biomass of each algae type that can be supported with the available resources, giving a mass balance.

$$\sum_k (n_{ik} B_k) + d_i + w_i = C_i$$

where;

i : type of nutrient

k : type of algae

B_k : biomass concentration of each algae type

n_{ik} : fraction of nutrient i per biomass concentration k

C_i : total readily available concentration

d_i : amount incorporated in dead algae

w_i : dissolved nutrient in water

Recycling of Nutrients:

The nutrient cycle is determined by uptake and release of nutrients into/from biomass, also including chemical transformations such as remineralization, nitrification etc. The readily available inorganic nutrients are uptaken by living biomass, and at each time step a certain amounts of biomass dies. A fraction of this biomass is sent into detritus (POC,N,P,Si), some preferably into labile organic pool, and the rest is sent back into the inorganic nutrients pool (autolysis). Detritus may be settled or remineralized or grazed. The formulation for different nutrients are the same, though the rates are defined accordingly.

$$\mathrm{d}d_i/\mathrm{d}t = \sum_k (f_p M_k n_{ik} B_k) - m_i d_i - s d_i$$

where;

M_k : mortality rate of algae type k (day^{-1})

m_i : remineralization rate constant of detritus (day^{-1})

f_p : fraction of dead algae sent to detritus pool

s : settling rate constant (day^{-1})

Energy Limitation:

Algae absorb light for photosynthesis and growth, also they have self shading effect throughout the water column. Due to the physics, light itself has penetration rates in the water column. Including the temperature effects on growth, mortality and respiration, the formulation of growth becomes a complicated process. Considering these effects, each type has its own efficiency of enegy use. As a function of temperature, the user defines a potential maximum growth rate, that is;

$$Pg_k^{max} = P_{1k} * (T - P_{2k})$$

Multiplication of Pg_k^{max} with efficiency factor E_k, with reference to optimal light intensity would yield a potential net growth rate for each type. Likely of growth rates, mortality and respiration rates are determined accordingly.

$$M_k = M_{1k} * M_{2k} \text{ and } R_k = R_{1k} * R_{2k}$$

With respect to those, total energy budget is formulized as follows;

$$\frac{dB_k}{dt} = (Pg_k^{max} * E_k - M_k - R_k) * B_k$$

where;

B_k : biomass of algae type k (g m^{-3})

M_k : mortality rate of algae type k (day^{-1})

R_k : respiration rate of algae type k (day^{-1})

E_k : depth and time averaged production efficiency factor of algae type k

Pg_k^{max} : potential maximum growth rate of algae type k

For the optimization procedure of E_k, the reader should refer to Delft3D-WAQ User Manual. It should also be stated that the formulation of growth rates defines a dynamic determination of net

growth rates for each time step.

Grazing:

Rather than defining the mortality rates in which they are modified to include grazing terms, BLOOM prescribes (user defined) a forcing function on phytoplankton as a grazing term. Likely of phytoplankton, grazers also have their own stochiometry, growth, mortality and respiration rates, they for each time step act to reach the predefined biomass. If the food is available, the grazers keep the prescribed biomass. If there is a lack of food, the grazer biomass drops to a certain level, and at each time step they graze on detritus and phytoplankton to reach the prescribed biomass concentration.

To well define competition, for each individual, seperate biomasses are calculated for each type with respect to energy, nutrient, growth and mortality limitations, and selects the best adopted biomass. This selection criteria is done to achive the maximum production available.

CHAPTER 3

METHODS OF DATA COLLECTION AND PREPARATION OF INPUT PARAMETERS

To simulate the circulation, mixing, stratification and primary production, realistic and detailed data were needed for model simulations. For the model testing and analysis stage, real *in-situ* data were used if possible. If those were not available, other forcing fields were taken from reliable model simulations and analyses. Acquired data, and its relevant field of use is listed below.

- Topography (hydrodynamics)
- Initial conditions (hydrodynamics and ecosystem)
- Boundary conditions (hydrodynamics and ecosystem)
- Heat balance (hydrodynamics)
- Wind stress (hydrodynamics)
- River discharges (hydrodynamics and ecosystem)
- Evaporation and precipitation (hydrodynamics)
- Surface solar radiation (ecosystem)
- Atmospheric and riverine nutrient input (ecosystem)

3.1 *In-Situ* Measurements

Cruises were conducted in Mersin Bay, as part of the project ”URBAN WASTEWATER MANAGEMENT ALONG COASTAL AREAS OF TURKEY: REIDENTIFICATION OF HOT SPOTS AND

SENSITIVE AREAS, DETERMINATION OF ASSIMILATION CAPACITIES BY MONITORING AND MODELLING AND DEVELOPMENT OF SUSTAINABLE WASTEWATER INVESTMENT PLANS", funded by TUBİTAK (Scientific and Technological Research Council of Turkey). Data were collected by R/V Bilim during 11 cruises between the years 2008-2010, in shelf regions of Mersin Bay (Figure 3.1). The times of the cruises were selected to observe the seasonal changes in both physical and ecosystem characteristics of the bay. Therefore winter, spring, mid-summer and early-autumn data were available for model testing and analysis.

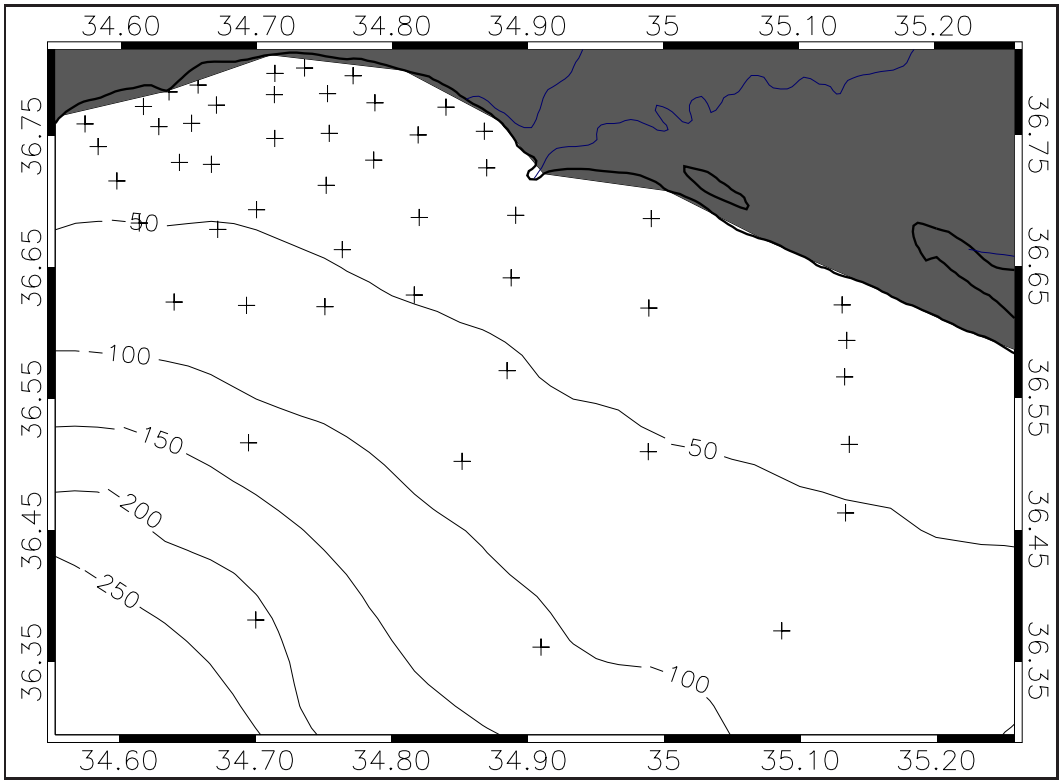

Figure 3.1: Cruise Map of Mersin Bay

50 stations were covered during each cruise, along with smaller coastal cruises, during September 2008, January, February, March, May, August, October 2009, February, April, July and October 2010. During each cruise, standard CTD profiles were obtained at each station using a SBE-9 CTD, equipped with pressure, temperature, conductivity, PAR and oxygen sensors. For chemistry related studies, inorganic nutrients (NO_3, NH_4, PO_4 and Si), particulate and dissolved organic nutrients (POC,N,P - DOC,N,P), chlorophyll-a, total suspended solid, pH and oxygen measurements were made. Additionally micro and macro sized autotroph and heterotroph species distributions were studied.

The seasonal riverine nutrient discharge, oxygen and pH levels were measured by the Chemical Oceanography Department of Institute of Marine Sciences (IMS-METU). The measurements were

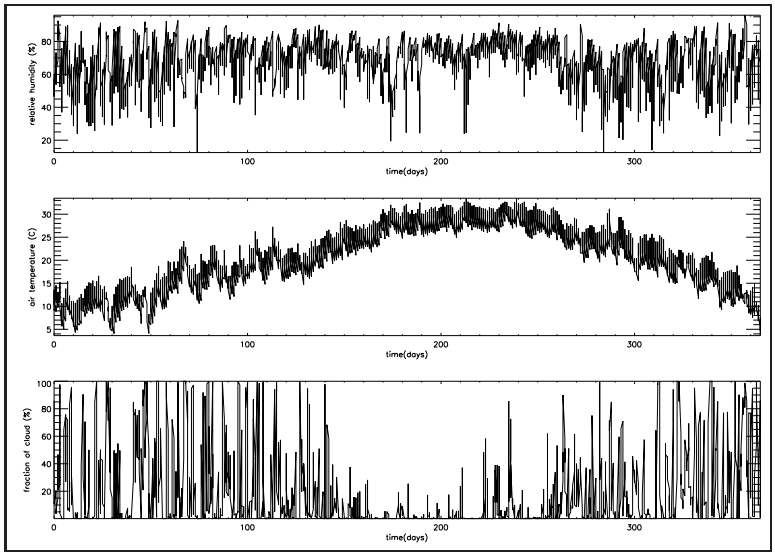

Figure 3.2: Parameters used for the Ocean Heat Flux model

held at the river bed near the discharge point in the sea. Data was available for the rivers Seyhan, Ceyhan, Berdan and Göksu. The atmospheric measurements were recorded in a coastal tower station in Erdemli. Nutrients were input to the model in inorganic form, NO_3, NH_4 and PO_4, and long term data were available (Koçak, 2010).

3.2 Heat Balance

For the heat balance calculations, the built-in Delft3D heat flux model was used. The percentage of the sky covered by clouds was prescribed . The effective back radiation and the heat losses due to evaporation and convection were computed by the model. Additionally, when air and water densities and/or temperatures were such that free convection occurs, free convection of latent and sensible heat was computed by the model. This model formulation is typically applied for large water bodies. The domain used for the modeling of Cilician Basin was valid for such a heat flux computation.

For calculation of surface heat flux parameters, relative humidity (r_{hum}), air temperature (T_a) and cloud fraction (F_c) were prescribed. The related heat forcing data was taken from INTERIM reanalysis data of ECMWF (European Center for Medium-Range Weather Forecasts). Values were taken from analysis of 2008 and 2009 with 6h time intervals. Relative humidity values were calculated from 2m dewpoint temperature values following the formula of Lawrence (2005) where RH = 100 - 5(T - T_d). The prescribed values are presented in Figure 3.2.

3.3 Topography

For the hydrodynamic model runs, GEBCO (General Bathymetry Chart of the Oceans) 1 minute resolution topography data was used. The final model bathymetry is seen in Figure 1.1.

3.4 Wind Stress

The prevailing wind patterns for the Cilician Basin were described in the introduction part of this thesis. For model simulations, space and time varying wind data were needed. To create the most reliable wind forcing fields, the suitability of the available *in-situ*, remotely sensed and reanalysis data were compared. The coastal measurement sites were too few and they were inadequate to distribute the available data to the whole domain, the ECMWF reanalysis data, which included the open-sea domain was too coarse. The choice was to use the satellite images of QuikSCAT/Seawinds data. The resolution was high enough to govern the surface forcing. 6 hour interval of u-v wind data was used with 0.25 degree resolution over the whole basin.

For each time step, using an additional set of files, the model calculations were referenced to a coarser wind grid, in this case the Seawinds grid, and the wind data were interpolated over the whole domain for each grid point. The grid structure of the satellite wind data can be found in Figure 3.3.

3.5 Surface Solar Radiation

In contrast to the ”Ocean Heat Flux Model” applied when running the hydrodynamics model, the ecosystem model in Delft3D requires a separate radiation function. A time series of radiation should be prescribed by user in W/m^2. For the 3D model, rather than prescribing accumulated radiation exposure, an average exposure should be prescribed (Figure 3.5). Surface net solar radiation data were retrieved from the ECMWF-INTERIM reanalysis at 6 hour time intervals. Formulation of Delft3D-ECO has a built-in day length function dependent on the latitude of the domain. Therefore average daily radiation values were prescribed from 6 hour ECMWF-INTERIM data.

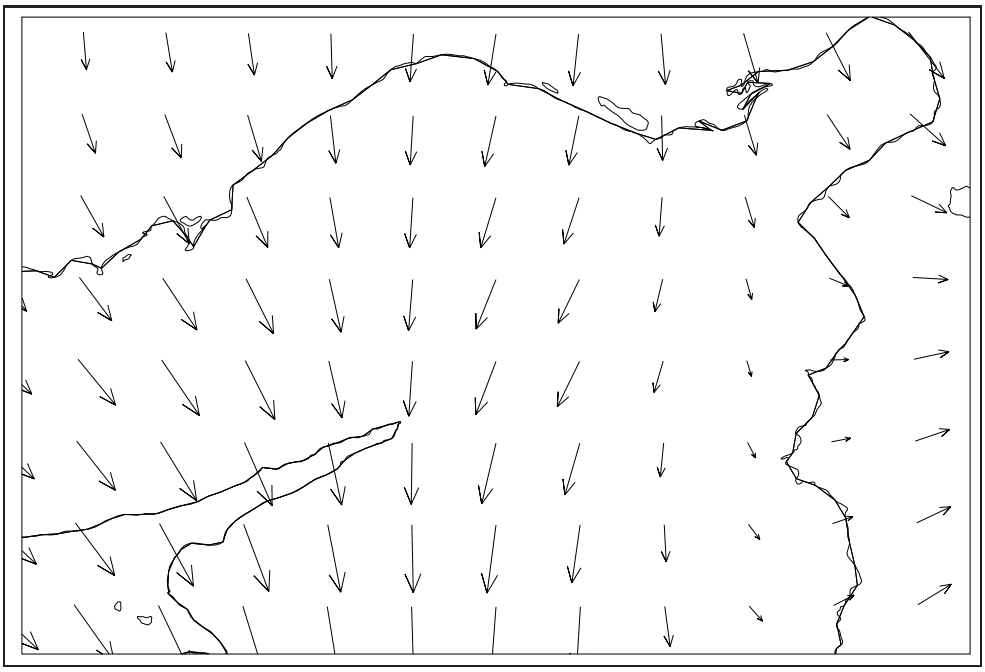

Figure 3.3: Grid structure of satellite wind data

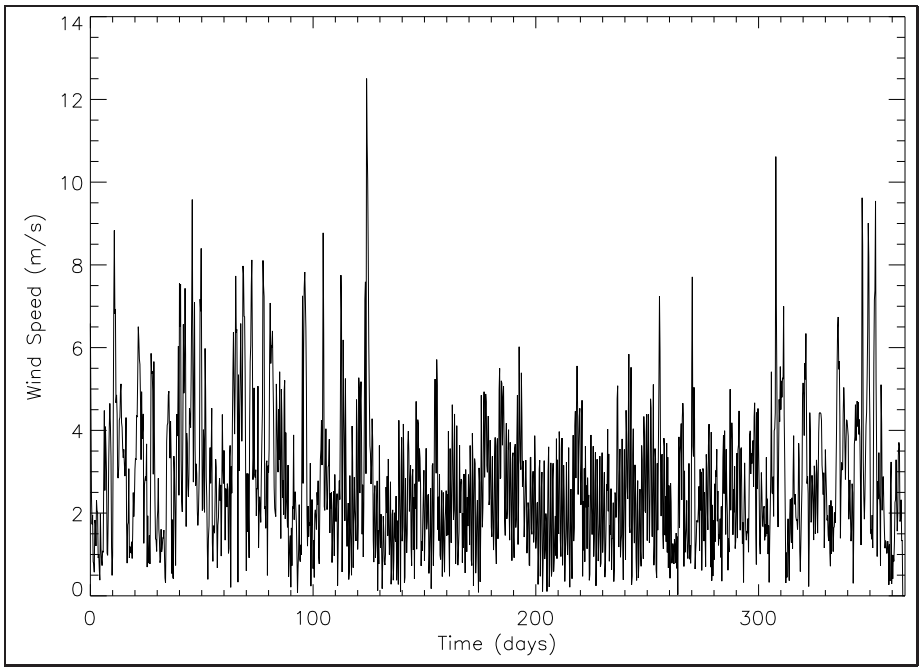

Figure 3.4: Time series of remotely sensed ocean winds at the offshore station (Figure 4.20) of Mersin Bay

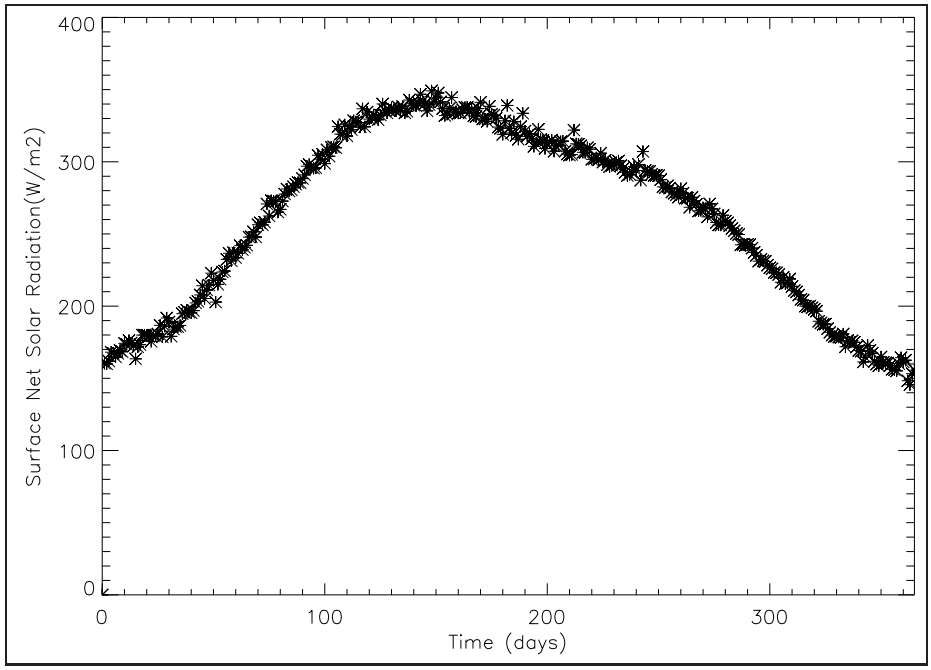

Figure 3.5: Surface net solar radiation used as a forcing function in ecosystem model simulations (ECMWF-INTERIM reanalysis

3.6 River Discharges

There is a substantial freshwater input to the model domain throughout the year. The 4 largest rivers discharging to the Cilician Basin are Seyhan, Ceyhan, Berdan and Göksu Rivers. These 4 river discharges were included in the hydrodynamic model setup to define the fresh water and sea water interactions in coastal areas. The rivers mostly have higher discharges in spring season, though the discharges continue throughout the year.

In addition to the river discharges, the wastewater discharge of Mersin also plays an important role when defining the ecosystem characteristics of Mersin Bay. As stated before, the area of concern was Mersin Bay, and because such discharges have negligible effects on circulation, wastewater discharges of other major cities were neglected. Monthly long term averaged freshwater fluxes were defined using statistics provided by the State Hydraulics Institute of Turkey (DSI). They were defined as point discharges at single grid cells, constant throughout the water column in m^3/s. (Figure 3.6)

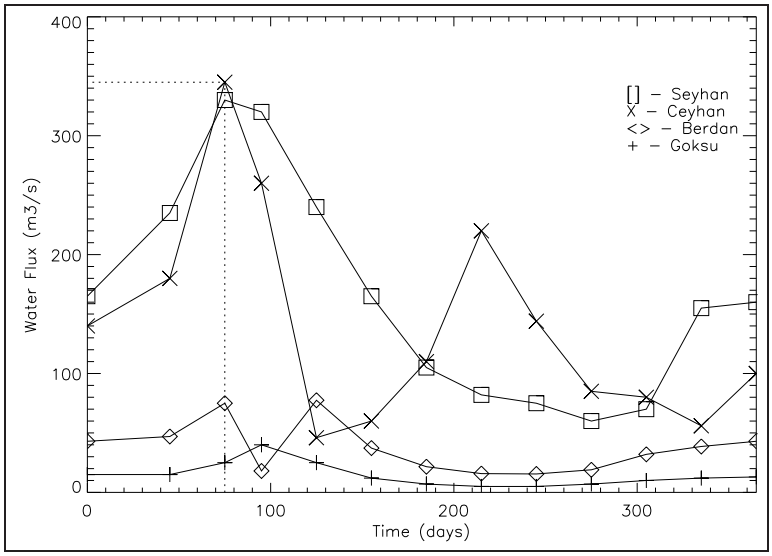

Figure 3.6: Yearly freshwater fluxes set for hydrodynamic simulations

3.7 Coupled 3D Eco-hydrodynamic Model Setup

3.7.1 Hydrodynamic Model Setup

In this study, the hydrodynamic and the ecosystem models were coupled offline. The reference hydrodynamic simulation start time was 01.01.2008 to meet the requirements of comparing *in-situ* measurements and model results. As stated in Section 3.1 of this study, *in-situ* measurements of Mersin Bay were started in September 2008 and carried out till November 2010. Therefore model simulations were done for the time interval of 2008-2009, while most extensive *in-situ* data availability was for the year 2009, where 6 cruises were conducted in different seasons covering winter, transition and summer periods.

The hydrodynamics model was run for the year 2008 to stabilize the model domain and its internal parameters and used solely as a spin-up run. Offline coupling of the hydrodynamics and ecosystem model compartments was done for the year 2009. Although there have been cruises conducted during 2010 in Mersin Bay, simulation of the year 2010 were not conducted in the scope of this study because of insufficiently detailed or unavailable forcing data, such as ECMWF-Interim, satellite imagery of winds and simulation results of CYCOFOS High Resolution Levantine Forecast. Simulation of the year 2010 will be conducted in further studies when data becomes available.

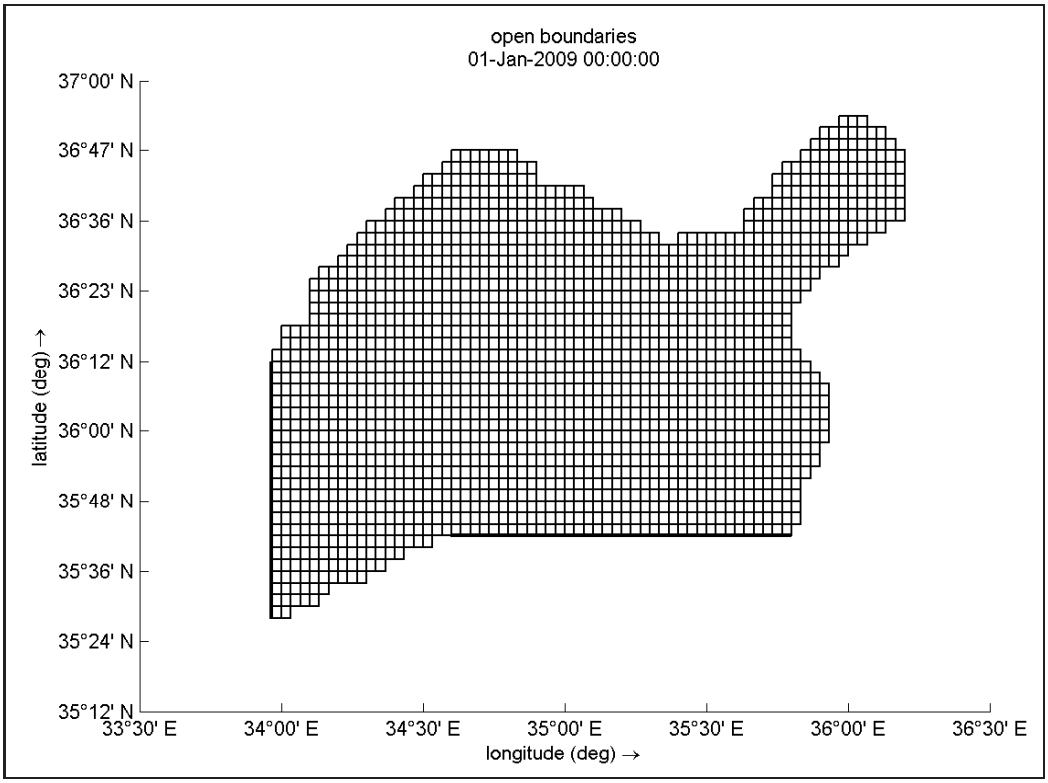

Figure 3.7: Hydrodynamic Model Grid

3.7.1.1 Model Domain and Initial Data

The term Cilician Basin is used in reference to the northeastern corner of Mediterranean Sea, east of longitude 33.5 (Shaw and Bush, 1978).The western boundary of the domain was located to the east of 33.5. The model domain also covers the Bay of Iskenderun and extends down to the northeastern corner of Cyprus. The precise decimal degree boundary location of the model domain were 33.9667 east which is the western open boundary and 35.7 north which is the southern open boundary. The Cilician model is covered by uniform orthogonal grid with 2 minute (approximately 3.3 km) resolution in both the east-west and north-south directions (Figure 3.7).

The Cilician hydrodynamic model covers an area of approximately 2.5 x 10^{10}m^2 between the coasts of Turkey and Cyprus, and consists of 69x45 grid points with two open boundaries. The southern open boundary is located at 35.7 degree north, where it extends from the northeastern corner of Cyprus to Syria. The western open boundary is located at 33.9667 degree east, where it extends from the south coast of Turkey (Taşucu) to the northern coast of Cyprus. Both open boundaries are indicated with solid lines in the domain in Figure 3.7. This setup of grid covers an extensive area around Mersin Bay, the area of concern. The reason for defining the open boundaries outside the region of interest was to eliminate the unrealistic effects of open boundaries on the bay.

The main aim of this study was to simulate and investigate the ecosystem dynamics. Rather than capturing the fine resolution circulation of the basin, grid structure was defined to simulate summer stratification and winter mixing in the water column. Therefore a coarse grid size was selected due to computational time restrictions. The reasoning behind this was, if general circulation of the bay with river discharges can simulate summer stratification and winter mixing for nutrient cycling and production sufficiently, the grid size and structure would satisfy the aims of this study. The validity and effectiveness of this approach will be discussed in detail in Chapter-4.

The initial conditions of the hydrodynamic model run were formed from a high resolution Levantine forecast model run at CYCOFOS (Cyprus Coastal Ocean Forecasting and Observing System) which dates to its result of 01.01.2008 at 12:00 pm. The CYCOFOS model has a grid resolution of uniform orthogonal 1 min size. For offline nesting concerns, the Cilician models grid points were defined so that they would coincide with the CYCOFOS model grid points. Rather than directly coupling the initial conditions with the CYCOFOS model, to relaxing the Cilician model numerically, initial velocities were defined as 0 m/s for both u and v. The free surface of CYCOFOS model was multiplied by 0.1, and temperature and salinity fields were directly taken without scaling. All parameters, T,S,ζ, u, v were initially smoothed along the domain using a technique adopted from the Delft3D-QUICKIN tool. For nesting the CYCOFOS model with the Cilician model, sigma levels (σ) were set equal to the CYCOFOS model. The σ-levels were defined such that the high stratification in summer months was captured. This resulted in very compact upper sigma levels. The CYCOFOS model has 24 sigma layers, so does the Cilician model. (σ = 0.0, -0.00183824, -0.00367647, -0.00735294, -0.0147059, -0.0294118, -0.0588235, -0.117647, -0.176471, -0.235294, -0.294118, -0.352941, -0.411765, -0.470588, -0.529412, -0.588235, -0.647059, -0.705882, -0.764706, -0.823529, -0.882353, -0.941176, -0.970588, -0.985294, -1.0)

3.7.1.2 Open Boundary Conditions

The open boundaries were set as far from the area of concern as possible with computational time consumption considered. To meet the numerical stability requirements of Delft3D-FLOW, the southern open boundary was set as 3D velocity profile boundary and the western open boundary was set to be the water level boundary. Daily velocity and water level fields were obtained from the CYCOFOS model. For the 3D velocity profile boundary, daily velocity data were input offline as velocities perpendicular to the boundary for every sigma level and every point. A similar procedure was ap-

plied to the western boundary. At each point of the boundary, water level data were imported from CYCOFOS. For transport boundary condition equations, 3D temperature and salinity profiles for each sigma level and point for both of the open boundaries were imported from the same model. Transport boundary conditions also have daily fields.

3.7.1.3 Hydrodynamic Model Scenarios

Tuning of the hydrodynamic model simulations was done to achieve an environment of water mass structure that allows good representation of primary production and nutrient cycling. With this in mind, the tuning procedure was focused on freshwater input from point sources and the river discharges. Although, as stated before, the river discharge values were taken as long term average discharges from the State Hydraulics Institute of Turkey, the results showed inconsistencies with the *in-situ* data. At certain times of simulation, hydrodynamic model results showed that too much freshwater has been input. The detailed discussion will be done in following sections.

Reference Scenario (Scenario-1):

The reference hydrodynamic scenario run was started at 01.01.2008 at 12:00 PM. Two runs have been simulated. The first run, a spin-up run, was for the year 2008 and the second run was for the year 2009. The initial conditions for the 2009 run were selected from the results of simulation done for the year 2008, at 31.12.2008 at 12:00 PM respectively. Therefore the results of 2009 only were considered as the reference model run. Time step for the simulations was 1 minute, with respect to the courant number calculation for the ADI time integration method explained in Chapter-2 of this study. Detailed setup configuration can be seen in Table 3.1

Table 3.1: Hydrodynamic simulation Scenario-1 setup

Parameter	**Source**	**Resolution**	**Used As**
Grid	-	2min x 2min	Domain Grid
Bathymetry	GEBCO	1min x 1min	Domain Bathymetry
Time Step	-	1 min	Simulation Time Step
Velocity and Water Level	CYCOFOS	1 min x 1 min	Initial Conditions
Velocity and Water Level	CYCOFOS	1 day	Open Boundary Conditions

Parameter	Source	Resolution	Used As (Continued)
Temperature and Salinity	CYCOFOS	1 min x 1 min	Initial Conditions
Temperature and Salinity	CYCOFOS	1 day	Open Boundary Conditions
Horizontal Eddy Viscosity	-	20 m^2/s	Background Viscosity
Horizontal Eddy Diffusivity	-	20 m^2/s	Background Diffusivity
Vertical Eddy Viscosity	-	10^{-6} m^2/s	Background Viscosity
Vertical Eddy Diffusivity	-	10^{-6} m^2/s	Background Diffusivity
3D Turbulance	-	k-Epsilon	Model for 3D Turbulance
Roughness Formula Formula	Chezy	U:65 V:65	Bottom Roughness
Relative Humidity	ECMWF Interim	6 hours	Ocean Heat Flux Model
Air Temperature	ECMWF Interim	6 hours	Ocean Heat Flux Model
Fraction of Cloud Coverage	ECMWF Interim	6 hours	Ocean Heat Flux Model
River Discharge	DSI	1 month	Freshwater Input
Winds	SEAWINDS	6 hours	Surface Forcing

Scenario-2:

With respect to the reference simulation, in Scenario-2, the freshwater influx was decreased. The simulation spin-up was kept as before, but for the simulation of the year 2009, the river freshwater flux was decreased to 1/3 of the original. This adjustment was done to represent the decreasing trend

of precipitation of rain and snow on coastal areas (Ludwig, 2009). Because the area of concern is Mersin Bay, this tuning was applied to the Seyhan River, which is the major freshwater input in the area.

Scenario-3:

Similar to Scenario-2, in Scenario-3 decreasing the Seyhan River freshwater input to 1/3 of the original has also been applied for the spin-up year 2008. While all of the coefficients were kept in their default values. Therefore simulations were carried out with physical forcing parameters to represent the environmental conditions of Cilician Basin.

Scenario-4 and Scenario-5:

The Delft3D-FLOW compartment has built-in heat flux models as explained in Chapter-2. Parameters like surface and back radiation were computed by model equations, and parameters such as air temperature, humidity and sky cloudiness were user defined. Besides those, some constants were required for calculations, such as water surface area, dalton and stanton numbers. These two numbers, dalton and stanton, are constants used in computation of latent and sensible heat fluxes. These constants were used in air-sea interface heat interactions. Basically their role was to define how much the surface water was being affected by the changes in structure of the atmosphere (heat and wind). Further tuning of the model was done by changing these constants. Default values of stanton and dalton were 0.0013 for both. In Scenario-4, these were changed to 0.0015 and in Scenario-5 to 0.0011 to define a range of sensitivity.

3.7.2 Ecosystem Model Setup

Transport of matter through advection and dispersion, water temperature and salinity were taken from the hydrodynamic results at time intervals of 6 hours. A 6 hour interval was considered adequate for the ecosystem model simulations, where most of the parameters were set daily. As discussed before, coupling of the ecosystem was done for the year 2009 only due to the availability of seasonal *in-situ* data.

The default parameterization of the ecosystem model was adjusted for more productive marine environments by Deltares, such as North Sea (Los, 2009). If compared with the Mediterranean, the

North Sea is exposed to less sunlight, is colder, and is connected to the Atlantic Ocean. Therefore the North Sea represents a very different environment than the Mediterranean, which is exposed to high amount of sunlight, high stratification and is also subject to nutrient limitation, which results in smaller primary production rates. Due to these restrictions, before scenario analyses stage, pre-tuning of the parameters for the Mediterranean case was required.

3.7.2.1 Ecosystem Dynamics

A summary ecosystem model compartments can be seen in Figure 3.8. At the bottom of the food chain are the inorganic nutrients, NH_4-N, NO_3-N, PO_4-P and Si. Algae, through photosynthesis, uptake these inorganic nutrients and store them in form of organic matter. While organic matter is formed by photosynthesis, dissolved oxygen is released into water. At the same time, algae also consume this organic matter for maintenance and respiration purposes, so some of the uptaken inorganic nutrients are sent back to the nutrients pool, via respiration. Although algae have high growth rates, they also have relatively high mortality rates. When algae die, organic matter is sent into three different pools in the model. Predefined percentages decide how much is sent to each pool. The particulate and easily decomposable organics are sent into a special particulate matter pool called DETRITUS. For this study, less decomposable compartment called OTHER ORGANICS were modified to represent the dissolved organic matter, so that their decomposition rates were increased and their settling was ceased. The rest of dead algae is sent back to the inorganic nutrients pool by a process called autolysis. Dead algae processes are governed by mortality rates of algae, where production is governed by growth and respiration rates. Respiration also requires dissolved oxygen. Particulate and dissolved matter, also undergo chemical processes. Their decomposition into more simple matter, the inorganics, is called mineralization by decomposers. The life cycle of decomposers are not included in the model, but their effect on the ecosystem in parameterized by mineralization rates. The mineralized nutrients are sent into the inorganic nutrients pool. Mineralization processes consume oxygen. Particulate matters, due to their weight, settle down into the sediment layer, which is online modelled with the water column. Mineralization and resuspension processes take place in the sediment layer. Together with these, nitrification and denitrification, input and output from neighbor grids, and atmospheric input complete the cycle of nutrients.

3.7.2.2 Calibration of Ecosystem Parameters for Cilician Case

The default parameterization of ecosystem dynamics was calibrated by Deltares for more productive marine environments than the Mediterranean Sea, such as the North Sea. Rather than simulating the model with the default setup, further and detailed analyses had to be carried out to lower the production rates. The starting point of parameters were chosen from the study of coupled ecosystem modelling of the Marmara Sea (Blauw *et. al.*, 2009). The difference between the default parameters and the Marmara Sea case study was the dependency of algae on nutrients. They defined the Marmara Sea as oligotrophic, so they increased the N,P,Si/C ratios. Since the Mediterranean is ultraoligotrophic, nutrient limitation (P/C) was further modified in this study (Table 3.6).

The algae pool in this study includes 4 primary producer groups. They are Diatoms, Flagellates, Dinoflagellates and Bacteria. With Delft3D-ECO more algae groups can be included in the model, but for the sake of simplicity and because these groups were dominant in Mersin Bay (Uysal, 2010; TARAL-SINHA, 2010, 2009), the rest of the algae groups were neglected in this study. Diatoms, flagellates and dinoflagellates represent the phytoplankton species, with diatoms having the highest dry matter, settling velocity and chlorophyll-a. (Tables 3.5 and 3.6). The bacteria group was included and parameterized to represent the small phytoplankton and bacteria groups in the bay. They have less dry matter and are less nutrient dependent.

The reference scenario was formed to represent the present ecosystem characteristics of Mersin Bay. Sensitivity analyses studies were done by further tuning the parameters and changing the inputs of the reference scenario. Comparison of reference scenario and available data was done for Mersin Bay. Although results existed for the whole domain, likewise in hydrodynamics results, results of Mersin Bay will be the focus of this study.

Initial and boundary conditions, river input

The open boundary locations were kept the same as for the hydrodynamics model, so the boundaries were distant from Mersin Bay to eliminate their influence on the ecosystem. Hydrodynamic model Scenario-5 was chosen for the offline coupling of the reference ecosystem run. Hydrodynamic model simulations were started in January, the same 1 year time interval was kept for ecosystem simulations as well. Initial conditions were formed from *in-situ* data collected in January 2009, taking the average of all stations. Boundary conditions were defined from the most offshore station of the

cruises. Defining the initial conditions with reference to a single cruise and neglecting the spatial distributions may seem unrealistic, but simulations were conducted for more than 1 year to remove the effect of initial conditions. The values assigned for initial and boundary conditions can be seen in Table 3.2. River discharges were set according to the data acquired from the Chemical Oceanography Department of Middle East Technical University. Measurements from 2009 were included for rivers Seyhan, Ceyhan, Berdan, Göksu rivers and Mersin city discharge point. Available data for each discharge were for months February, April, July and October.

Table 3.2: Initial and Boundary Conditions of Reference Simulation

Parameter	**Initial**	**Boundary**
DetC (gC/m^3)	0.03	0.015
DetN (gN/m^3)	0.005	0.0025
DetP (gP/m^3)	0.00035	0.00022
DetSi (gSi/m^3)	0.00035	0.00035
DOC (gC/m^3)	0.03	0.015
DON (gN/m^3)	0.005	0.0025
DOP (gP/m^3)	0.00035	0.00022
DOSi (gSi/m^3)	0.00035	0.00035
NH_4 (gN/m^3)	0.00544	0.000875
NO_3 (gN/m^3)	0.002	0.000875
PO_4 (gP/m^3)	0.00062	0.00015
Si (gSi/m^3)	0.0214	0.0035
DO (g/m^3)	7.27	7.5
Diatoms-E (gC/m^3)	0.0003537	0.0
Diatoms-N (gC/m^3)	0.0003537	0.0
Diatoms-P (gC/m^3)	0.0003537	0.0
Flagellates-E (gC/m^3)	0.0003537	0.0
Flagellates-N (gC/m^3)	0.0003537	0.0
Flagellates-P (gC/m^3)	0.0003537	0.0
Dinoflagellates-E (gC/m^3)	0.0003537	0.0
Dinoflagellates-N (gC/m^3)	0.0003537	0.0
Dinoflagellates-P (gC/m^3)	0.0003537	0.0
Bacteria-E (gC/m^3)	0.0003537	0.0
Bacteria-N (gC/m^3)	0.0003537	0.0

Parameter	Initial	**Boundary** continued
Bacteria-P (gC/m^3)	0.0003537	0.0

Process Parameters

Growth, mortality, respiration rates, nutrient stoichiometry and chemical reaction rates can be seen in Tables 3.5, 3.6 and 3.7. It was mentioned that further tuning of phosphorus dependency was done using the Marmara case stoichiometry. The change was the increased P/C ratio of Flagellate-P types and decreased P/C ratio of Bacteria-P types. There were two reasons for doing this, one was to increase the competition of diatoms and flagellates over phosphorus and the other one was to make bacteria more nutrient efficient due to its low light and growth efficiency at high temperatures. Recent studies and cruise data of 2009 show diatom and flagellate dominance in spring and bacteria dominance in summer (TARAL-SINHA, 2009). The modifications were done in reference to this ecosystem character of the bay.

Besides nutrient stoichiometry, modification of growth, mortality and respiration rates were done as well. To increase the diatom dominance and effectiveness, growth rates of diatoms were increased and growth rates of flagellates were decreased. Growth rates of bacteria types were also decreased slightly to overcome the complete dominance of bacteria in summer. To fit the results to the *in-situ* data, mortality and respiration rates of all types were increased (Table 3.7). Although the rates may be higher than those in literature, it should be kept in mind that all models calculate parameters differently and also further modification of rates is performed at each time step using light efficiency curves.

After reference run, further calibration of parameters and input values was done to adjust the model setup to an oligotrophic marine environment. Changes were named as RUN-#, and tuning of parameters were mostly concentrated on chemical and physical parameters rather than biological parameters such as growth rates or stoichiometry etc. The offshore station was included in the cruise plan to provide reference data representing the oligotrophic North East Mediterranean. Calibration of the ecosystem model at this station is important in that manner. Because the station is relatively more affected by offshore waters, boundary conditions have important effects on this station. Therefore, while calibrating the reference scenario, adjustments were first applied to boundary conditions.

RUN-01

For the reference run, to observe the internal dynamics of coastal environment, boundary data input was kept at too low values. In this scenario, however, nutrient input at the boundaries increased to the original *in-situ* data at the offshore station. Data input from the open boundaries were adjusted to represent the seasonal changes as well, so time dependent data input was set at the open boundaries. In addition to that, threshold values for inorganic nutrients were included in calculations to limit the excess production in the system (NH_4=0.1 μM, NO_3=PO_4=0.02 μM and Si=0.5 μM). Boundary data can be observed in Table 3.3.

RUN-02

RUN-02 is a follow up scenario, to tune the nutrient structure of the ecosystem after a major change in boundary conditions. Originally, minor amounts of dead algae were sent into the dissolved organics pool. Most of the dead algae were sent into the particulate (detritus) organics pool and into the inorganics pool. Observations, however, show a different nutrient distribution. Therefore, dissolved organic nutrient parameterization was modified to implement a balanced ratio of particulate and dissolved organics. In some cases, dissolved organics show slightly higher concentrations than particulate organics. To achieve such layout, the fraction of dead algae was modified, with a ratio of 45/35 (particulate/dissolved). The reason they do not have similar percentages was that, particulates have larger mineralization rates and also they have settling velocities.

RUN-03

RUN-03 focused on open boundary conditions similar to RUN-01. The difference between them was the way the boundary conditions were implemented. In RUN-01, constant in water column, but varying in time concentrations of inorganic, organic nutrients and oxygen were set. In RUN-03, depth varying, but constant in time concentrations were set. These adjustments were made to observe the sensitivity of the model to boundary conditions. RUN-01 focuses on seasonal changes of the environment, whereas RUN-03 focuses more on the pumping of nutrients from the bottom layers, so that nutrient concentrations increased gradually in deeper layers at the boundaries. The idea was to observe how much primary production was affected by the pumping of nutrients from the bottom layers due to mixing.

Cases-01,02 and 03

Cases-01,02, and 03 focus on the influence of river discharge into the bay. Nutrient load in Case-01

was increased by 50%, in Case-02 by 100% and in Case-03 the nutrient load was ceased. The aim in these scenarios was to observe the effect of nutrient discharge in coastal and offshore locations. Specifically it was intended to determine which regions of the bay were more influenced by river discharge and which regions would be influenced by offshore circulation, and hence the boundary conditions.

Cases-04 and 05

Cases-04 and 05 focused on the influence of the atmospheric discharge into the domain. The reference scenario taken for this simulation was the 0 nutrient load scenario, RUN-03, to observe the influence on both the coastal and offshore locations. In Case-04, yearly averaged atmospheric loads were included from the study of Koçak (2010). In Case-05, atmospheric discharge was doubled. In both Cases-04 and 05, both dry and wet depositions were included in the total discharge.

Table 3.3: Nutrient, oxygen and chlorophyll-a profile for the offshore station

Depth	**NH_4 (μM)**	**NO_3 (μM)**	**PO_4 (μM)**	**Si (μM)**	**DO (mg/L)**	**Chl-a (mg/m^3)**
	January 2009					
0	0.24	0.13	0.02	0.79	7.22	0.08
10	0.10	0.13	0.02	0.80	7.19	0.07
20	0.05	0.13	0.02	0.78	7.30	0.08
30	0.05	0.09	0.02	0.78	7.23	0.08
50	0.04	0.12	0.02	0.78	7.18	0.10
75	0.04	0.09	0.02	0.75	7.13	0.06
100	0.06	0.13	0.02	0.74	7.11	0.05
150	0.04	0.19	0.03	0.80	7.09	-
200	0.22	0.26	0.03	0.84	7.28	-
	February 2009					
0	0.05	0.11	0.03	0.81	7.42	0.15
5	0.11	0.06	0.02	0.80	7.40	0.18
10	0.05	0.09	0.02	0.81	7.41	0.14
20	0.05	0.09	0.02	0.81	7.53	0.10
30	0.06	0.09	0.02	0.79	7.40	0.13
40	0.05	0.07	0.02	0.79	7.44	0.10
50	0.05	0.08	0.02	0.79	7.39	0.11
60	0.05	0.05	0.02	0.79	7.41	0.10

Depth	NH_4 (μM)	NO_3 (μM)	PO_4 (μM)	Si (μM)	Oxygen mg/L	Chl-a mg/m^3
75	0.10	0.08	0.02	0.82	7.32	0.10
100	0.10	0.09	0.02	0.81	7.4	0.12
150	0.16	0.13	0.02	0.81	7.39	0.13
200	0.20	0.39	0.02	1.00	7.39	-
	March 2009					
0	0.22	0.23	0.03	0.92	7.47	0.12
10	0.08	0.23	0.03	1.07	7.47	0.13
20	0.38	0.41	0.04	0.94	7.50	0.10
30	0.06	0.23	0.02	0.89	7.53	0.13
40	0.19	0.31	0.02	0.90	7.46	0.14
50	0.22	0.27	0.02	0.87	7.51	0.12
75	0.15	0.23	0.02	0.87	7.46	0.12
100	0.18	0.44	0.02	0.91	7.41	0.09
125	0.22	0.55	0.02	0.97	7.35	0.06
150	0.27	0.61	0.02	1.01	7.31	0.03
200	0.24	0.31	0.02	1.12	7.56	0.08
	April 2009					
0	0.34	0.12	0.04	1.53	7.68	0.06
5	0.32	0.10	0.03	1.11	7.68	0.06
10	0.26	0.09	0.03	1.17	7.66	0.05
20	0.24	0.14	0.04	1.37	7.63	0.10
35	0.21	0.13	0.03	1.56	7.66	0.21
65	0.22	0.45	0.03	1.72	7.46	0.09
75	0.38	0.52	0.05	1.87	7.34	0.02
100	0.44	0.80	0.04	1.74	7.42	0.09
150	0.43	0.79	0.05	2.22	7.56	0.17
200	0.59	1.34	0.07	2.64	7.10	0.25
	August 2009					
1	0.92	0.08	0.03	0.83	6.26	0.03
3	0.92	0.08	0.03	0.83	6.34	0.02
7	1.14	0.09	0.03	0.97	5.70	0.02
20	1.02	0.09	0.03	0.82	6.42	0.03
35	1.21	0.08	0.04	1.52	6.73	0.25
45	1.25	0.20	0.03	1.19	7.46	0.14
75	0.99	0.15	0.02	0.82	7.74	0.12

Depth	NH_4 (μM)	NO_3 (μM)	PO_4 (μM)	Si (μM)	Oxygen mg/L	Chl-a mg/m^3
90	1.20	0.16	0.03	0.96	7.60	0.12
150	0.91	0.15	0.03	0.84	7.23	0.03
200	1.04	0.59	0.05	1.43	7.00	0.02
	October 2009					
0	0.17	0.09	0.03	1.08	6.57	0.04
5	0.27	0.07	0.03	1.08	6.54	0.03
10	0.16	0.08	0.03	1.07	6.54	0.06
20	0.24	0.07	0.03	1.05	6.54	0.03
30	0.12	0.06	0.03	0.94	6.94	0.05
50	0.40	0.07	0.02	0.92	7.84	0.05
75	0.26	0.52	0.03	1.46	7.30	0.16
100	0.16	0.39	0.02	0.94	7.22	0.05
150	0.11	1.09	0.03	1.21	7.01	0.02
200	0.19	2.06	0.03	1.81	6.89	0.00

Table 3.4: Nutrient, oxygen and chlorophyll-a profile for the river discharge station

Depth	NH_4 (μM)	NO_3 (μM)	PO_4 (μM)	Si (μM)	DO (mg/L)	Chl-a (mg/m^3)
	January 2009					
2	0.10	0.24	0.04	0.94	7.49	0.08
4	0.12	0.19	0.04	0.92	7.53	-
8	0.04	0.16	0.04	0.92	7.52	0.14
13	0.16	0.20	0.06	0.99	7.52	-
18	0.47	0.18	0.04	0.93	7.53	0.16
27	0.61	0.21	0.06	0.97	7.53	-
29	0.67	0.22	0.07	0.98	7.55	0.24
	February 2009					
2	2.29	4.86	0.06	3.56	7.76	0.11
5	2.11	4.12	0.05	3.08	7.73	0.24
10	0.92	0.44	0.02	0.93	7.57	0.20
15	0.82	0.18	0.02	0.85	7.57	0.21

Depth	NH_4 (μM)	NO_3 (μM)	PO_4 (μM)	Si (μM)	Oxygen mg/L	Chl-a mg/m^3
20	0.73	0.12	0.02	0.81	7.59	0.19
30	0.99	0.27	0.03	0.93	7.62	0.22
	March 2009					
1.5	2.21	3.76	0.07	4.34	8.59	0.32
3	2.23	3.08	0.08	3.55	7.94	0.56
5	1.76	1.89	0.02	2.00	7.89	0.41
10	1.63	1.30	0.02	1.62	7.79	0.40
14	1.53	1.25	0.03	1.59	7.78	0.27
24	1.62	0.86	0.04	1.39	7.64	0.36
	April 2009					
0	0.22	0.45	0.08	1.07	7.95	0.80
5	0.17	0.24	0.05	0.61	8.12	0.65
10	0.06	0.22	0.04	0.60	7.99	0.35
15	0.13	0.24	0.04	0.65	8.25	0.41
25	0.33	0.52	0.06	1.09	7.42	0.93
	August 2009					
0	2.01	1.92	0.13	8.08	6.47	0.82
3	0.16	0.18	0.06	2.58	6.44	0.43
5	0.31	0.10	0.05	1.60	6.39	0.36
8	0.11	0.08	0.06	0.91	6.33	0.26
14	0.07	0.06	0.03	1.05	6.26	0.09
20	0.11	0.07	0.03	1.48	6.17	0.20
30	1.15	0.38	0.09	3.22	5.78	0.51
	October 2009					
0	1.10	0.86	0.05	5.33	7.14	0.99
3	1.22	0.80	0.05	4.97	7.11	0.84
5	1.05	0.60	0.04	4.56	7.10	0.83
10	0.85	0.19	0.02	2.45	6.51	0.11
15	0.90	0.17	0.02	1.89	6.54	0.07
20	0.84	0.16	0.02	1.88	6.51	0.08
25	0.66	0.16	0.03	1.91	6.49	0.11
30	0.93	0.22	0.03	1.95	6.54	0.14

Table 3.5: Mineralization and sedimentation rates of state variables

	Sedimentation Rate (m/d)		Mineralization Rate (1/d)
DetC	0.1	**DetC**	0.12
Diatoms-E	0.5	**DetN**	0.12
Diatoms-N	1.0	**DetP**	0.08
Diatoms-P	1.0	**DetSi**	0.08
Flagellates-E	0.0	**DOC**	0.04
Flagellates-N	0.5	**DON**	0.04
Flagellates-P	0.5	**DOP**	0.04
Dinoflagellates-E	0.0	**DOSi**	0.04
Dinoflagellates-N	0.0		
Dinoflagellates-P	0.0		
Bacteria-E	0.0		
Bacteria-N	0.0		
Bacteria-P	0.0		

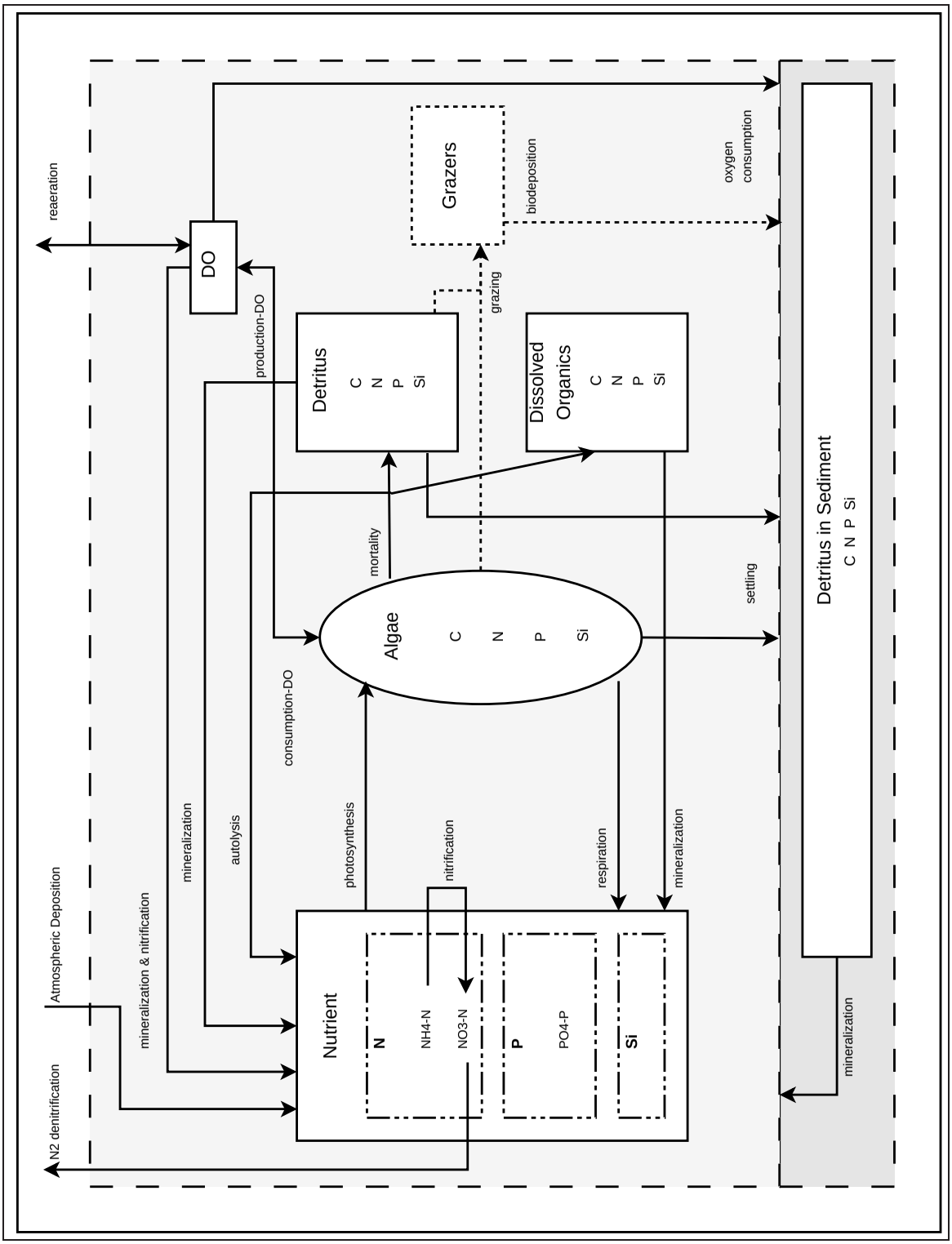

Figure 3.8: Ecosystem Model Flowchart

Table 3.6: Comparison of ecosystem parameters of Delft3D defaults (D), Marmara Case (M) and Cilician Case (C)

Ratio (g/g)	**N/C**			**P/C**			**Si/C**			**Chl-a/C**		
Case	**D**	**M**	**C**	**D**	**M**	**C**	**D**	**M**	**C**	**D**	**M**	**C**
Diatoms-E	0.255	0.255	0.255	0.0315	0.0315	0.0315	0.447	0.525	0.45	0.0533	0.04	0.04
Diatoms-N	0.07	0.141	0.141	0.012	0.021	0.021	0.283	0.525	0.45	0.01	0.025	0.025
Diatoms-P	0.105	0.2	0.2	0.0096	0.02	0.02	0.152	0.375	0.25	0.01	0.025	0.025
Flagellates-E	0.2	0.14	0.2	0.02	0.015	0.015	0.0	0.0	0.0	0.0228	0.0286	0.0286
Flagellates-N	0.078	0.2	0.14	0.0096	0.01125	0.0125	0.0	0.0	0.0	0.0067	0.0167	0.0167
Flagellates-P	0.113	0.113	0.113	0.0072	0.007	0.012	0.0	0.0	0.0	0.0067	0.0167	0.0167
Dinoflagellates-E	0.163	0.1625	0.1625	0.0168	0.01675	0.01675	0.0	0.0	0.0	0.0228	0.0286	0.0286
Dinoflagellates-N	0.064	0.115	0.115	0.0112	0.0175	0.0175	0.0	0.0	0.0	0.0067	0.0167	0.0167
Dinoflagellates-P	0.071	0.1275	0.1275	0.0096	0.015	0.015	0.0	0.0	0.0	0.0067	0.167	0.0167
Bacteria-E	0.22	0.22	0.22	0.025	0.025	0.025	0.002	0.002	0.002	0.033	0.033	0.033
Bacteria-N	0.113	0.113	0.113	0.015	0.015	0.015	0.002	0.002	0.002	0.02	0.02	0.02
Bacteria-P	0.17	0.17	0.17	0.015	0.015	0.013	0.002	0.002	0.002	0.02	0.02	0.02

Table 3.7: Growth (1/d), mortality (1/d) and respiration (1/d) rates at 0^{o}C and temperature dependencies with 1=linear and 2=exponetial dependencies

Type	Growth	Growth-T	Mortality	Mortality-T	Respiration	Respiration-T
Diatoms-E	0.095[1]	-1.75	0.15[2]	1.072	0.1[2]	1.066
Diatoms-N	0.09[1]	-2	0.16[2]	1.085	0.1[2]	1.066
Diatoms-P	0.09[1]	-2	0.16[2]	1.085	0.1[2]	1.066
Flagellates-E	0.073[1]	-1	0.15[2]	1.072	0.1[2]	1.066
Flagellates-N	0.07[1]	-1	0.16[2]	1.085	0.1[2]	1.066
Flagellates-P	0.07[1]	-1	0.16[2]	1.085	0.1[2]	1.066
Dinoflagellates-E	0.132[1]	5.5	0.15[2]	1.072	0.1[2]	1.066
Dinoflagellates-N	0.113[1]	4.75	0.16[2]	1.085	0.1[2]	1.066
Dinoflagellates-P	0.112[1]	4.75	0.16[2]	1.085	0.1[2]	1.066
Bacteria-E	0.28[2]	1.083	0.07[2]	1.08	0.025[2]	1.072
Bacteria-N	0.24[2]	1.095	0.09[2]	1.085	0.025[2]	1.072
Bacteria-P	0.24[2]	1.095	0.09[2]	1.085	0.025[2]	1.072

CHAPTER 4

RESULTS AND DISCUSSION

This chapter includes a comparison of the model results to the *in-situ* data. First, hydrodynamic simulations were compared to the corresponding *in-situ* CTD data. Data were compared along the two transects indicated in Figure 4.1 and as surface distributions. Some cruises during 2009 did not cover all of the 50 stations in Mersin Bay, so where data were not adequate to plot surface or transect distributions of physical characteristics, no comparison is presented. Following the hydrodynamic model results, ecosystem model setup, scenario and sensitivity analyses will be discussed in detail.

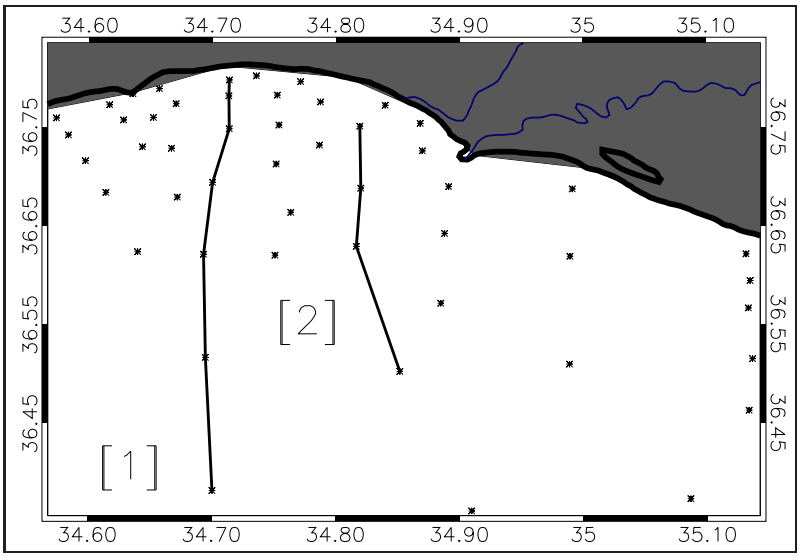

Figure 4.1: Location and name of CTD transects used to assess the reliability of model results

4.1 Results of Hydrodynamic Simulations

This section begins with a comparison of the reference simulation to the available observations and continues with a comparison of reference simulation to the scenario simulations. This section aims to provide an assesment of the hydrodynamic model and the sensitivity of results to changing fresh-water inputs. *In-situ* data were not available for the offshore waters of the Cilician Basin, and for

this reason, model results located outside of Mersin Bay were not included in the comparisons.

During the development stage of the hydrodynamics model, the initial and boundary conditions were set and the structure of the grid was defined. Because the Mersin Bay area was the main focus of this study, defining a larger domain that covered an extensive area compared to Mersin Bay (Figure 3.7) was not needed. Therefore first simulations were defined for a smaller domain that covered an area within the boundaries of Mersin Bay (Figure 4.2). This setup had certain advantages and disadvantages. The most important advantage was reduced computational time. Moreover, because the domain boundaries were closer to the coasts, wind profiles from local atmospheric stations could be considered. CTD data were available to set the initial conditions, eliminating the introduction of errors from an offline model that would have been used otherwise. The disadvantage was the open boundary setup of the domain. The grid structure defined the open boundaries too close to the area of interest, meaning model results were highly influenced by open boundary characteristics. Therefore, the boundaries had to be set away from Mersin Bay as much as possible. The best option was to locate the open boundaries adjacent to Cyprus, to form a closed basin.

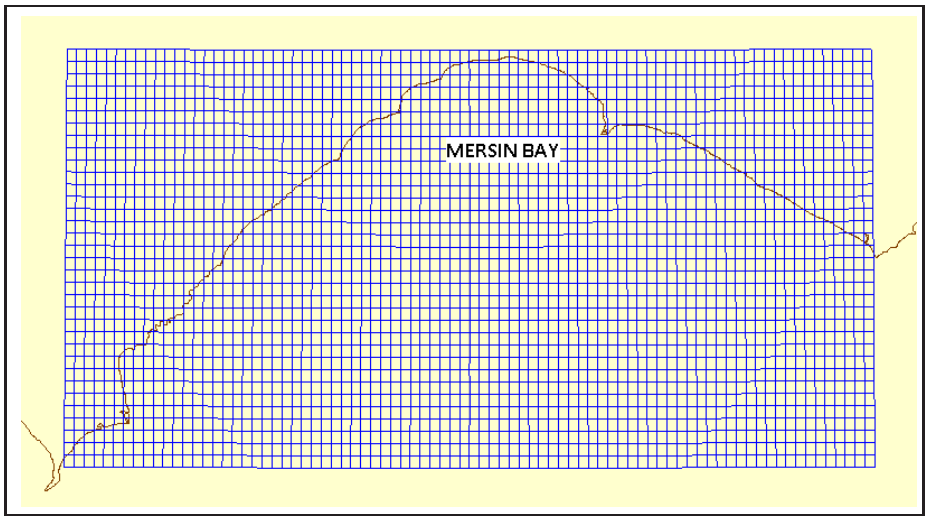

Figure 4.2: Structure of a smaller domain for hydrodynamic model simulations

To capture the ecosystem dynamics of Mersin Bay, uniform grid size had to be increased, but the vertical resolution was kept as fine as possible to capture mixing and stratification. The domain included topography as deep as 1500 m and continental shelf (Figure 1.1). The resulting vertical grid setup created a very fine vertical resolution even at 200 m over the shelf area. The problem at this point emerged in computation of horizontal spreading of freshwater input in coastal areas. This phenomena will be discussed in Section 4.1.2.

Around Cyprus, near the open boundaries, CTD data were not available, but it was necessary to define temperature, salinity, velocity and free surface fields to compute the governing flow equations. Therefore CYCOFOS High Resolution Levantine Forecast data was used at the open boundaries and as initial fields. At every grid point at the open boundaries, daily fields were taken from CYCOFOS. At the open boundaries velocity fields were multiplied by 0.1 to give the Cilician model the flexibility to define its own internal patterns with reference to T,S and wind forces. Validation of this approach was done with comparisons of CTD data at the bay. Also this approach eliminated the instabilities of offline nesting at the boundaries.

4.1.1 CTD Measurements

As discussed in Chapter-1, due to excess amount of evaporation over precipitation, the Mediterranean Sea exhibits high saline properties in general, with increasing salinity towards east. At certain times of the year, salinities above 39.5 ppt can be observed in Mersin Bay. Due to its geographical setting in northeastern corner of Mediterranean, the Cilician Basin shows high salinity characteristics. Although the Cilician Basin has high salinity characteristics, it receives high amounts of freshwater from the coasts in the form of river input. River fluxes are important freshwater input, especially in Mersin Bay due to its close location to high mountains, where the source of freshwater is the precipitation over land. Therefore, throughout the year 2009, CTD casts exhibited low salinity waters near the coastal areas of Mersin Bay, especially in winter-transition months (Figures 4.3d and f). Besides its implications on the physical structure of the bay, river input is also important for the biology of the environment due to the discharge of nutrients, hence primary production. Although, the coasts had varying salinity structure in the year 2009, the same situation was not valid for the offshore waters of the shelf area. As can be seen in CTD casts (Figures 4.3, 4.4, 4.5 and 4.6), both surface and profile plots show salinities range between 38.5-39.75 and 39.5 in average at the surface, with the exception of April 2009 (Figure 4.4b). Also in agreement with the surface distributions, in summer month transects, layer of high saline waters at the surface can be observed (Figures 4.6d and f).

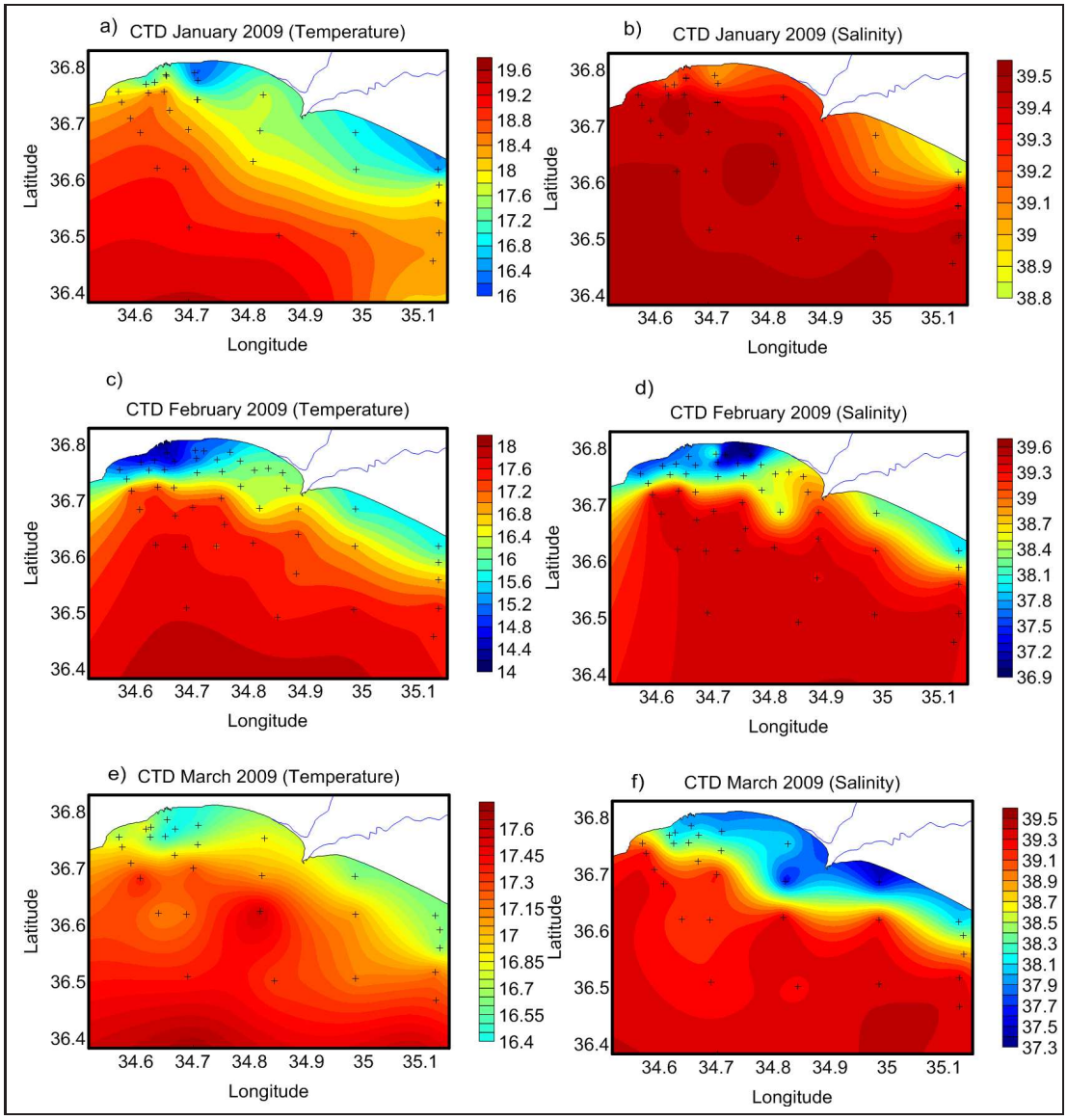

Figure 4.3: Cruise surface measurements for 2009, a)January temperature b)January salinity c)February temperature d)February salinity e)March temperature f)March salinity

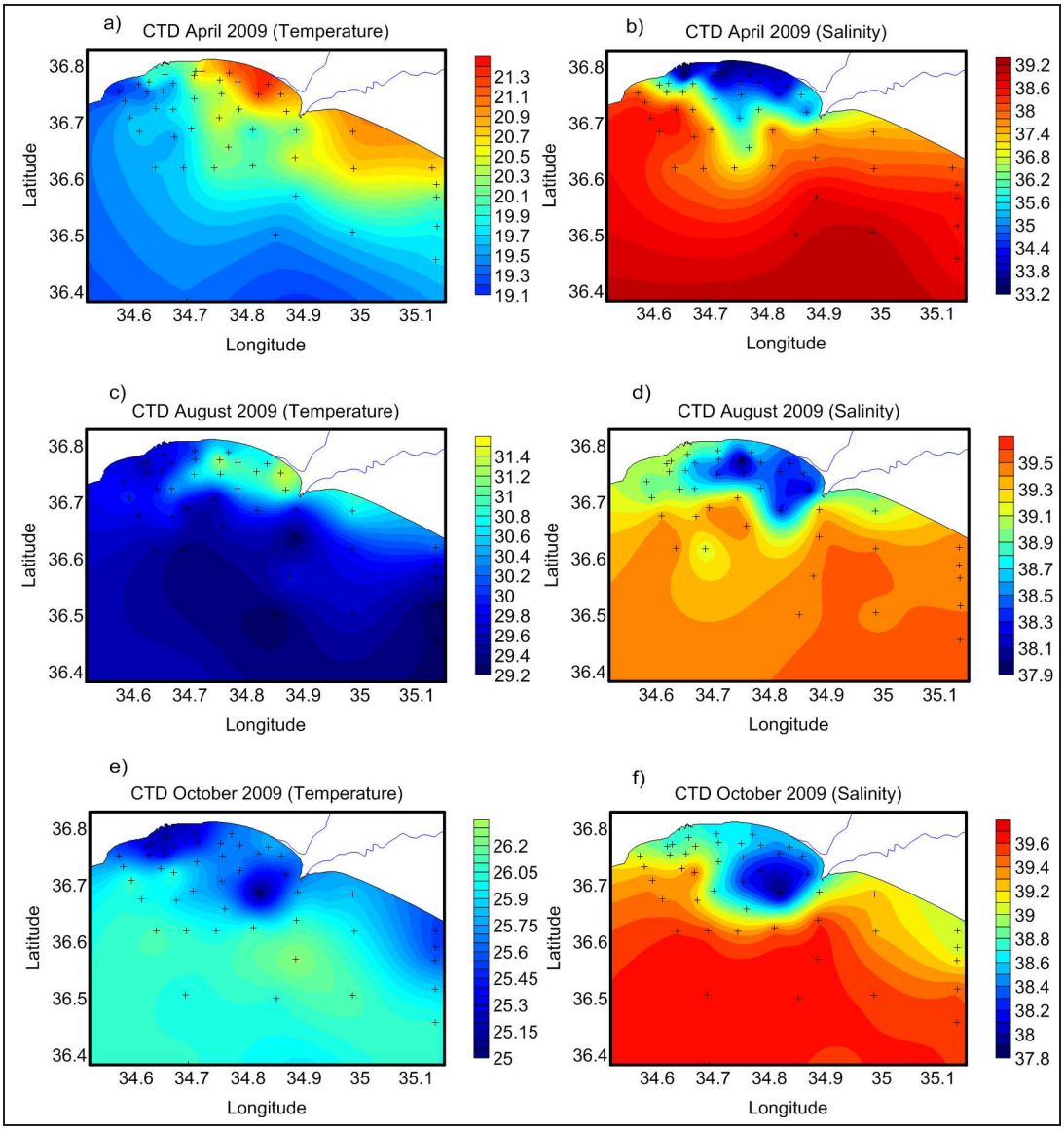

Figure 4.4: Cruise surface measurements for 2009, a)April temperature b)April salinity c)August temperature d)August salinity e)October temperature f)October salinity

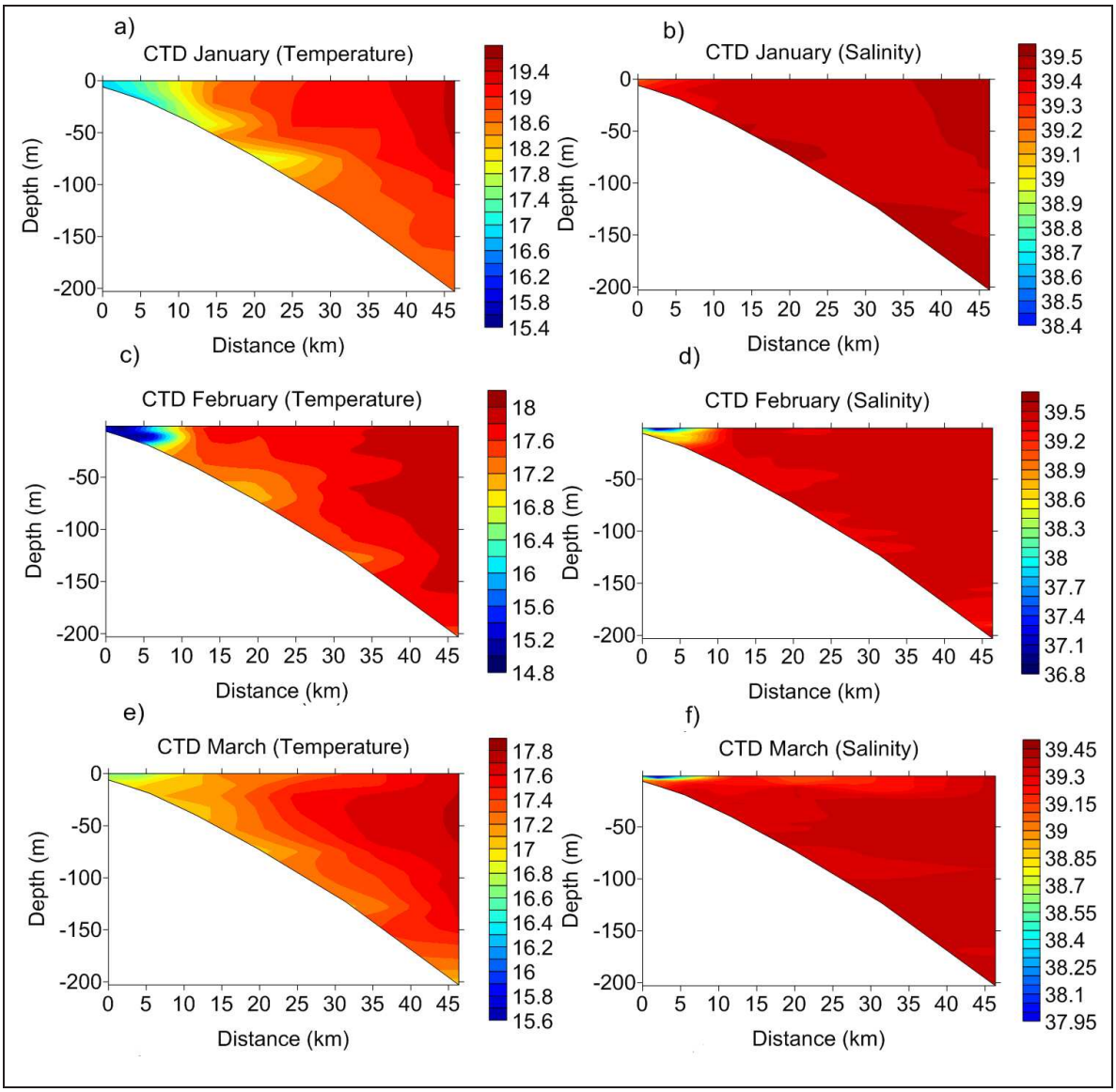

Figure 4.5: Cruise Transect-1 measurements for 2009, a)January temperature b)January salinity c)February temperature d)February salinity e)March temperature f)March salinity

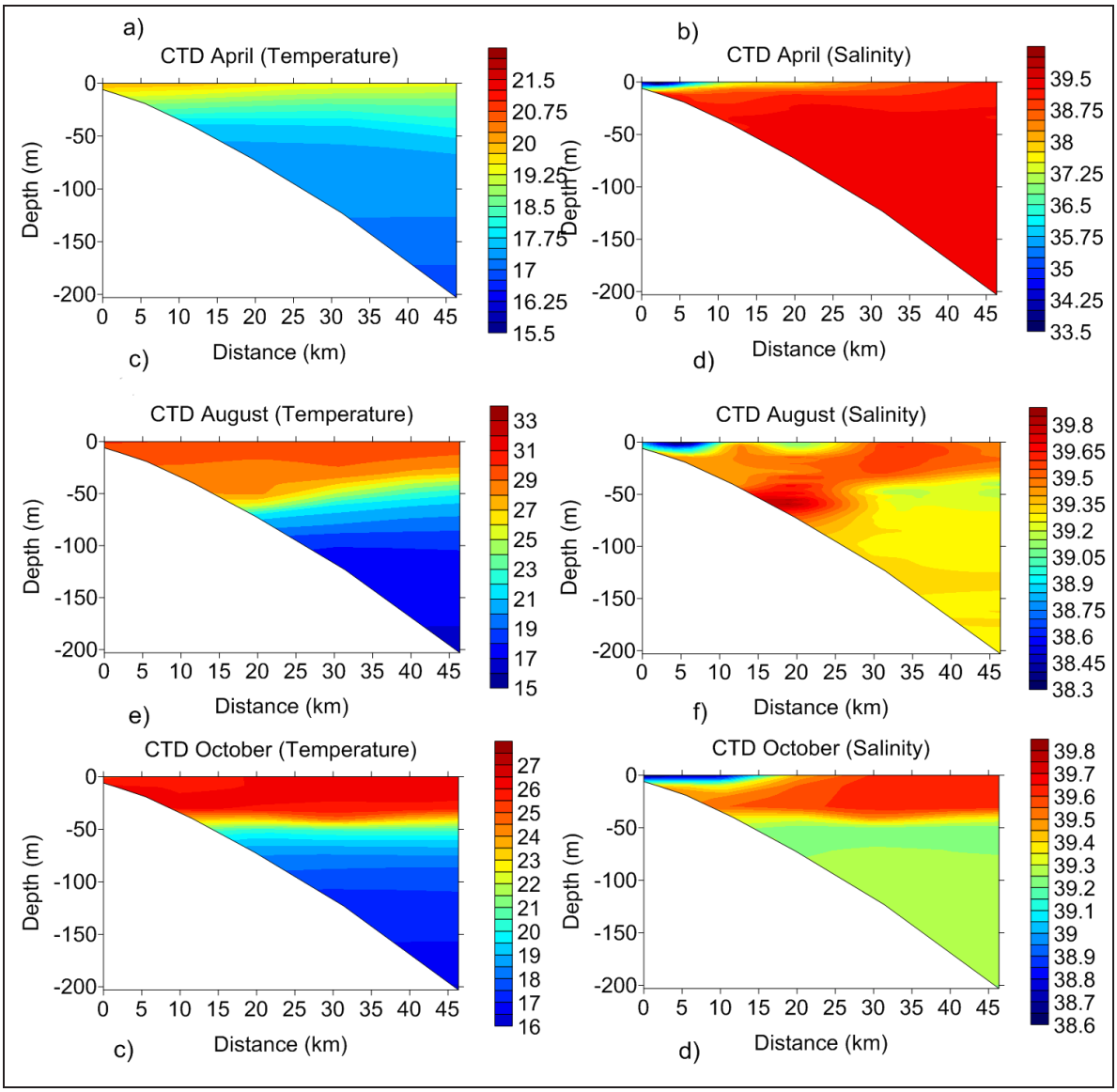

Figure 4.6: Cruise Transect-2 measurements for 2009, a)April temperature b)April salinity c)August temperature d)August salinity e)October temperature f)October salinity

Temperature distributions exhibit similar patterns as salinity. The effect of freshwater input as river discharges, decreased the temperature of the inner Mersin Bay, especially in winter and spring months. This change for the winter and spring was due to the increasing flux of freshwater discharge and the cold temperatures of snow-melt waters. In winter months, especially in February and March, the influence of air-sea heat interaction can be observed with temperatures as low as 17^oC in offshore waters (Figures 4.3c and e). In summer, the surface layers were heated up to as high as 30^oC (Figure 4.4c). The importance of temperature changes in the domain is that, such changes cause mixing and stratification of the water column. In winter months, the effect of mixing can be observed in Figures 4.5a, c and e, where similar temperatures were observed from surface down to 150 m depth. The same character can also be seen in the salinity profiles. On the contrary, in summer months, water masses with high temperatures were found within a narrow surface layers. This was due to the cessation of mixing in the water column due to the stable density structure. In summer months (Figures 4.6c and e) because density was mostly driven by temperature, less dense warmer waters became trapped at the surface and gradually their temperature increased further, which resulted in such stratified profiles.

4.1.2 Scenarios-1, 2, and 3

Omitting the numerical computation restrictions of river plumes and turbulence, CTD casts only showed a single location and time in a year, therefore model-data misfit was expected throughout the simulations. Spatial distribution patterns of low salinity waters were the main points that was considered during model data comparison. Also, the mixed layer structure was given consideration. These were important because nutrient input from rivers, or pumping of nutrients from bottom layers was directly influenced by such physical dynamics. Influences of these results, therefore, were traced in primary production processes.

As described in Chapter-3, DSI freshwater flux data was used in Scenario-1, whereas 1/3 of the original flux was used only for the year 2009 in Scenario-2 and in Scenario-3 the year 2008 flux data was used as well. The influence of river discharge on the bay can be easily distinguished by modeled salinity and temperature results throughout the year. In Figures 4.7 and 4.8, river discharge penetration can be traced in the bay both at the surface and bottom layers. Salinity ranges do not compare well with CTD measurements but water flux introduced at a single grid cell at the coast may not reflect the observed dynamics. It was observed in CTD measurements that freshwater influence can be traced down to the latitude 36.7, but the configuration of water flux in Scenario-1 extends this low salinity barrier down to latitude 36.6 (Figure 4.7).

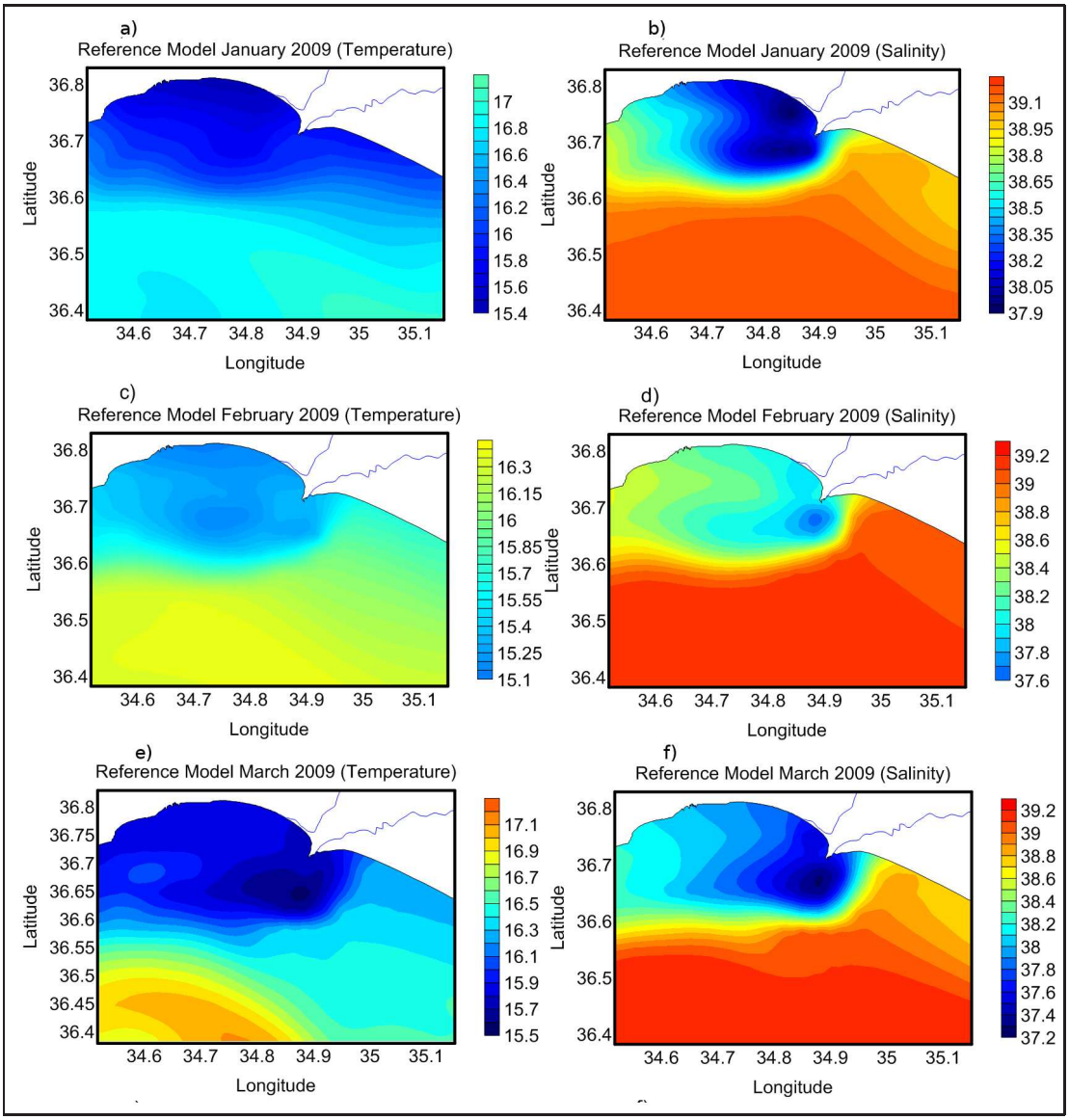

Figure 4.7: Reference model (Scenario-1) surface distributions for 2009, a)January temperature b)January salinity c)February temperature d)February salinity e)March temperature f)March salinity

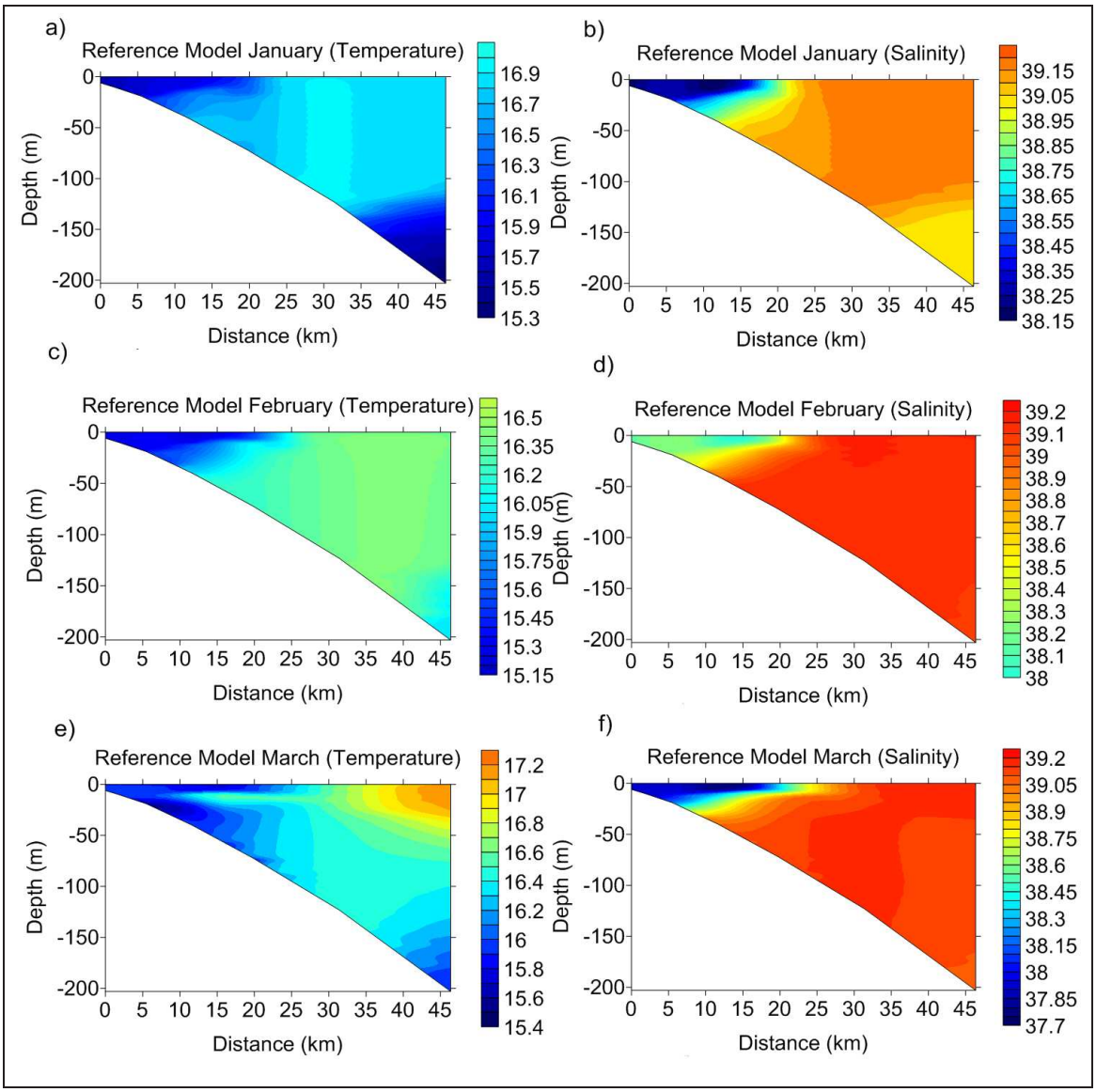

Figure 4.8: Reference model (Scenario-1) Transect-1 distributions for 2009, a)January temperature b)January salinity c)February temperature d)February salinity e)March temperature f)March salinity

Rather than expecting matching salinity ranges, freshwater intrusion patterns into the bay should be investigated as a first step, because such a case implies that nutrients deposited from rivers will be carried too far into the bay. That will in turn influence the ecosystem dynamics. Therefore, tuning of freshwater input was required. There were several possible reasons for such a result. In Chapter-3, it was mentioned that long term averages of nearly 50 years of river discharges were set as point sources. Year 2009 alone may not fit well with the climatological averages. By using the averages, the freshwater flux may be overestimated. Another scenario was that, considering year 2009 discharge fits well with the average data, the grid size may be too coarse for the model to define its spreading. Either of the two, model setups of Scenario-1 had to be tuned. Not only the spreading of nutrients is important for the ecosystem, but the loads would also be influenced. As the flux increases or decreases, loads of nutrients will be linearly affected (Load[g/s]=Flux[m^3/s]xConcentration[g/m^3]). For this reason, the flux from Seyhan River was decreased to its 1/3 value in Scenarios-2 and 3.

Scenario-2 and Scenario-3 had the same setup but the initial conditions for 2009 were different. In Scenario-2, year 2008 data with original river flux values were kept, and flux for year 2009 was divided by 3. In Scenario-3, both of the years 2008 and 2009 river fluxes were divided by 3. Extension of river influence in the bay decreased as expected in these scenarios. Freshwater intruded less offshore and the decrease in salinity were observed more at the coastal areas, which was the case similar to the CTD observations. In Figures 4.9 and 4.10, it is clearly seen that the freshwater was trapped more towards northeast of the bay. In the Reference Scenario setup, the western domain of the bay was also influenced by the rivers whereas in reality, the western part should show more offshore characteristics (Figures 4.3b and f).

Temperature is influenced by several factors such as radiation and air-sea interactions. Model equations describing the heat balance have been discussed in Chapter-2 of this study. Therefore, besides boundary conditions, and freshwater input, temperature is a function of heat gain and loss across the air-sea interface. This creates a sinusoidal shaped time-series profile of temperature more confined at the surface. As the Mediterranean region is a mid-latitude region, water temperature varies significantly throughout the year. CTD casts showed surface temperature range of 17.8-30 ^oC at the offshore stations (Figures 4.3e and 4.4c). The river discharge area was more influenced by cold water input from land. Due to water heat capacity, heat was absorbed mostly at the surface. Below a certain depth, variability in temperature was highly reduced. This can be observed in deep transect plots. Even in August, below 100 m, temperature was 15-17 ^oC (Figure 4.6c). Thermocline, sharp decrease of temperature, was observed in summer months around 50-60 m depth. This behavior had

implications for ecosystem dynamics and will be discussed in the following sections, for that reason it was crucial to capture this behavior in the model simulations.

When investigating the model results of temperature, in Scenario-1 and 3, the winter months had lower surface temperatures compared to data. CTD casts showed surface temperatures offshore in January of 18-19.5 ^{o}C (Figures 4.3a 4.5a) but two of the simulations showed temperature range between 16.5 and 17.2 ^{o}C (Figures 4.7a, 4.8a, 4.9a and 4.10a). Model results were two degrees less than observations on average. Similar remarks can also be made for results of months February and March. To better represent the temperatures, further tuning of heat balance parameters is required, which was done in Scenarios 4 and 5.

4.1.3 Scenarios 4 and 5

It was discussed that surface temperature results for January were on average 2 degrees less than those observed. The reason for this, in January, was because of initial conditions for simulation of year 2009. Initial conditions for 2009 can not be easily modified because they were defined from results of a previous simulation for the year 2008. Therefore the constants stanton and dalton numbers for sensible and latent heat fluxes were modified. In winter months, as stated, the model lost excess heat in Simulations-1,2,3 so that initial conditions derived from the 2008 spin-up had unrealistically low temperatures (Figure 4.11). The original model run and Scenario-3 with constants 0.0013, had distinctly lower temperatures for December compared to Scenarios 4,5 and CYCOFOS results for 2008. Although high temperature values were reached in Summer 2008, the model lost excess heat during the following months. Therefore modifications to these numbers were required. This phenomena requires detailed sensitivity analysis but due to computational time restrictions, it was only possible to conduct two additional simulations with constants Dalton = Stanton = $0.0013^{+}_{-}0.0002$.

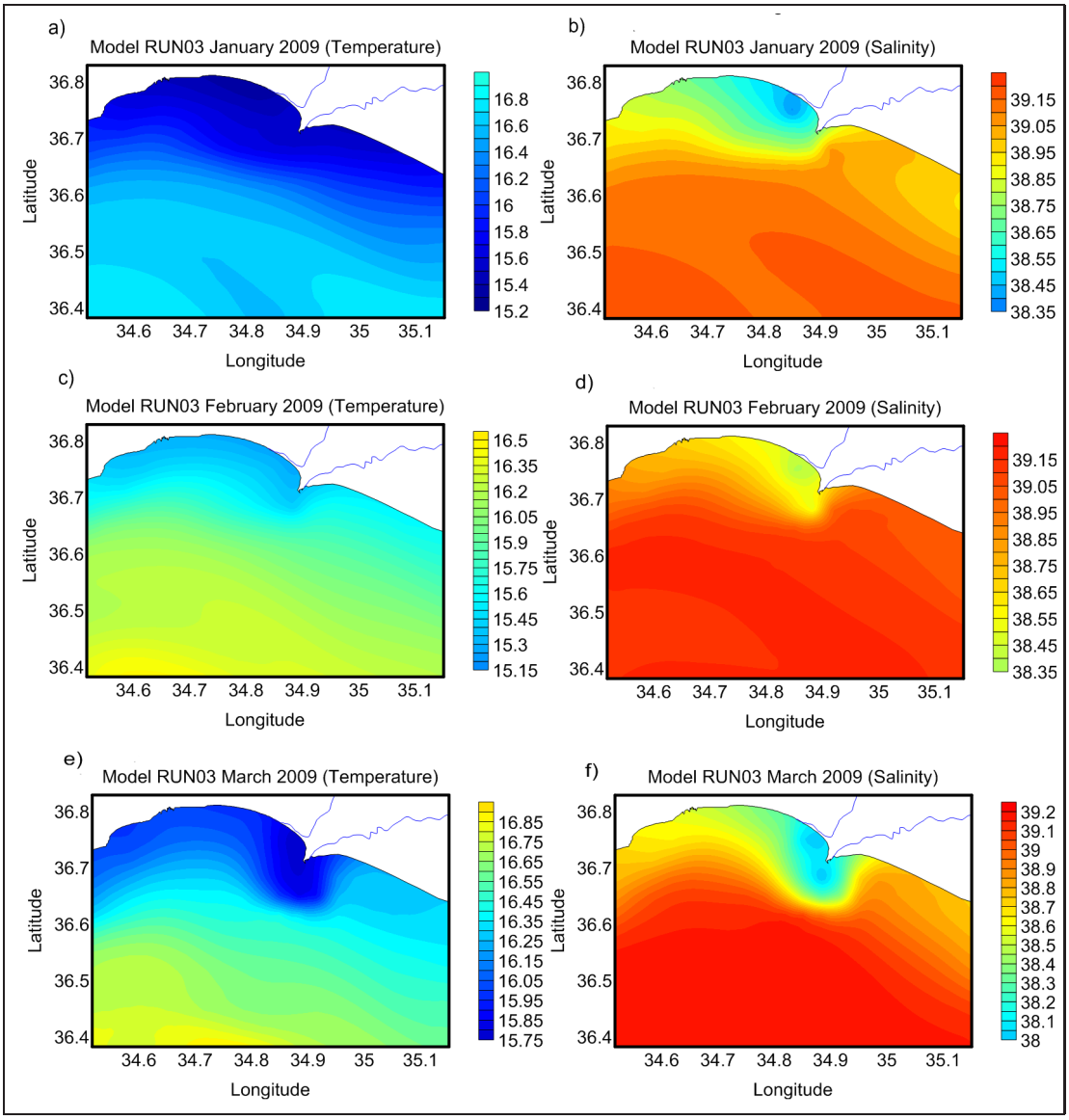

Figure 4.9: Scenario-3 surface distributions for 2009, a)January temperature b)January salinity c)February temperature d)February salinity e)March temperature f)March salinity

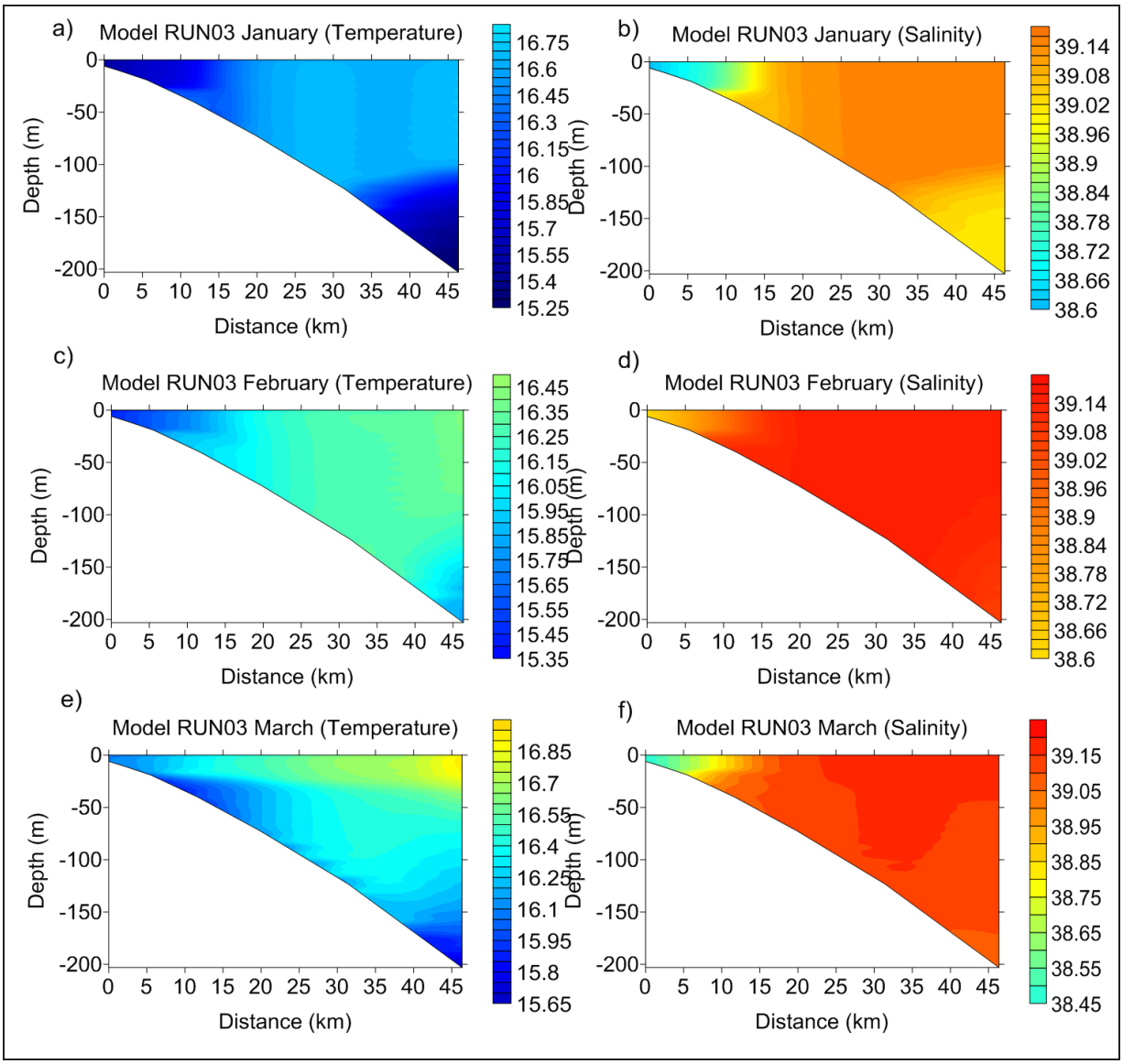

Figure 4.10: Scenario-3 Transect-1 distributions for 2009, a)January temperature b)January salinity c)February temperature d)February salinity e)March temperature f)March salinity

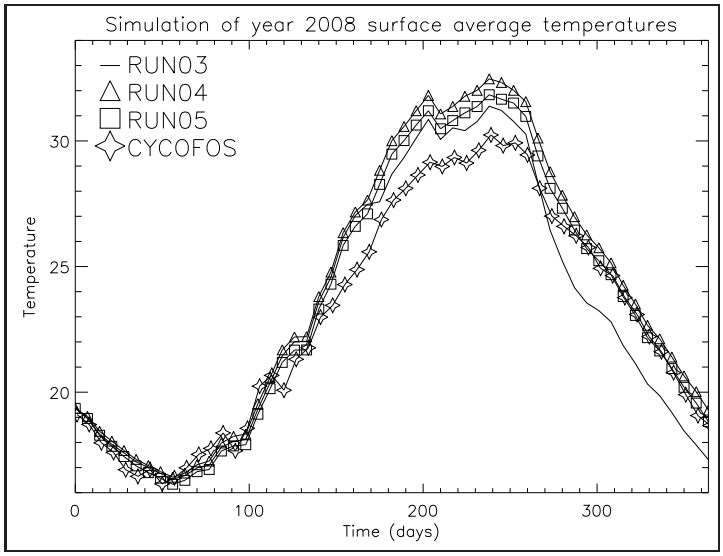

Figure 4.11: Comparison of averaged surface temperatures of Scenario-3, Scenario-4, Scenario-5 and CYCOFOS simulations for year 2008

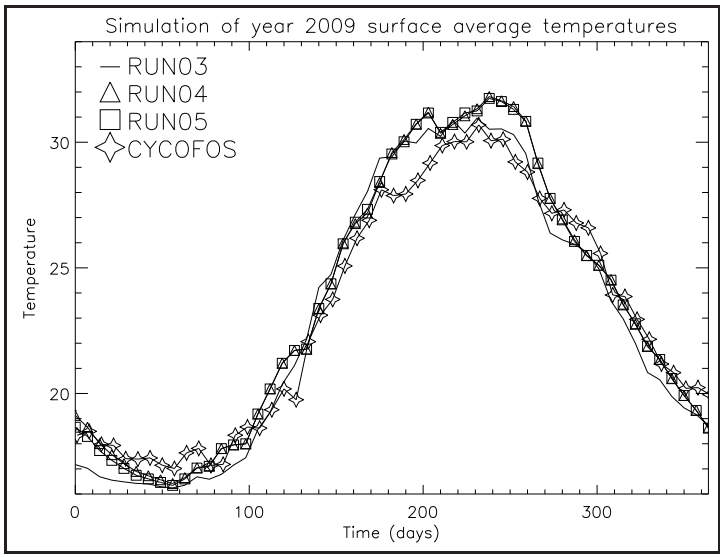

Figure 4.12: Comparison of averaged surface temperatures of RUN03, RUN04, RUN05 and CYCOFOS simulations for year 2009

Better results were obtained in Scenarios-4 and 5 compared to Scenario-3, as temperature results showed increased values (Figure 4.13). Temperature as high as 18.9 ^{o} can be observed at offshore in Scenario-5. This increasing trend can also be observed for deeper layers of the water column. However, further tuning of these constants should be made, because as time passed, in March (Figure 4.14), the domain again lost more heat than observed values. The highest temperature difference in January between CTD measurements and model results of Scenario-5 at the surface was 0.6 ^{o}C, also in March the difference is similar. This implies that water lost less heat in winter months compared to Scenarios-1,2,3. Low temperature initial conditions for 2009 can be seen in Figure 4.12. Although such tuning has been applied for scenarios, in February the model still lost more heat compared to

CYCOFOS data and gained more heat in summer. To fix this problem, as stated more tuning should be applied.

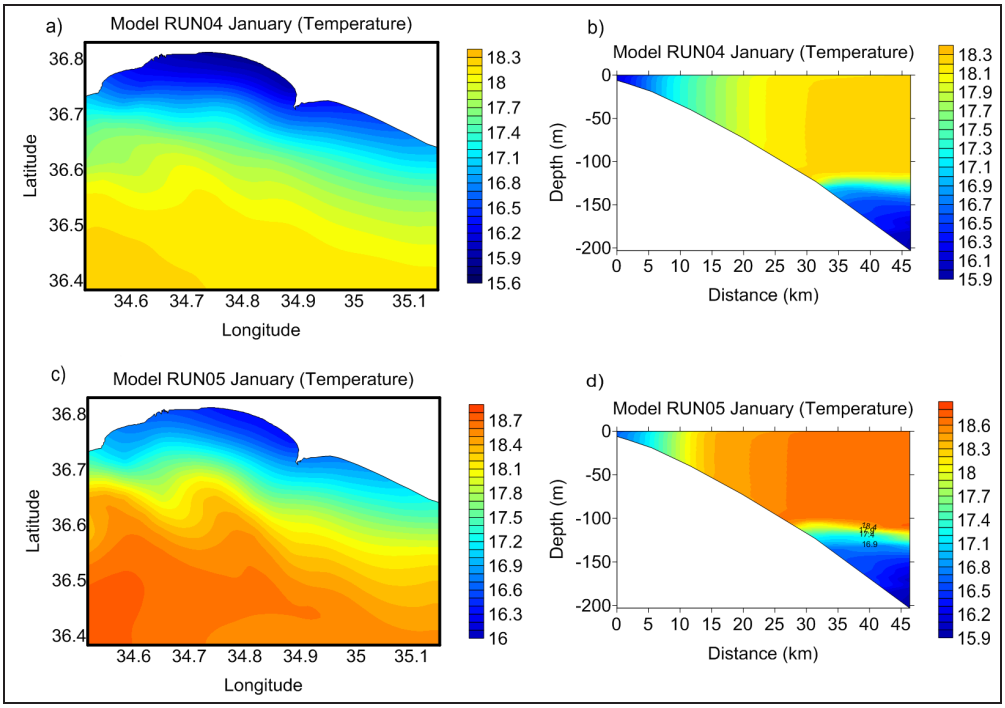

Figure 4.13: Model results of temperature distribution for January 2009 a)Scenario-4 surface b)Scenario-4 Transect-1 c)Scenario-5 surface d)Scenario-5 Transect-1

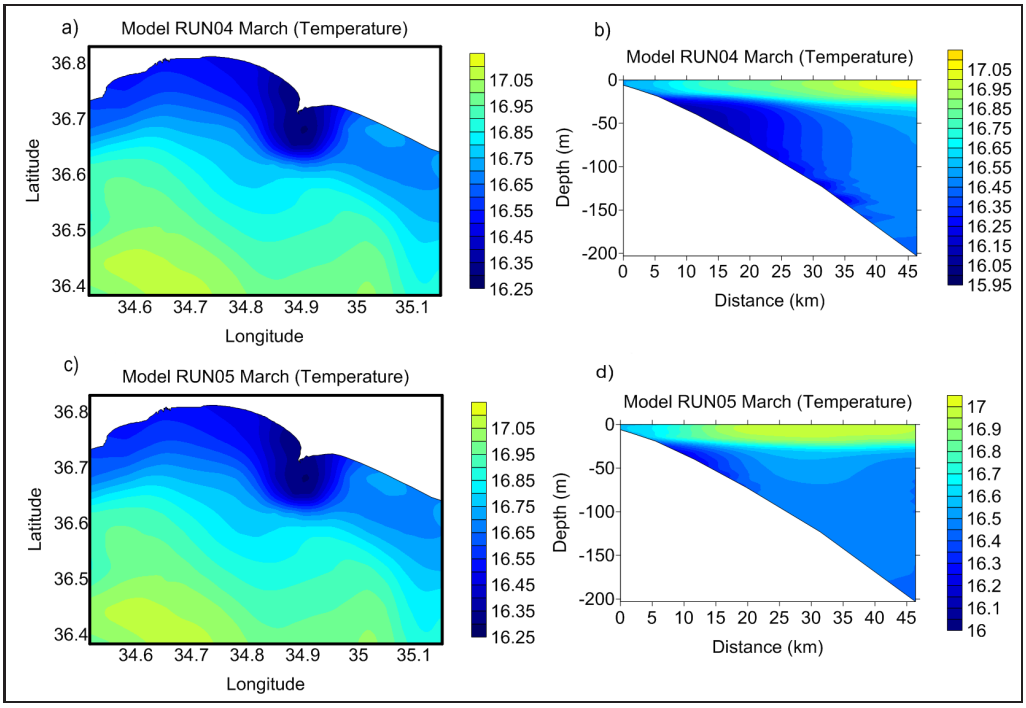

Figure 4.14: Model results of temperature distribution for March 2009 a)Scenario-4 surface b)Scenario-4 Transect-1 c)Scenario-5 surface d)Scenario-5 Transect-1

The offline coupling method was applied to Scenario-5 circulation results, because realistic circulation patterns with an order of magnitude velocity fields (0.1-0.2 m/s on average) including realistic temperature and salinity distributions were simulated by this setup. The general Cilician Basin circulation patterns were described in Chapter-1. The dominant flow is from the east to west direction and is called the Asia Minor Current. Besides this main current, there are small eddies along the coasts of the Cilician Basin, which interact with the offshore waters and freshwater inputs in form of river discharges. In this study, since the main focus was to investigate the primary production in Mersin Bay, coastal area circulation play an important role in the study.

CTD temperature and salinity distributions, as well as model results, showed that the physical characteristics of the bay create two distinct environments. Especially in winter, this distinction was significant. Coastal waters were less saline and colder compared to the offshore waters, where offshore waters had similar characteristics to the Cilician Basin waters outside the bay. This implies that, the coastal areas of Mersin Bay was highly influenced by river discharges and were trapped at the coast by the offshore circulation, and had minor interaction with the offshore waters. These can be seen in Figures (4.15, 4.16, 4.17, 4.18 and 4.19). The offshore waters throughout the year show different circulation patterns compared to coastal areas. The residence time of the domain was calculated to be 1.6 years, which means the domain water masses' recycling rate was fast and constantly new freely available nutrients entered the domain through the boundaries. This circulation character of the bay is very important in defining its ecosystem dynamics and will be discussed in Section 4.2

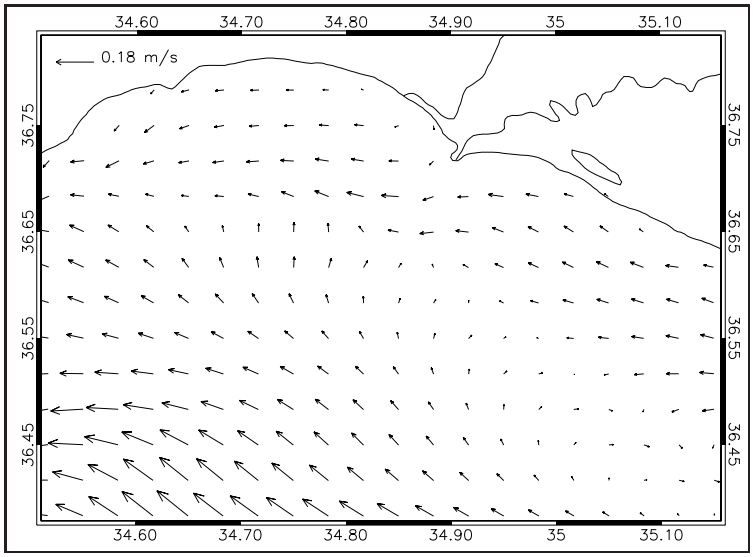

Figure 4.15: Surface horizontal velocity fields of RUN05 for 20^{th} day of 2009

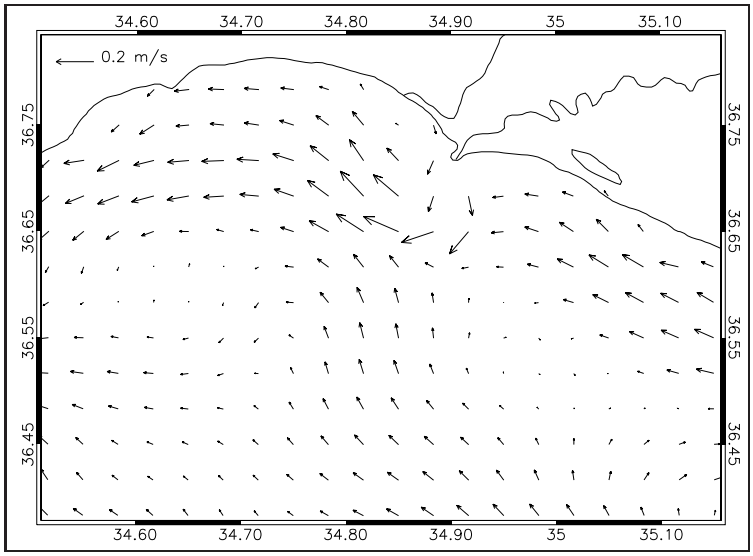

Figure 4.16: Surface horizontal velocity fields of RUN05 for 60th day of 2009

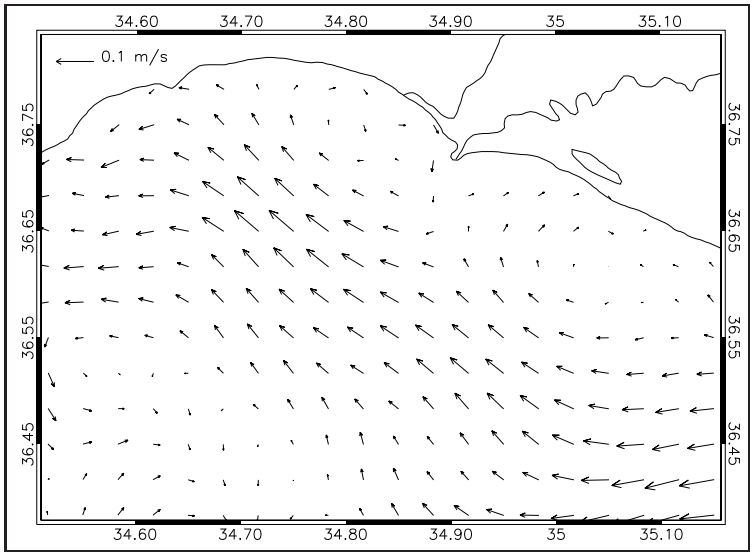

Figure 4.17: Surface horizontal velocity fields of RUN05 for 150th day of 2009

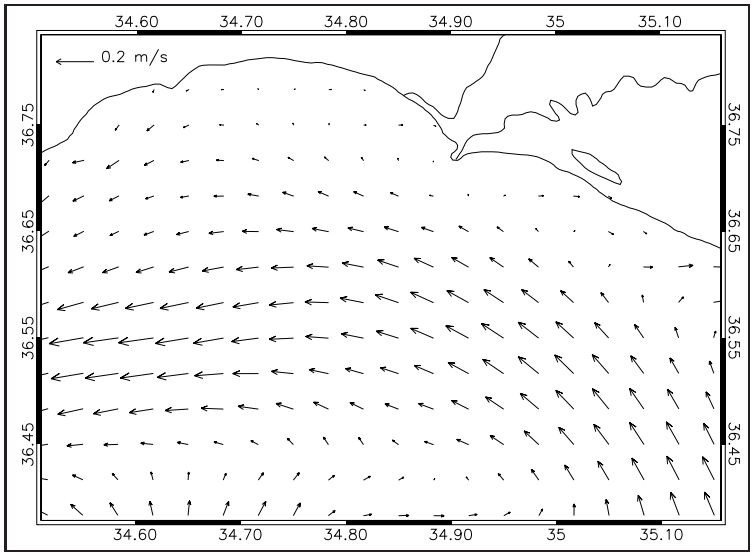

Figure 4.18: Surface horizontal velocity fields of RUN05 for 225th day of 2009

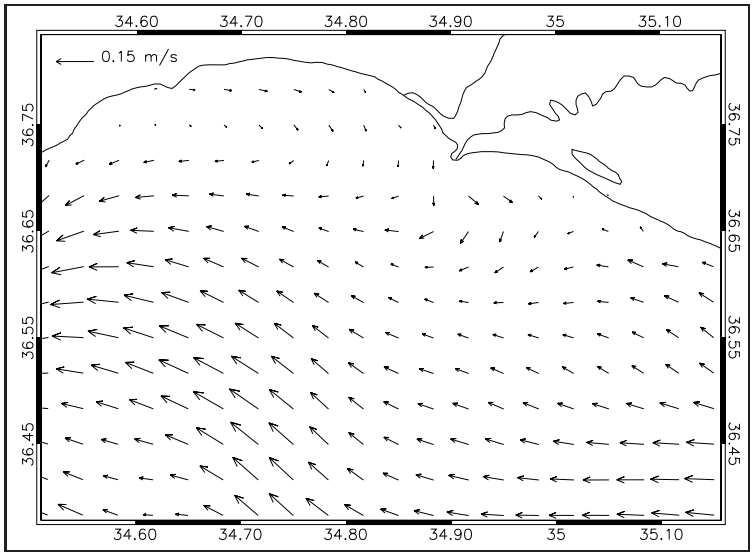

Figure 4.19: Surface horizontal velocity fields of RUN05 for 275th day of 2009

4.2 Ecosystem Simulation Results

A reference ecosystem model was set that provided the first comparisons with the available *in-situ* data. To eliminate the unrealistic effects of initial conditions, the reference model was run for 3 years until a steady state was reached. In the scenario setup, it was mentioned that constant values were given as initial conditions, instead the model was run for a year, and its final time step solution was used as initial conditions.

The aim of the reference simulation was to acquire comparable results that follow the seasonality of the *in-situ* data. A reference simulation was done before sensitivity analyses to tune the ecosystem parameters for the ultra-oligotrophic Mediterranean Sea case study as explained in detail in Chapter-3. The following results and sensitivity analyses were investigated with reference to these analyses. Their parameterization can be seen in Tables 3.5, 3.6 and 3.7. *In-situ* data was compared with model results at two locations of the bay, in the river discharge area and at an offshore station (Figure 4.20). These stations were selected for comparison due to the availability of most extensive chemistry and biology data (Tables 3.3 and 3.4).

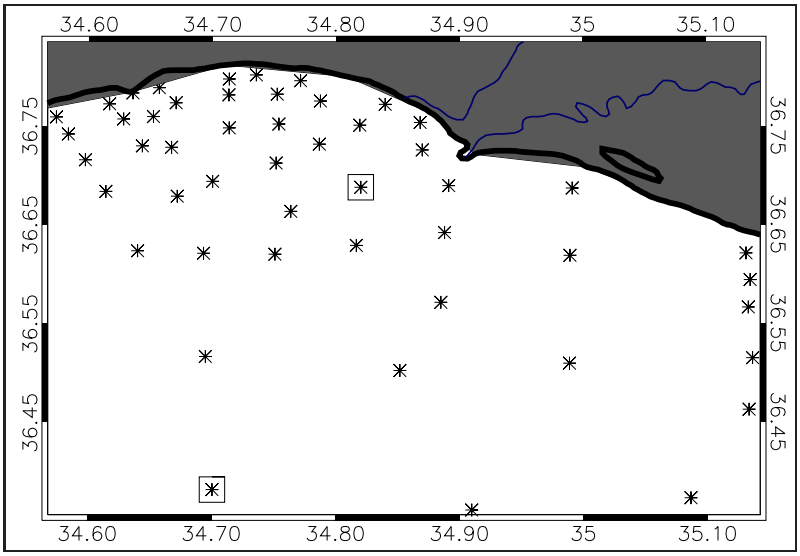

Figure 4.20: Locations of stations used for model results and *in-situ* measurement comparisons

Comparison of chlorophyll-a and primary production rates of offshore and river discharge stations (Figures 4.21 and 4.22) show that due to discharge, the river area was more productive (4 times) throughout the year, and algae blooms can be clearly seen in the spring season. When the model results and data were compared, figures show that model results slightly overestimated observations in both stations. Modeled chlorophyll-a results were higher compared to data, especially in winter months. This discrepancy may stem from model hydrodynamics as unrealistic mixing results in excess nutrient availability that was in turn was available for production. Alternatively this could be the result of the numerical solver of the model. As was described in Chapter-2, the Delft3D-ECO model was developed for estuarine and coastal environments, so the model at each time step maximizes the production. Because in winter months more nutrients were available, the model maximized the production (Figure 4.21b). This brings into question the need to adapt the ecosystem model which will be further analyzed as future work.

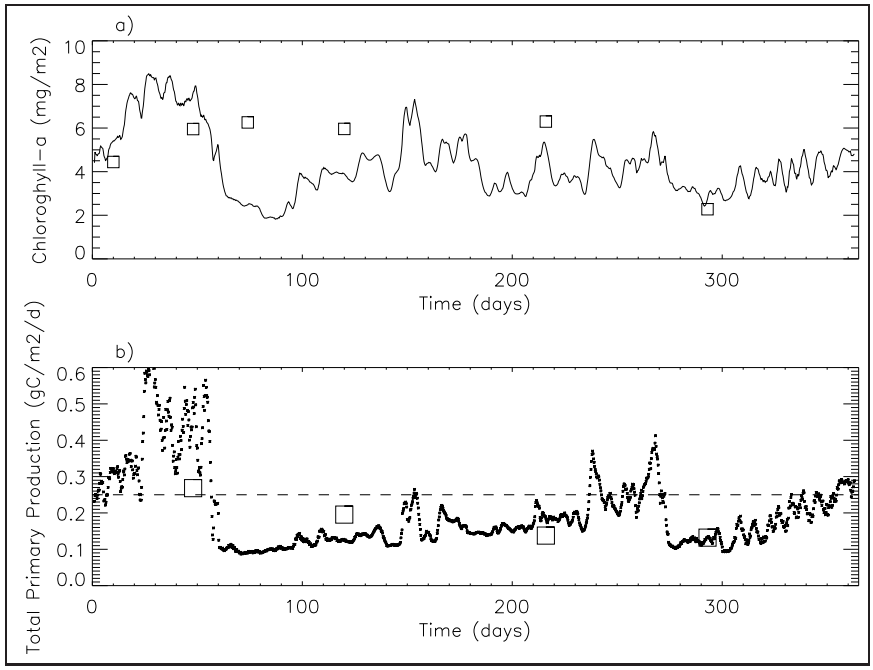

Figure 4.21: Depth integrated time series of a) chlorophyll-a concentration and b) primary production rates at the offshore station for the reference simulation. Boxes indicate observed *in-situ* values.

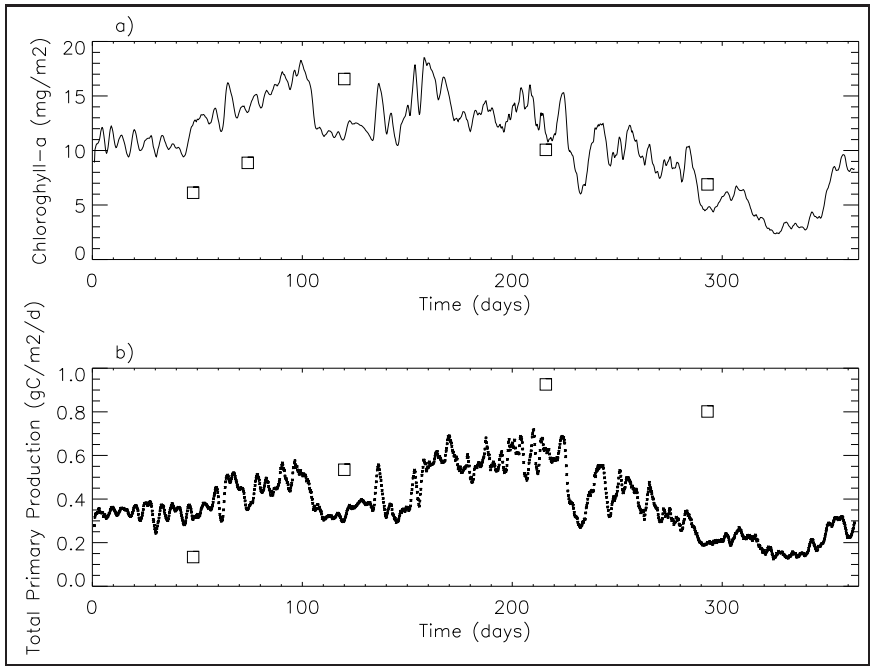

Figure 4.22: Depth integrated time series of a) chlorophyll-a concentration and b) primary production rate at the river discharge station from the reference simulation. Boxes indicate observed *in-situ* values.

For the reference simulation, to force the diatoms to dominate in winter and spring, their growth rates were increased accordingly. It can be easily observed in Figures 4.23 and 4.24) that throughout the year, among the phytoplankton (diatoms, flagellates and dinoflagellates), diatoms were the dominant large phytoplankton both at the onshore and offshore locations. Especially at the coast, diatom blooms followed winter and spring months. Total phytoplankton biomass increased in winter and spring months, whereas small phytoplankton and bacteria dominated in summer. To understand what drove this process and why large species dominated during winter and spring and why small species dominate in summer, growth rates and resource dependencies of algal types should be examined.

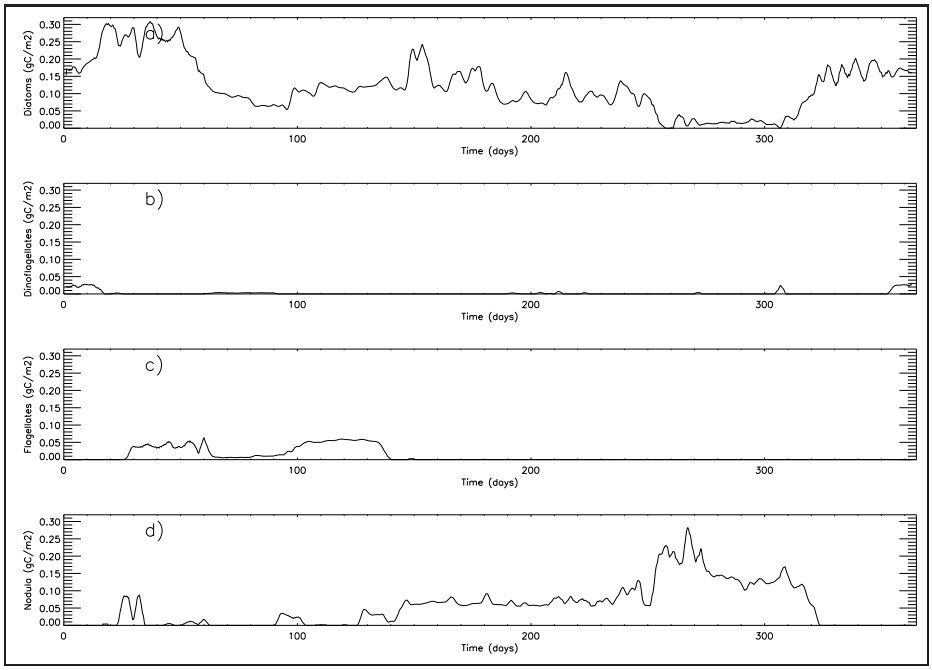

Figure 4.23: Depth integrated time series of a) Diatoms, b) Dinoflagellates, c) Flagellates and d) Bacteria concentration at the offshore station from reference simulation

The Delft3D-ECO (BLOOM) model defines two types of resources, energy (light) and nutrients. Limiting resources causes shifts in the dominance of algal types within different seasons (Figures 4.23 and 4.24). To understand phytoplankton and bacteria growth limitation or factors that favor the growth of a certain specie, results of the Reference Scenario were investigated in detail. The model results showed that the most dominant algae types were the types adapted for phosphorus limited environments. This showed that phosphate availability in general was the main limiting factor for phytoplankton growth in the model domain. When assigned carbon growth rates of P-type species were observed, diatoms formed the most efficient types of algae in cold, and bacteria formed the most efficient in warm water temperatures. In Figure 4.28, growth rates of diatoms and bacteria match each other at 26^{o}C. This indicated that, at temperatures below 26^{o}C, diatoms, and at temper-

atures above 26^{o}C bacteria, would have an advantage. However, during certain periods of the year when temperatures were below 26^{o}C, bacteria can dominate the system (Figure 4.25). This implies that there were factors that regulated the growth rates of bacteria other than the temperature.

The dependency of growth on nitrogen showed that diatoms relied more on nitrogen when algae nutrients dependencies were considered (Figure 4.29). Moreover, diatoms, for all temperatures within the range 15-32^{o}C are more phosphate dependent (Figure 4.30). This explains why bacteria dominated the system below certain temperature degrees. Especially near the surface in summer months, nutrients were depleted and algae types that were better adapted to low nutrient environments were favored. This shows in surface layers, when due to high growth rates and lower dependency on phosphorus, bacteria dominated the system. The effect of temperature should not be omitted in this case but, as water cooled down to temperatures of 24-26^{o}C, nutrient restrictions became more important for selection criterion. That is why the dominance of bacteria followed the mixed layer depth (Figure 4.25). As water started to mix due to cooling, more nutrients were pumped towards the surface, and because at colder temperatures diatoms had greater growth rates than bacteria, diatoms started to dominate the system. Similar characteristics exist for dinoflagellates and flagellates. At 20^{o}C, dinoflagellates and diatoms have the same growth rate but the phosphorus dependency of dinoflagellates lower than diatoms, so during December to January dinoflagellates dominated the system. As water cooled further in February-March, although all phytoplankton have similar growth rates, because flagellates are less phosphorus dependent, in surface waters (0-20m) flagellates dominated the system in spring.

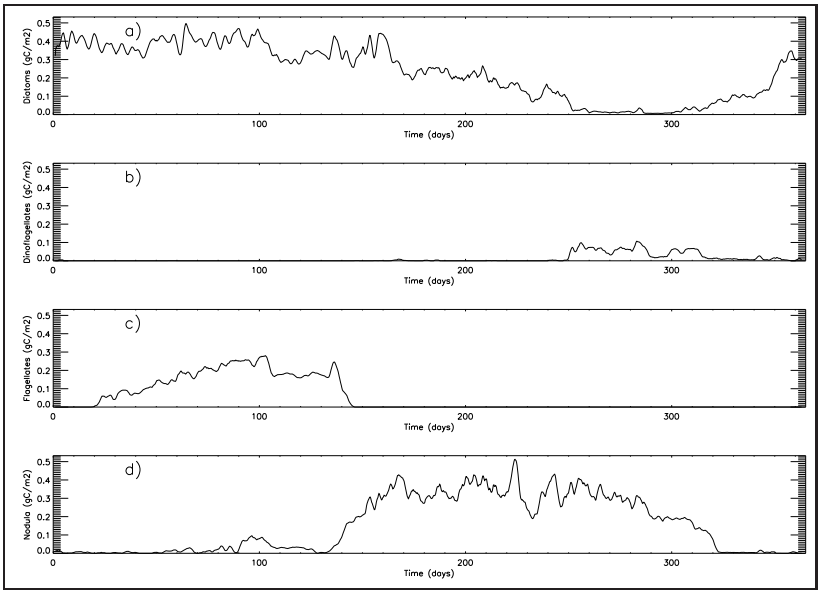

Figure 4.24: Depth integrated time series of a) Diatoms, b) Dinoflagellates, c) Flagellates and d) Bacteria concentrations at the river discharge area for the reference simulation

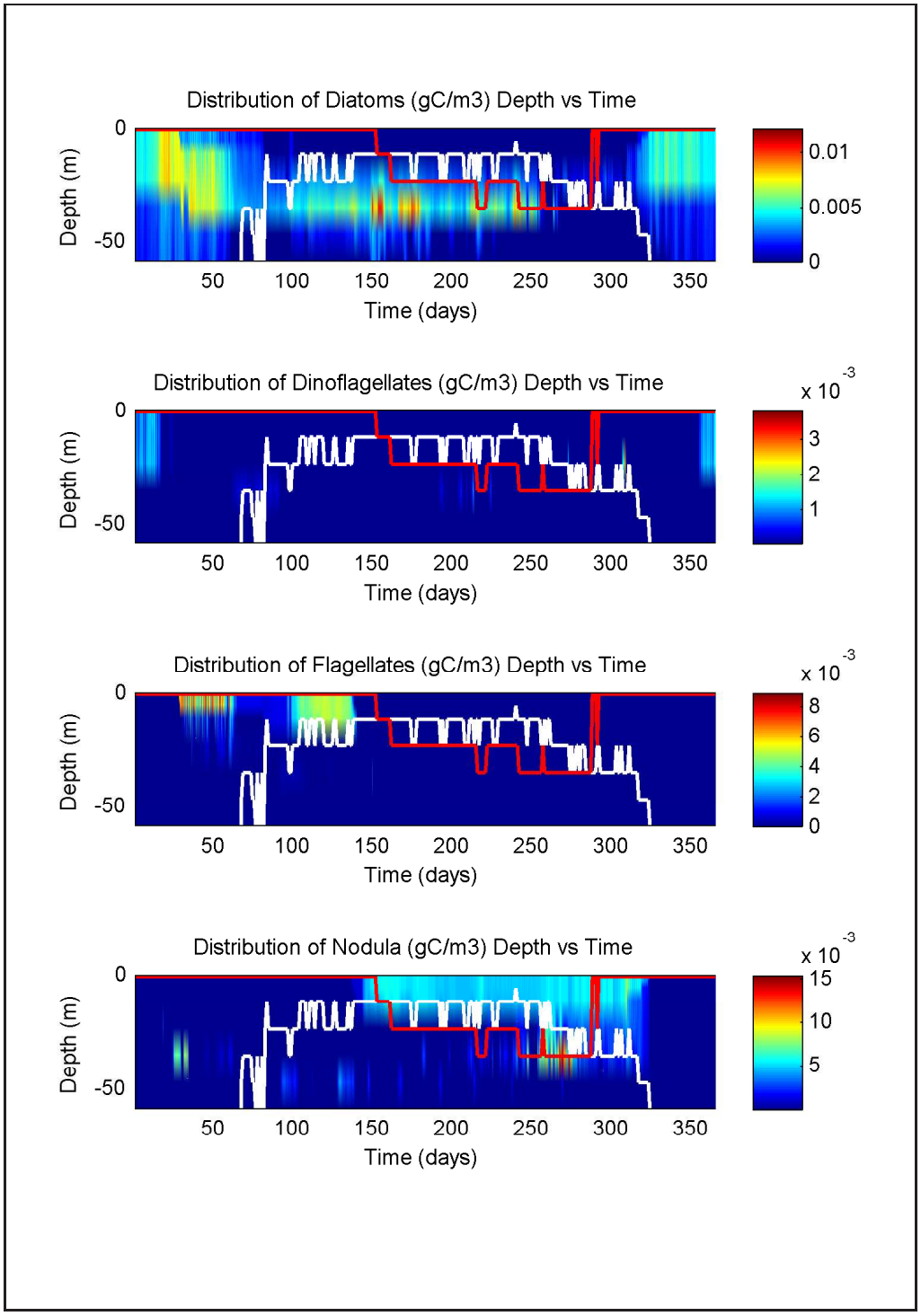

Figure 4.25: Depth vs time distribution of a)Diatoms, b)Dinoflagellates, c)Flagellates and d)Bacteria concentrations at the offshore station for the reference simulation. White line indicates mixed layer depth. Red line indicates temperature 26^{o}C

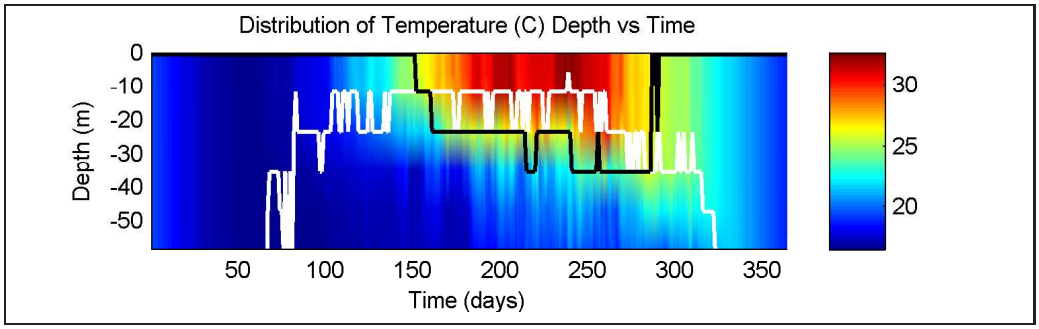

Figure 4.26: Depth vs time distribution of temperature at the offshore station. White line indicates mixed layer depth. Black line indicates temperature 26^{o}C

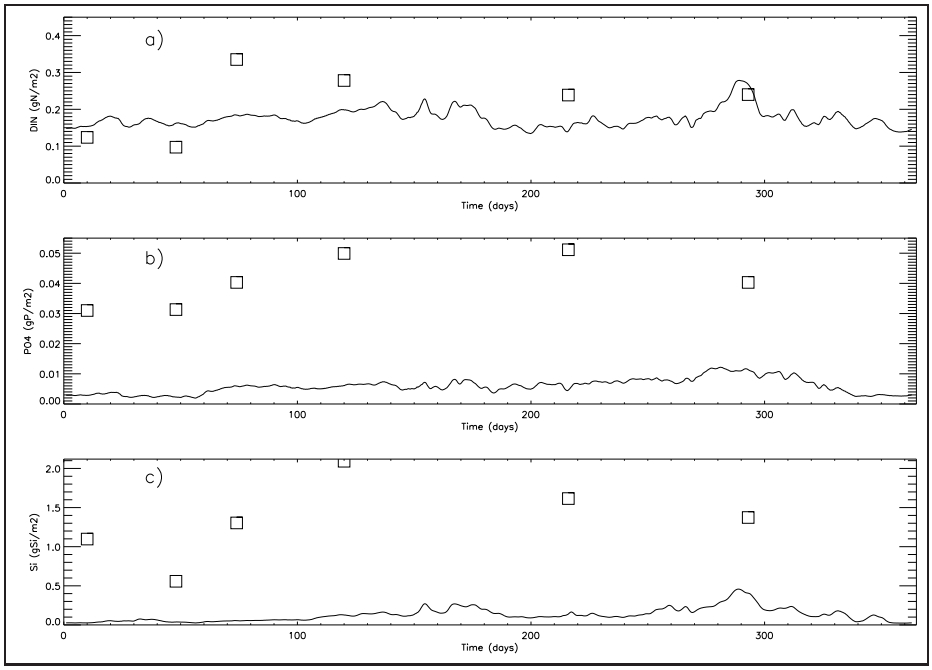

Figure 4.27: Depth integrated time series of concentrations of a) Dissolved Inorganic Nitrogen, b) Dissolved Phosphate and c) Dissolved Silicate

The effect of temperature and nutrient dependencies on ecosystem, only explains the domination of species within the limiting resources. However, it is important to understand the overall governing limitation of the environment. The principle of growth equations were explained in detail in Chapter-2. Algae, in order to grow, require several resources. These are nutrients (NH_4, NO_3, PO_4 and Si) and light. Excluding deep layers, light is not a limiting resource in the Mediterranean. BLOOM helps to understand which nutrients, N, P, Si, limit the overall production. Algae groups consist of subgroups within the BLOOM configuration. Each of the algae types are specified to adapt to different limiting environments. These are referred as energy (E), nitrogen (N), and phosphate (P) types. At each time step, grid and depth, the model calculates the ratio of net production and nutrient requirement, and decides which is the limiting resource for that specific algae group. The ratio, in turn decides which limiting type favors the growth. At each time step, only one type is

selected for each algae. By examining the dominant algae types, it is possible to determine which of the resources is limiting. The reference scenario shows phosphorus deficiency adopted species favor. This in turn explains that phosphorus is the governing limiting nutrient in the system.

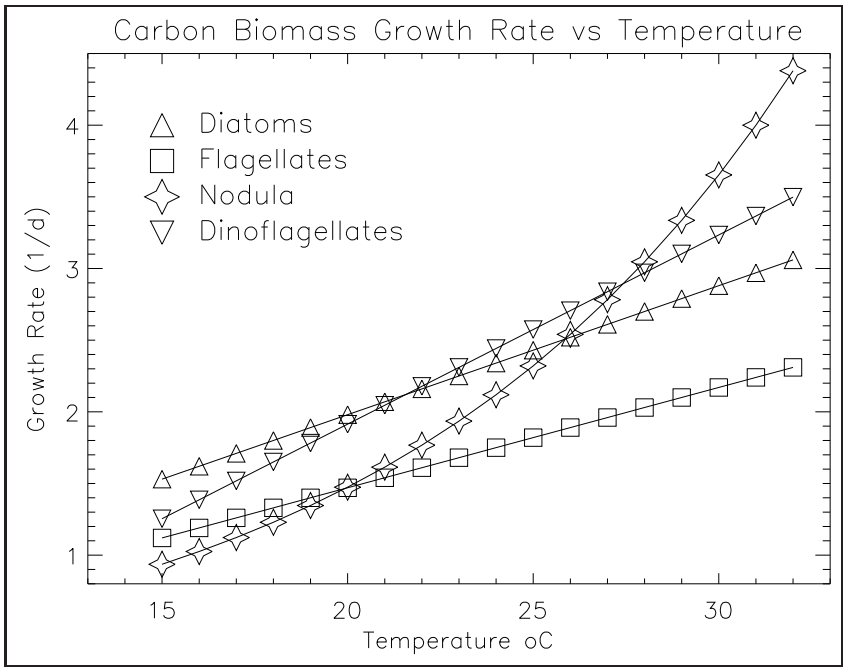

Figure 4.28: Biomass carbon growth rates vs temperature of P-type diatom, flagellate, bacteria and E-type dinoflagellate species parameterized in this study

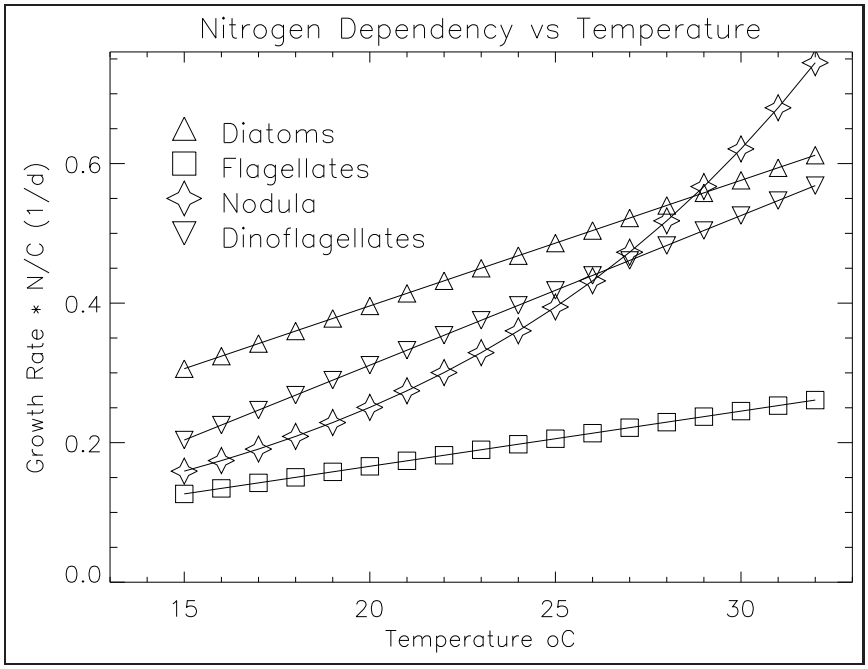

Figure 4.29: Nitrogen dependency of growth vs temperature of different P-type diatom, flagellate, bacteria and E-type dinoflagellate species parameterized in this study

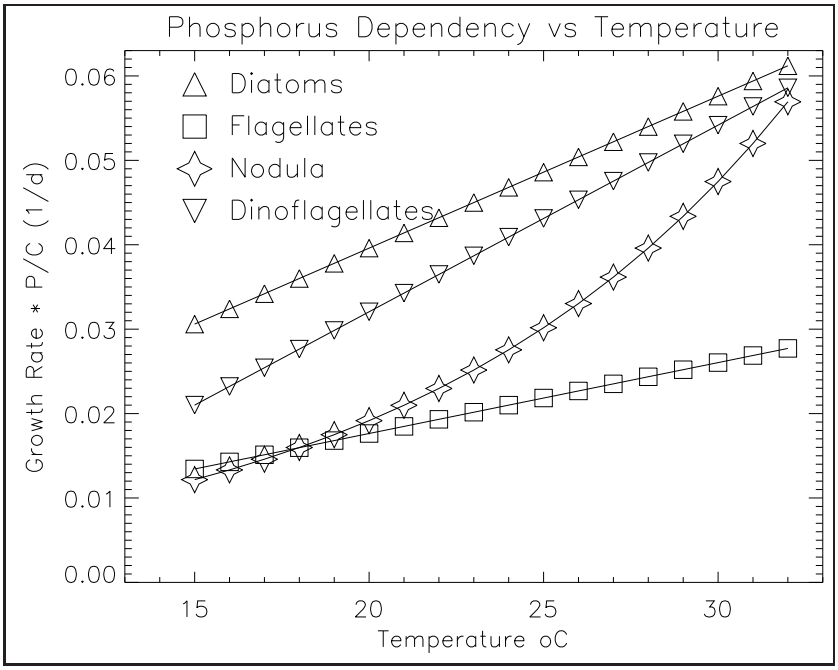

Figure 4.30: Phosphorus dependency of growth vs temperature of different P-type diatom, flagellate, bacteria and E-type dinoflagellate species parameterized in this study

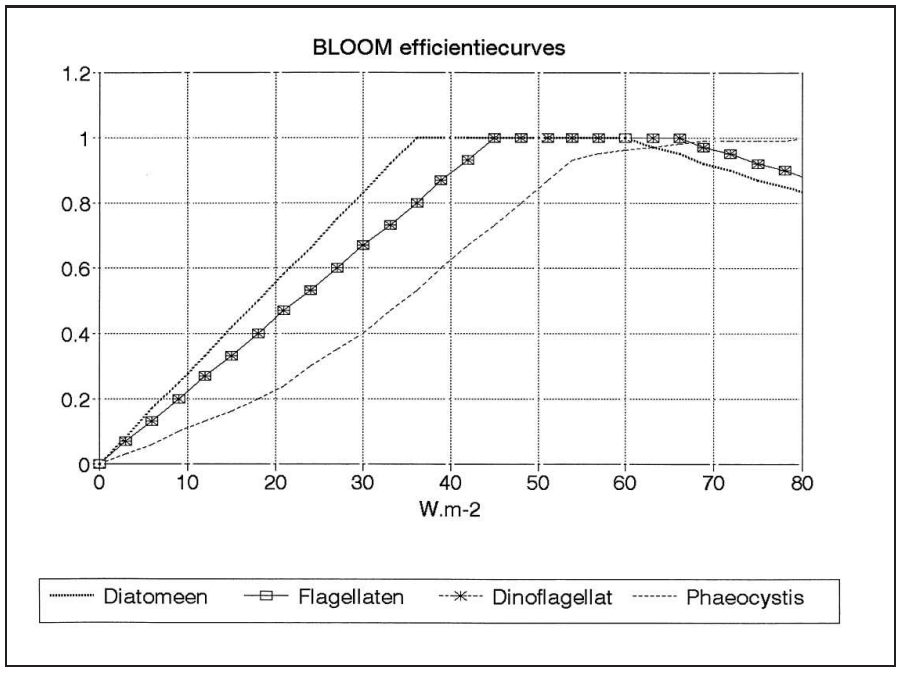

Figure 4.31: Light efficiency curves of different algae groups parameterized in this study (After Los, 2009)

4.2.1 RUN-01

Different cases for calibrating the reference scenario was given in Chapter-3 of this study. RUN-01 focused on the realistic time dependent boundary conditions, and the data sources were the *in-situ* data available from cruises at the offshore station. In addition to that, a lower concentration threshold was applied for inorganic nutrients to limit the maximum production. If inorganic nutrient distributions were compared between reference scenario (Figure 4.27 and Figure 4.33) and RUN-01 (Figure 4.32 and Figure 4.34), nutrient distributions approached the observed values. Although increasing the nutrient input from boundaries might result in higher production at the offshore station, setting a threshold limit to nutrient uptake balances the excess loss of nutrients, and gives good representation of nutrient distributions, but slight increases in production at the offshore station can still be observed (Figure 4.35). This is a good indicator that the offshore station was influenced by North East Mediterranean waters.

Another important result of RUN-01 was the oxygen concentration distribution. Oxygen is a good indicator for tracing the circulation. Therefore oxygen concentration at the offshore station was directly influenced by circulation and boundary conditions. For RUN-01, oxygen concentrations and nutrients were time dependent. Changes in oxygen concentration is seen in Figure 4.36. Nutrient, chlorophyll-a and oxygen results fit well with the *in-situ* data (Table 3.3).

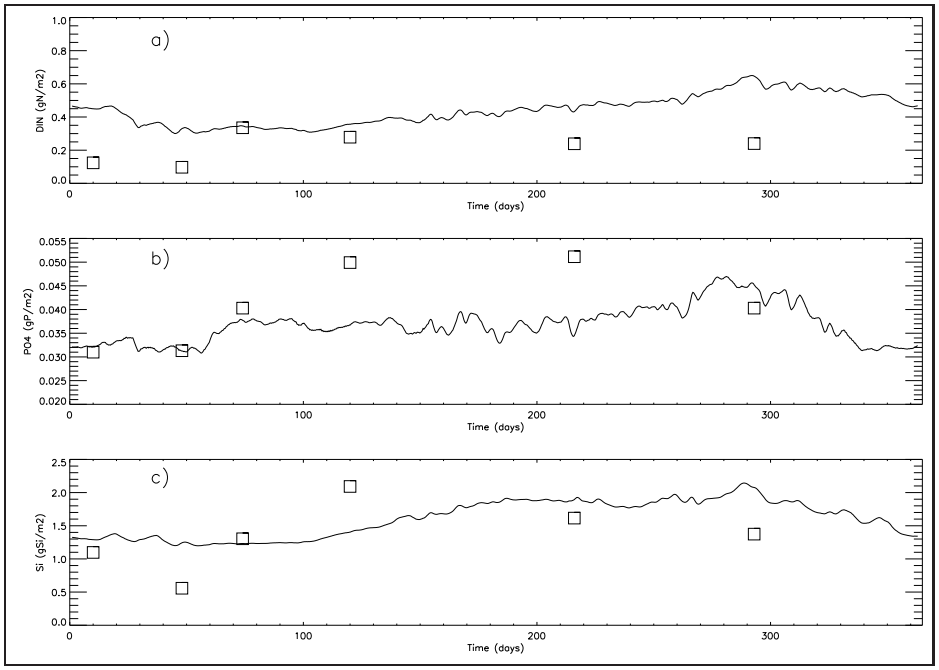

Figure 4.32: Depth integrated time series of RUN-01 of offshore station a) Dissolved Inorganic Nitrogen b) Dissolved Phosphate c) Dissolved Silicate

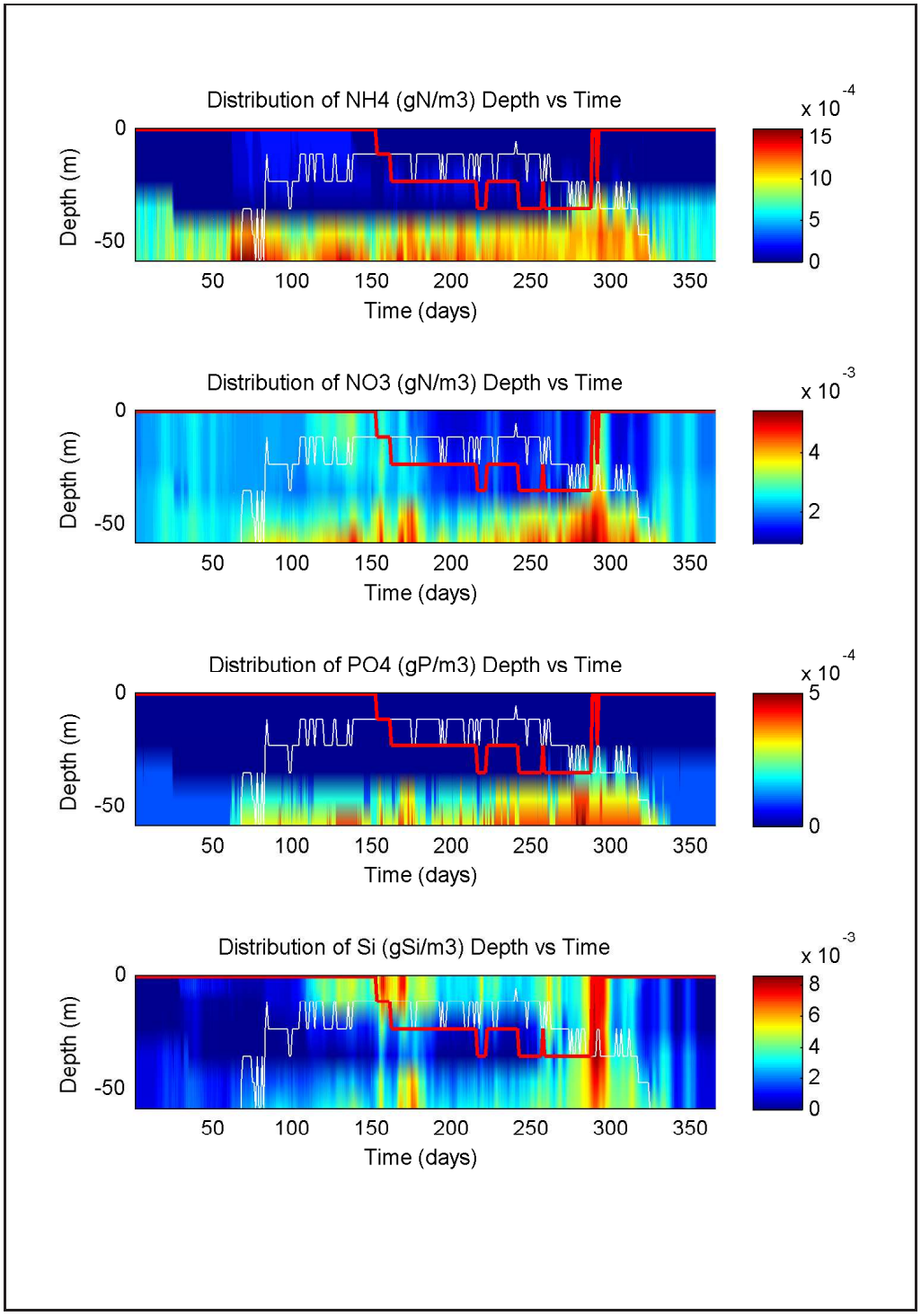

Figure 4.33: Depth vs time distribution of nutrients at the offshore station reference run. a)NH_4, b)NO_3, c)PO_4, d)Si. White line indicates mixed layer depth. Red line indicates temperature 26^{o}C

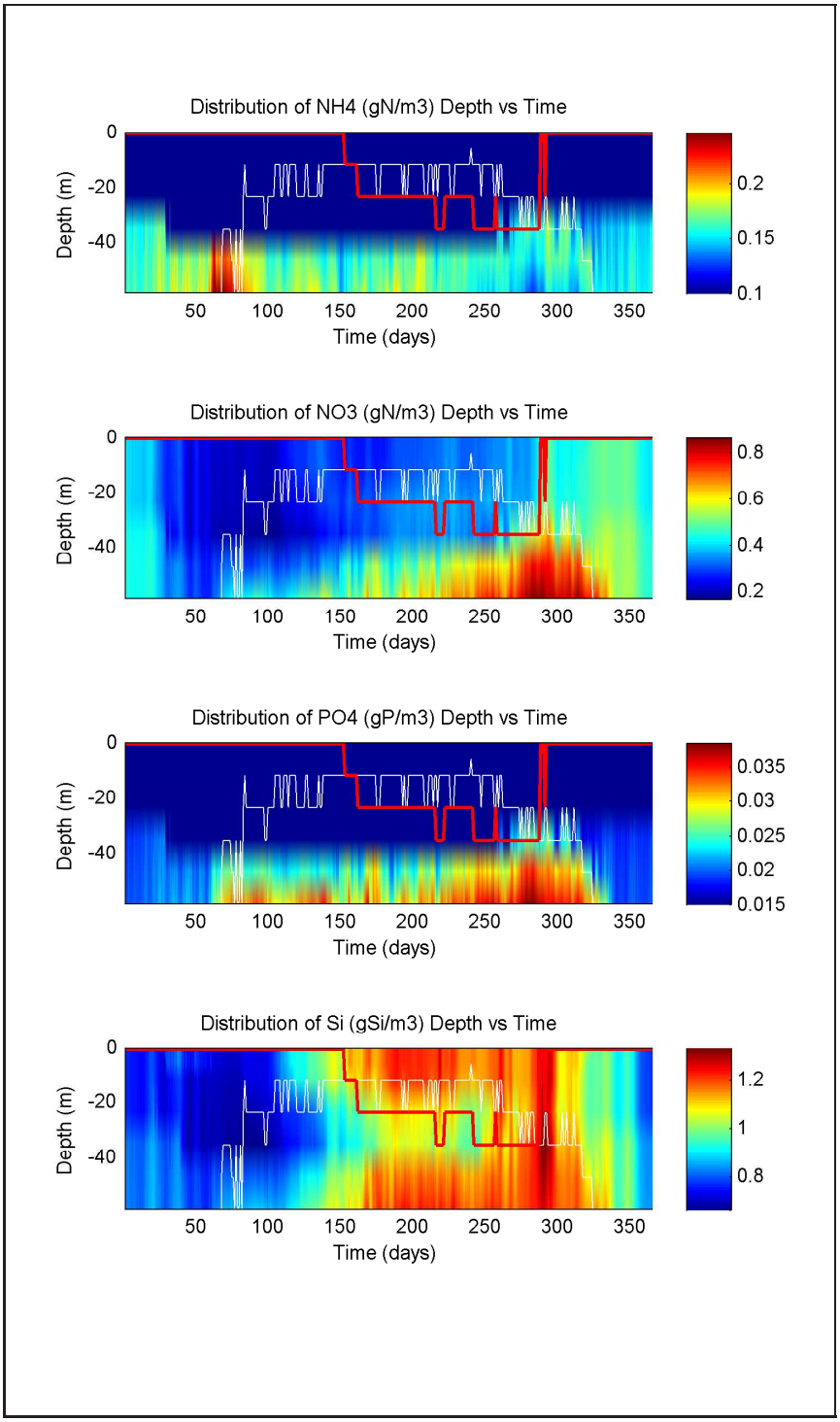

Figure 4.34: Depth vs time distribution of nutrients of RUN-01 at the offshore station. a)NH_4, b)NO_3, c)PO_4, d)Si. White line indicates mixed layer depth. Red line indicates temperature 26^oC

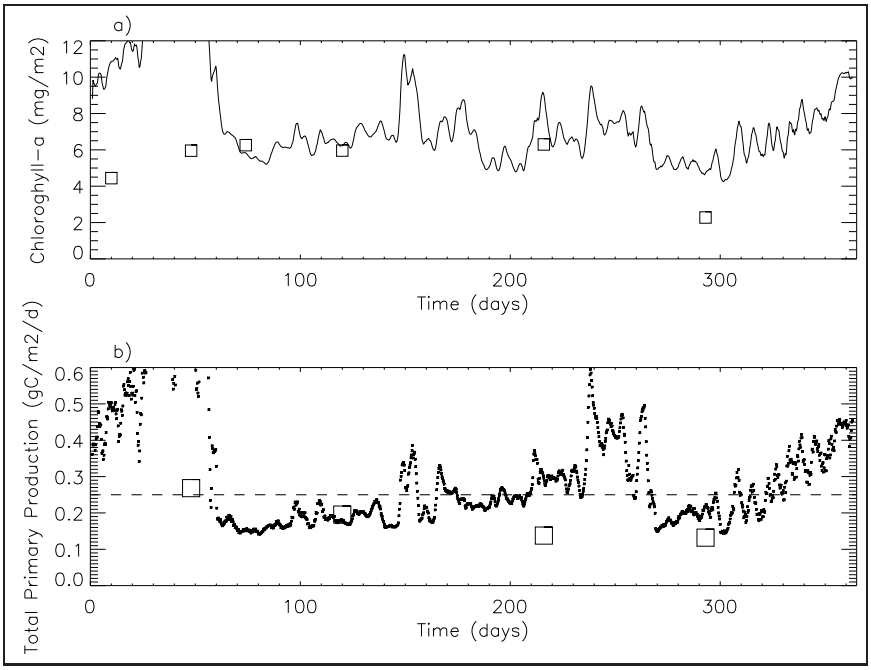

Figure 4.35: Depth integrated time series of RUN-01 of offshore station a) chlorophyll-a b) primary production. Boxes indicate observed *in-situ* values

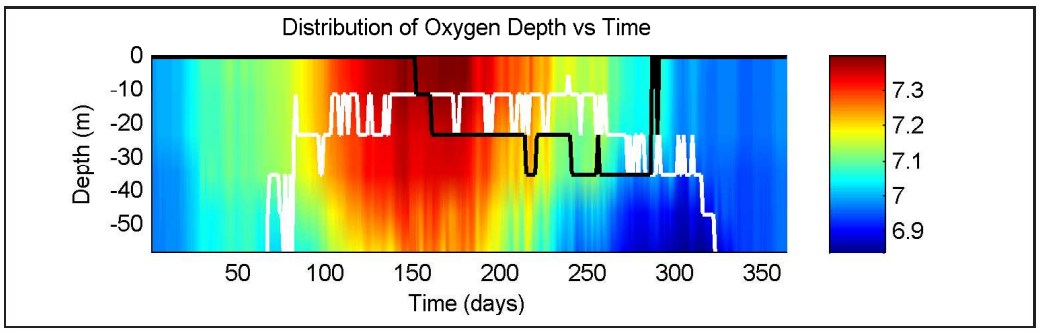

Figure 4.36: Depth vs time distribution of oxygen at the offshore station of RUN-01. White line indicates mixed layer depth. Black line indicates temperature 26^{o}C

4.2.2 RUN-02

In the scenario description in Chapter-3, it was explained that RUN-02 was implemented to acquire better representations of particulate and dissolved fractions of organic matter. Examining the rates of mineralization in Table 3.5, show that particulate matter have higher mineralization rates than dissolved organics. However, a major gap between magnitudes of dissolved and particulate organic matter occured in simulations (4.37 and 4.38). For better representation of the environment, this needed to be fixed. Such a distribution affects the primary production in the water column because of inorganic nutrient pumping due to process mineralization. This is one of the reasons why RUN-01 shows higher concentrations of chlorophyll-a compared to *in-situ* observations (Figure 4.35).

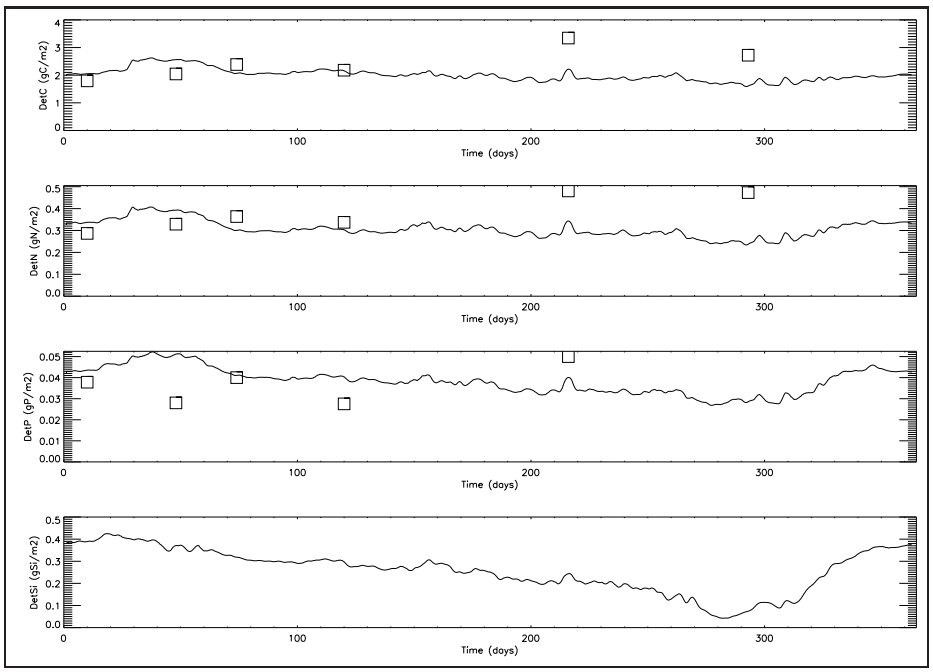

Figure 4.37: Depth integrated time series of RUN-01 of offshore station a) DetC b) DetN c)DetP d)DetSi. Boxes indicate observed *in-situ* values

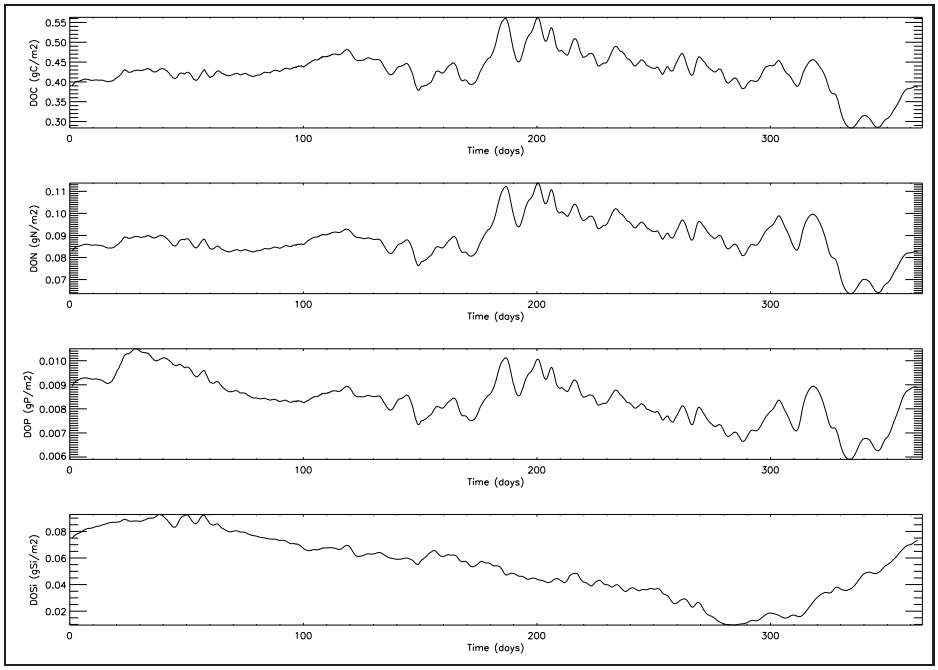

Figure 4.38: Depth integrated time series of RUN-01 of offshore station a) DOC b) DON c)DOP d)DOSi. Boxes indicate observed *in-situ* values

Distributing the dead algae into particulate and dissolved organics with respect to a balanced ratio (1 to 1) resulted in better model-data comparison (Figures 4.39, 4.40 and 4.41). Dissolved organic fraction of matter was not measured in cruises thus, particulate matter had to be taken as reference in comparing results with the data. Both of the organic pools, therefore were comparable with the observations, and with the adjustment done in RUN-02, the dissolved fraction was comparable to the particulate fraction of organic matter. Changes in chlorophyll-a were also observed, and by shifting the particulate matter into dissolved matter yielded similar concentrations of chlorophyll-a with data. These results show that the model was robust because comparable results were obtained by tuning the parameters of RUN-01.

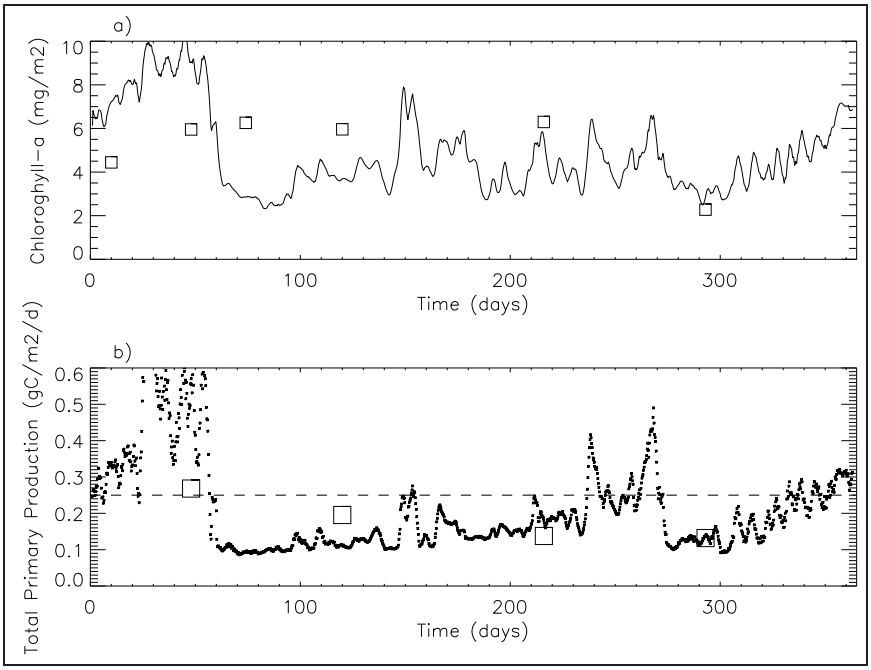

Figure 4.39: Depth integrated time series of RUN-02 of offshore station a) chlorophyll-a b) primary production. Boxes indicate observed *in-situ* values

The most important result of RUN-01 and RUN-02 was the influence of boundaries on the offshore station of the bay. As stated before, reference scenarios boundary conditions were kept to low values, while in RUN-01 and 02, boundary conditions were modified to fit the observed data. If Figures 4.21, 4.22, 4.35 and 4.42 were compared, the influence of boundary conditions was obvious at the offshore station. As the nutrient input increased at the boundaries, production increased proportionally. However, at the river discharge area, such influence was not observed. Still, results show similar concentrations. This implies that, the offshore station of Mersin Bay show open sea water characteristics of the North East Mediterranean.

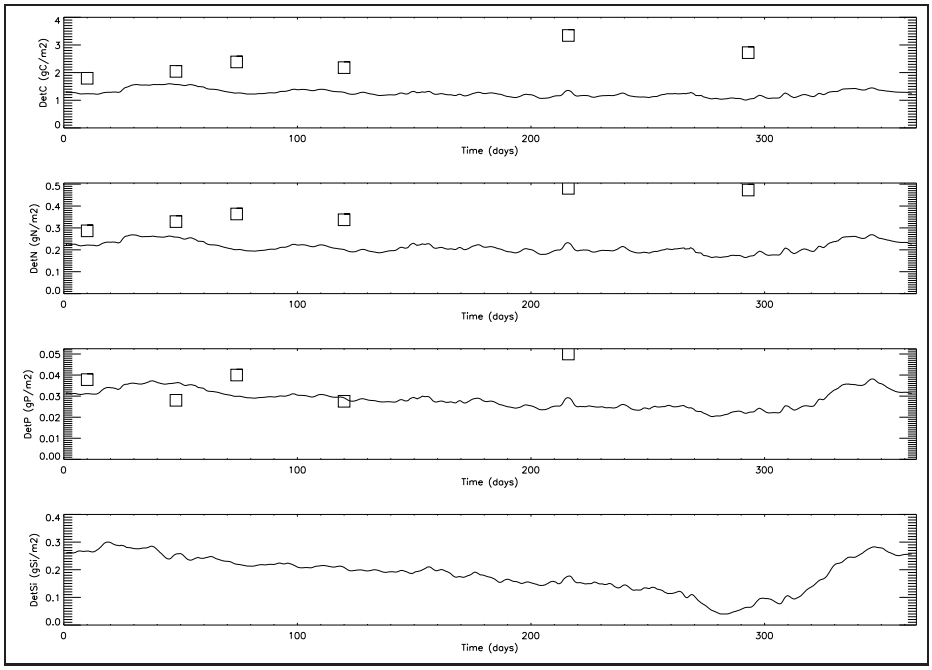

Figure 4.40: Depth integrated time series of RUN-02 of offshore station a) DetC b) DetN c)DetP d)DetSi. Boxes indicate observed *in-situ* values

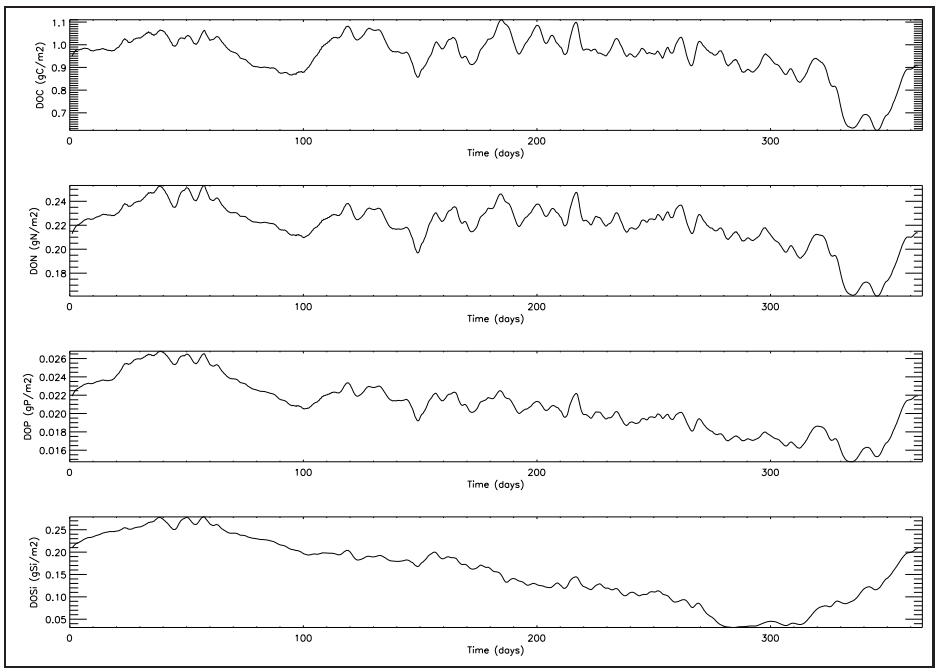

Figure 4.41: Depth integrated time series of RUN-02 of offshore station a) DOC b) DON c)DOP d)DOSi. Boxes indicate observed *in-situ* values

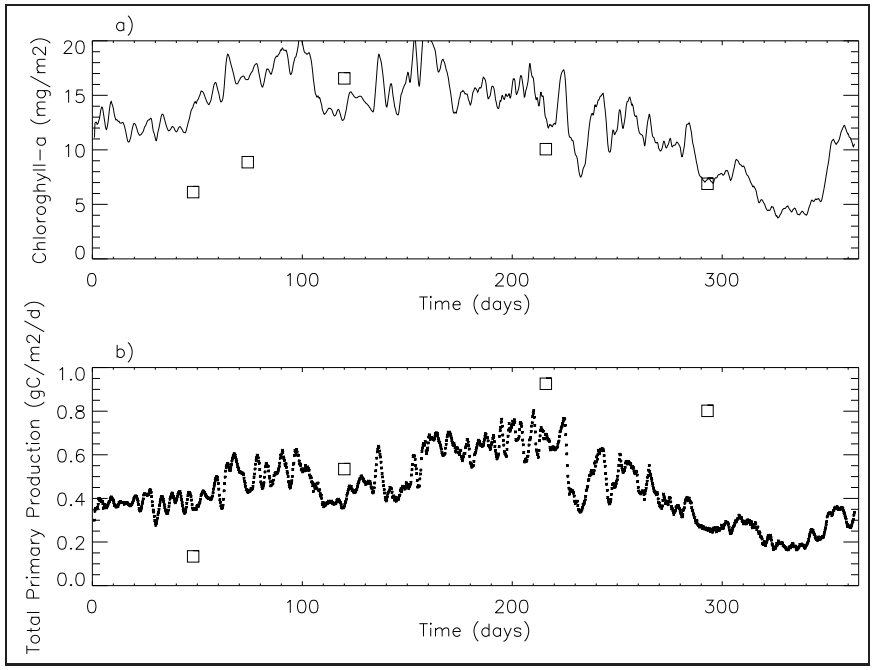

Figure 4.42: Depth integrated time series of RUN-01 of river discharge station a) chlorophyll-a b) primary production. Boxes indicate observed *in-situ* values

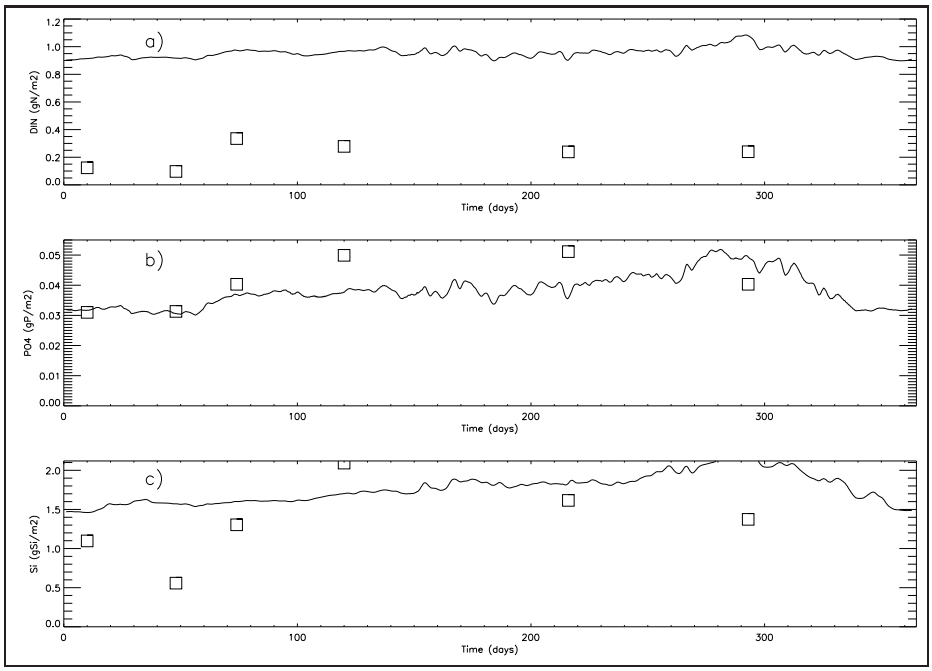

Figure 4.43: Depth integrated time series of RUN-03 of offshore station a) Dissolved Inorganic Nitrogen b) Dissolved Phosphate c) Dissolved Silicate

4.2.3 RUN-03

The open boundary nutrient and oxygen concentrations were modified in this simulation. Depth varying, but yearly mean nutrient concentrations were forced from the boundaries. Increasing concentrations of nutrients with depth were set at the boundaries. Profiles were acquired from averaging seasonal cruise data from the offshore station. Such an approach results in higher concentrations at certain times of the year compared to cruise data. Chlorophyll-a results can be seen in Figure 4.44. Slight increase of chlorophyll-a was observed. The reason for this was excess pumping of nutrients from bottom layers, and overestimating the nutrient concentration for certain times of the year, due to averaging the boundary data over the whole year. Excess nutrient pumping can be observed in Figure 4.43. A large increase in dissolved inorganic nitrogen was obvious in this case. Compared to RUN-01, nitrogen concentrations more than doubled, yet phosphorus values remained similar. This case confirms that the ecosystem reflected a phosphorus limiting environment. Intrusion of excess phosphorus caused a shift in primary production of the environment, but results did not show this increase of phosphorus. This implies that, phosphorus pumped into the system was immediately consumed, which further limited the production.

4.2.4 Cases-01, 02 and 03

Nutrient loads in setup were modified to observe the effect of river discharge into the bay. 0%, 150% and 200% of the original discharge was set for Seyhan River. The effect of different nutrient loads was distinct (Figure 4.45 and 4.46). There was a direct relationship between production and the discharge. The production increased and decreased proportionally with the discharge. However such an effect can not be seen in the offshore station. There were very minor changes in chlorophyll-a concentration but, when compared to the change in river discharge area, it can be concluded that offshore was not affected by these changes in river discharges. Circulation and boundary conditions fed the production. Another important result was that the winter bloom was not as effective without river discharge as it was with river discharge in coastal area. In addition to that, the winter bloom was present in all scenarios at the offshore station. This implies that, due to mixing of the water column in winter months, production increased offshore. In coastal areas however, because of shallowness, such nutrient pumping from bottom layers was not observed and the water column was not nutrient fed by circulation. This means, coastal water was trapped by the offshore circulation. Such conditions at the coasts have important effects in the ecosystem of the bay. This can be the reason why opposite ecosystem characteristics were observed at the coast and at the offshore waters of the bay.

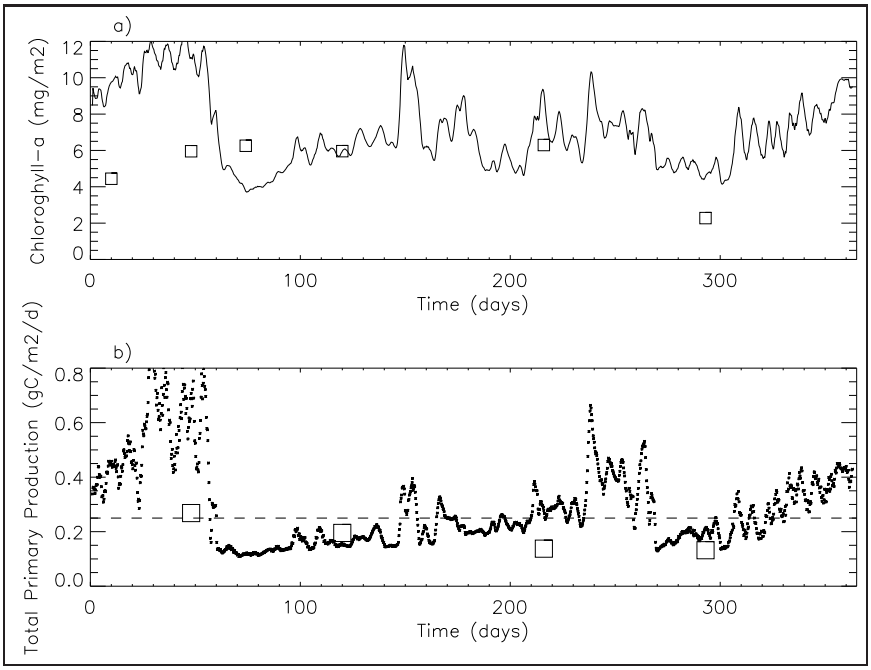

Figure 4.44: Depth integrated time series of RUN-03 of offshore station a) chlorophyll-a b) primary production. Boxes indicate observed *in-situ* values

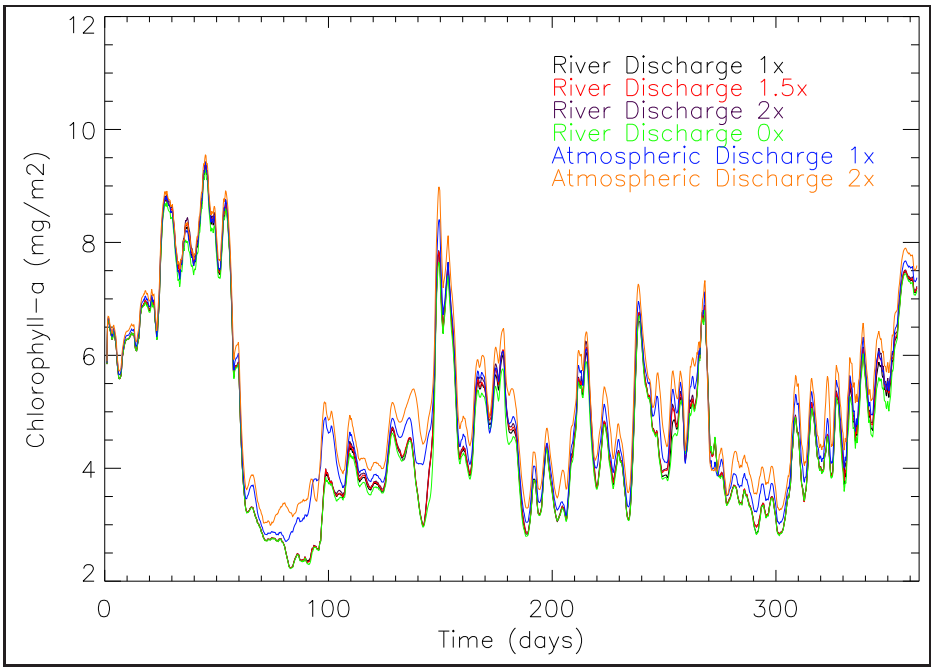

Figure 4.45: Depth integrated time series of Cases-01,02,03,04 and 05 of offshore station

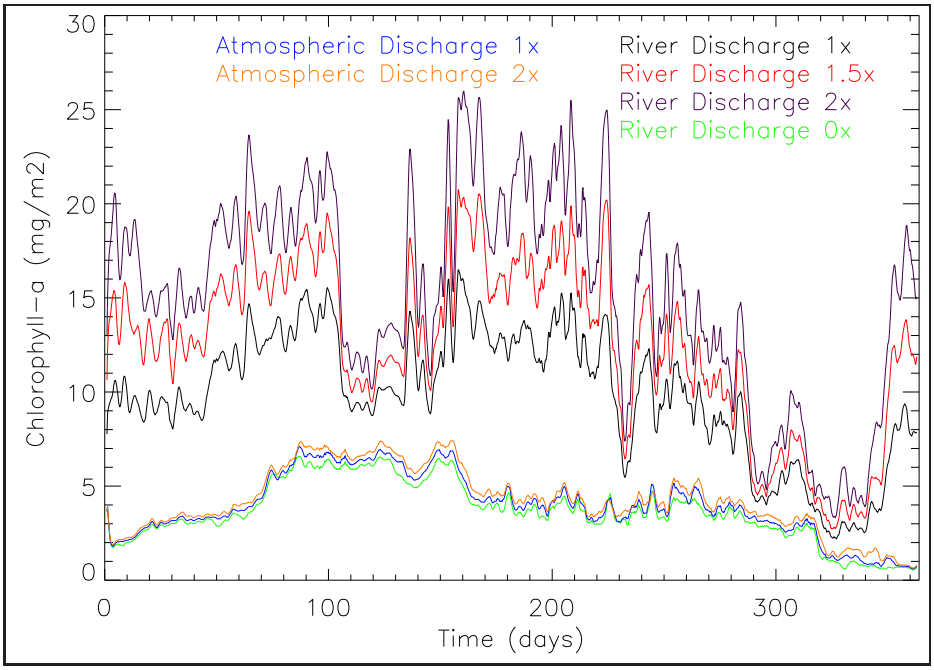

Figure 4.46: Depth integrated time series of Cases-01,02,03,04 and 05 of river discharge station

4.2.5 Cases-04 and 05

In Cases-04 and 05, atmospheric discharge was included as an additional nutrient source to Case-03, which had no nutrient load from rivers. Case-04 simulated observed and Case-05 simulated doubled atmospheric input. This was done to observe the changes in the environment due to atmospheric interactions. Both of the stations responded to atmospheric nutrient discharge because the discharge was implemented throughout the domain (Figure 4.45 and 4.46). However, although an increase in chlorophyll-a concentration was observed, the increase was relatively small compared to river discharge. It should be noted that, the offshore station where there was too small influence of river responded to the atmospheric deposition with significant amounts. This implies that, besides circulation, atmospheric discharge played an important role in production especially at times of the year where there was significant nutrient limitation. This phenomena can be clearly seen in results that show the post-bloom period of the simulation, between days 60 and 150 of the year 2009.

4.2.6 Final Run

The final ecosystem model run was simulated by combining RUN-01 initial and boundary conditions and RUN-02's fraction of organic matter distribution in result of mortality, including the atmospheric discharge of Case-04. This setup included the time dependent ecosystem boundary conditions from

RUN01, better distribution of dead algae matter into particulate and dissolved forms, and atmospheric deposition as a nutrient source. It should be stated that river discharge was already included in RUN01 and RUN02. Thus, the final run represented a completely recycled ecosystem dynamics, tuned for the ultra-oligotrophic Cilician Basin and eutrophic Mersin Bay coastal area. At the offshore station of the final run, peak chlorophyll-a concentration was 0.3 mg/m^3 (Figure 4.47) which was in good agreement with the observations (Table 3.3). An increase in productivity can be observed in winter and early-spring months throughout the water column, where production decreased below the mixed layer depth as the seasonal thermocline got shallower in summer months. The algae distribution in the water column was discussed in Section 4.2, where bacteria in warm seasons dominated the system above the mixed layer depth and large phytoplankton such as diatoms dominated where vertical mixing was significant in winter months (Figure 4.48). The nutrient abundance played an important role in defining the productivity in the system, where phosphorus was selected as the primary limiting nutrient throughout the year. Nutrient distribution in the water column, like algae are related to the mixed layer depth as well. As the water column mixed, the nutrients were dispersed in the water column which enhanced the production. However, in summer months, as the seasonal stratification got stronger, nutrients trapped at the surface completely diminished due to primary production by bacteria, whereasin below the mixed layer depth, pumping of nutrients from the bottom layers created a deep chlorophyll-a maximum near 30 m depth (Figure 4.49).

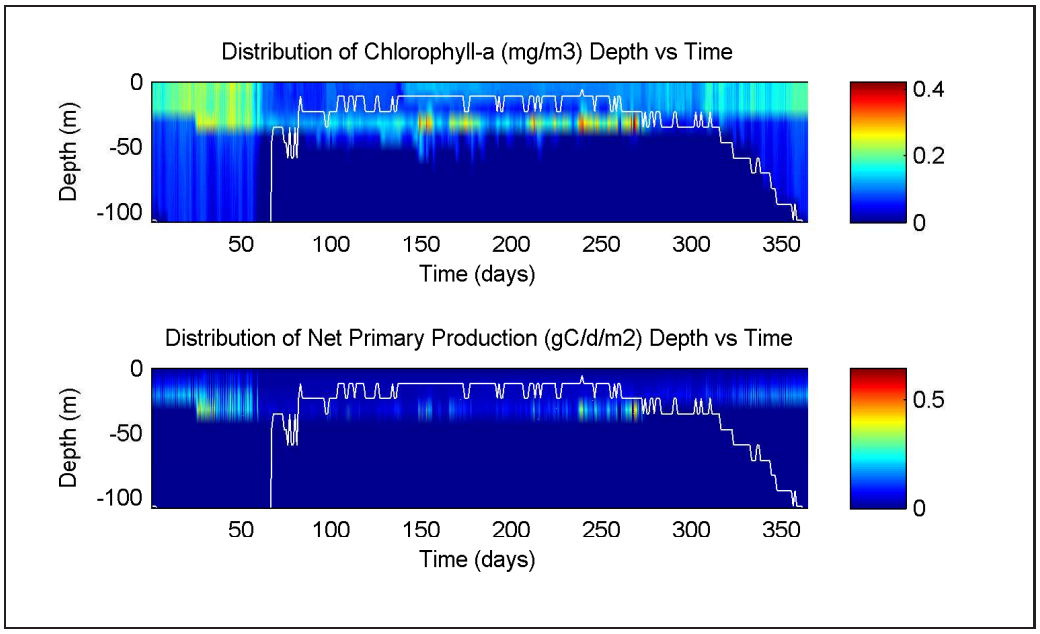

Figure 4.47: Depth vs time distribution of final run a) chlorophyll-a and b) net primary production at offshore station final run. White line indicates mixed layer depth

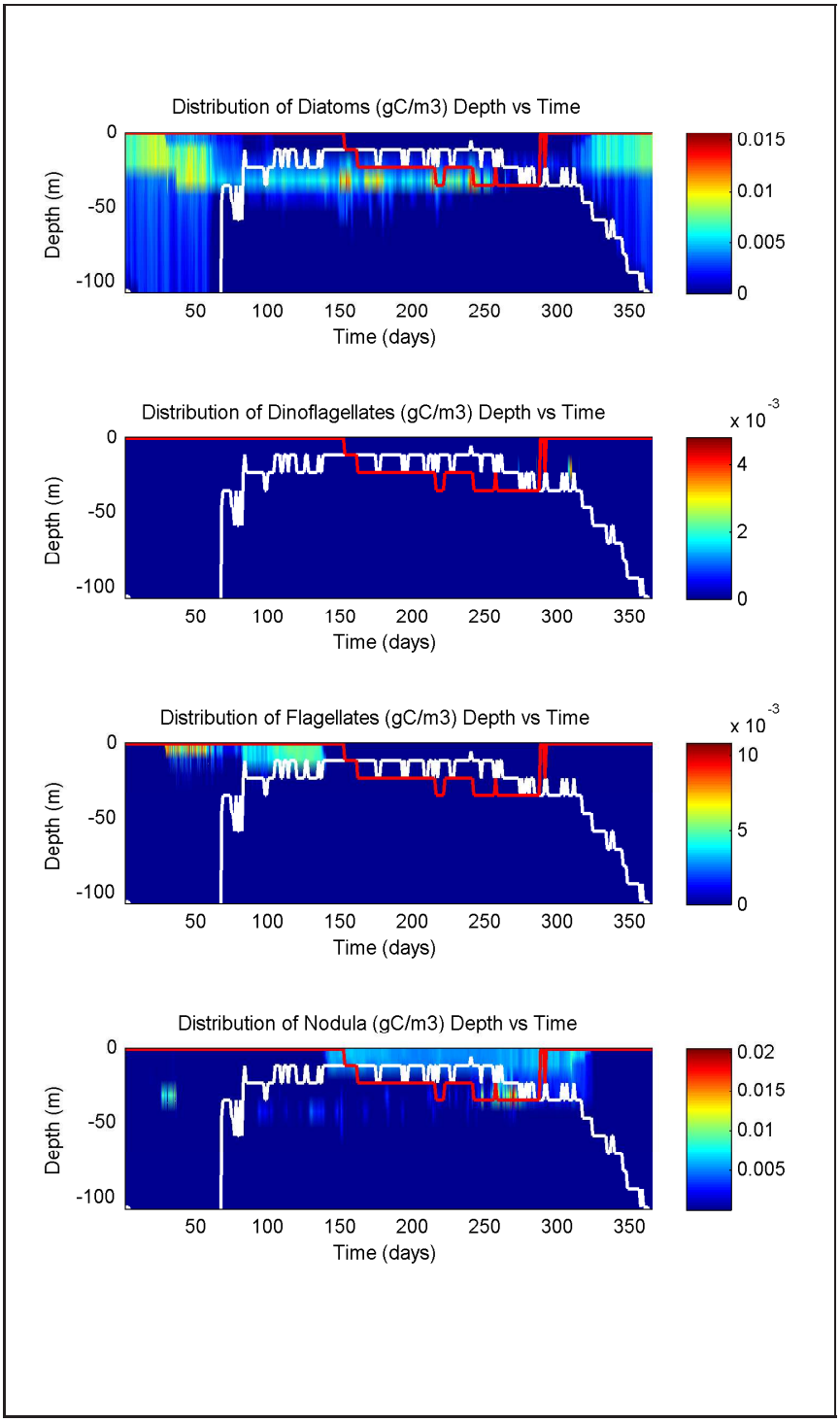

Figure 4.48: Depth vs time distribution of algae groups at the offshore station of final run. a)Diatoms, b)Dinoflagellates, c)Flagellates, d)Bacteria. White line indicates mixed layer depth. Red line indicates temperature 26^{o}C

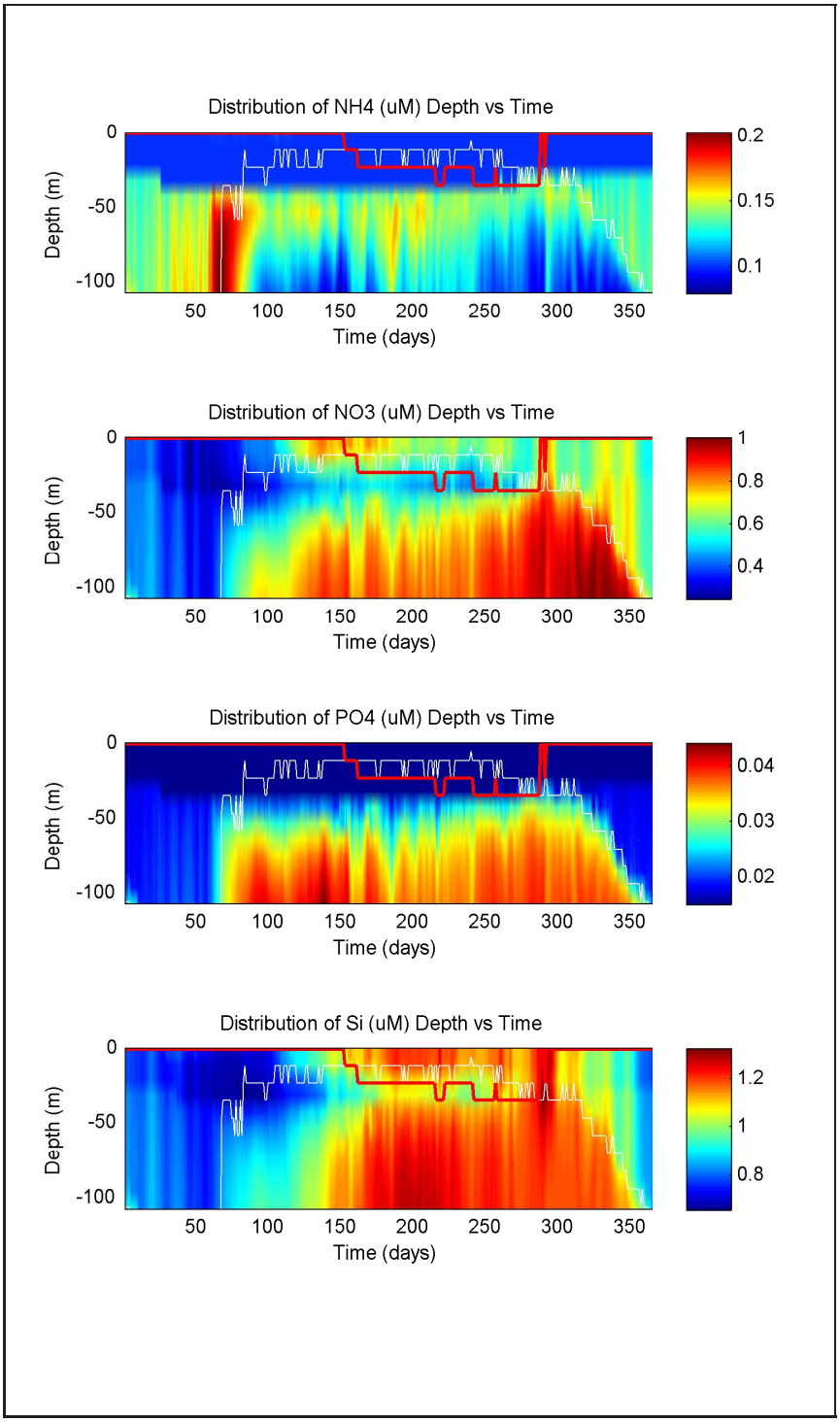

Figure 4.49: Depth vs time distribution of nutrients at the offshore station final run. a)NH_4, b)NO_3, c)PO_4, d)Si. White line indicates mixed layer depth. Red line indicates temperature 26^{o}C

CHAPTER 5

CONCLUSION

This study provides an analysis of primary production in Mersin Bay which exhibits distinctly different ecosystem characteristics in near shore and offshore regions. This is largely due to the prevailing circulation which restricts the influence of river plumes to the near-shore regions, where primary production is greatly enhanced. While the offshore waters of the basin show oligotrophic characteristics, the inner bay, due to the intrusion of nutrients through river and domestic wastewater discharges, show eutrophic characteristics.

Model results well represent the opposing characteristics of the inner and outer regions of Mersin Bay. The simulations reveal important characteristics of the bay. The coastal area is highly influenced by riverine discharges. The primary production of the coastal areas of Mersin Bay is directly influenced by nutrient input from Seyhan River. On the contrary, offshore waters do not show any significant response to nutrient discharge. This phenomena was tested with several river discharge scenarios. Nutrient loads from river discharges were modified in scenarios, from no discharge to doubling the nutrient concentrations. The response of the ecosystem in Mersin Bay varied in different regions. As expected, coastal areas were directly influenced by the changes in nutrient concentrations. However, offshore regions showed very little response. A simulation without river discharges was taken as reference for the comparisons and the annually averaged increase in production in the upper 60 m of the water column and at the surface at the offshore stations were 1.5%, and 2% respectively. The reason for this phenomena is the trapping of coastal waters by the offshore circulation. In parallel to river discharge scenarios, three atmospheric deposition scenarios were tested, no deposition, observed values and twice the observed values. The offshore waters of Mersin Bay responded significantly to the changes in nutrient load from atmosphere. The annually averaged increase in production found in the upper 60 m of the water column and at the surface was 10.5 %, and 15 % respectively when compared to the case with no atmospheric deposition. Moreover, in months where seasonal stratification is strong enough to form a stable water column, the increase in atmospheric deposition increases production by 25 %. These results show that production in the

offshore waters of Mersin Bay is mostly affected by the mixing in the water column and atmospheric nutrient deposition, especially in summer months. On the contrary, although atmospheric interactions play an important role in production in the coastal area of Mersin Bay, production is enhanced by river discharges.

Another important outcome of this study was the determination of limiting resources in the Cilician Basin. Sensitivity analyses show a phosphorus limited environment. This is not a new phenomena however, phosphorus limitation governs the dominant specie distribution of the marine ecosystem in Mersin Bay. The significance of this approach can be realized by examining the algae distribution throughout the year. Due to winter mixing, nutrients are homogenized in the whole water column, so that phytoplankton (mostly diatoms) dominate the system. As the stratification gets stronger in summer months, phosphorus limitation emerges and such low nutrient availability favors the bacterial growth. This phenomena can be related to the mixed layer depth. In conclusion, this suggests that algae biomass and distribution in the water column is directly proportional to mixed layer depth, and overall production is governed by phosphorus limitation, because in all scenario results, nitrogen is above the required amounts for growth.

In conclusion this study has provided a good description of the general circulation dynamics of Mersin Bay, allowing simulation of the ecosystem response to seasonal cycling and and determination of the limiting nutrients. However, in order to better understand the dynamics of the river discharge regions, further refinement of the physical model is neccessary. In particular a finer resolution in the horizontal plane is required in the region of the river discharges. Additionally, the acquisition of recent river flux data and local wind patterns from coastal stations is required in order to better capture the influence of small-scale physical features on the ecosystem dynamics of the region.

CHAPTER 6

REFERENCES

Alhammoud, B.,Béranger, K., Mortier, L., Crépon, M., Dekeyser, I., 2005. Surface circulation of the Levantine Basin: Comparison of model results with observations. Progress in Oceanography 66, 299-320

Antoine, D., Morel, A., Andre, J. M., 1995. Algal pigment distribution and primary production in the eastern Mediterranean as derived from coastal zone color scanner observations. Journal of Geophysics Research, 100, 16196-16209.

Ataktürk, S.S., 1980. Atmospheric Variability and Air-Sea Interactions in the Northern Margins of Cilician Basin. M.Sc. Thesis, Institute of Marine Sciences, METU, Mersin, Turkey.

Azov, Y., 1991. Eastern Mediterranean-a Marine Desert?. Marine Pollution Bulletin 23, 225-232

Bethoux, J.P., 1989. Oxygen consumption, new production, vertical advection and environmental evolution in the Mediterranean Sea. Deep Sea Research Part A 36, 769-781

Bethoux, J.P., Morin, P., Madec, C., Gentili, B., 1992. Phosphorus and nitrogen behaviour in the Mediterranean Sea. Deep Sea Research Part A 39, 1641-1654

Bethoux, J.P., Morin, P., Chaumery, C., Connan, O., Gentili, B., Ruiz-Pino, D., 1998. Nutrients in the Mediterranean Sea, mass balance and statistical analysis of concentrations with respect to environmental change. Marine Chemistry 63, 155-169

Blauw, A.N., Los, H.F.J., Bokhorst, M., Erftemeijer, P.L.A., 2009. GEM: a generic ecological model for estuaries and coastal waters. Hydrobiologia DOI 10.1007/s10750-008-9575-x. Collins, M.B., Banner, F.T., 1979. Secci disk depths, suspensions and circulation, North Eastern Mediterranean Sea. Marine Geology 31, M39-M46

Ediger, V., Velegrakis, A.F., Evans, G., 2002. Upper slope sediment waves in the Cilician Basin, northeastern Mediterranean. Marine Geology 192, 321-333

Ediger, V., Evans, G., Ergin, M., 1997. Recent surficial shelf sediments of the Cilician Basin (Turkey), northeastern Mediterranean. Continental Shelf Research 17, 1659-1677

Ediger, D., Tuğrul, S., Yılmaz, A., 2005. Vertical profiles of particulate organic matter and its relationship with chlorophyll-*a* in the upper layer of the NE Mediterranean Sea. Journal of Marine Systems 55, 311-326

Evans, G., Morgan, P., Evans, W.E., Evans, T.R., Woodside, J.M., 1978. Faulting and halokinetics in the northeastern Mediterranean between Cyprus and Turkey. GEOLOGY 6, 392-396

Koçak, M., Kubilay, N., Tuğrul, S., Mihalopoulos, N., 2010. Atmospheric nutrient inputs to the northeastern levantine basin from a long-term observation: sources and comparison with riverine inputs. Biogeosciences, 7, 1-14.

Krom, M.D.; Thingstad, T.F.; Brenner, S.; Carbo, P.; Drakopoulos, P.; Fileman, T.W.; Flaten, G.A.F.; Groom, S.; Herut, B.; Kitidis, V.; Kress, N.; Law, C.S.; Liddicoat, M.I.; Mantoura, R.F.C.; Pasternak, A.; Pitta, P.; Polychronaki, T.; Psarra, S.; Rassoulzadegan, F.; Skjoldal, E.F.; Spyres, G.; Tanaka, T.; Tselepides, A.; Wassman, P.; Wexels Riser, C.; Woodward, E.M.S.; Zodiatis, G.; Zohary, T., 2005. Summary and overview of the CYCLOPS P addition Lagrangian experiment in the Eastern Mediterranean. Deep Sea Research II 52, 3090-3108.

Krom, M.D., Herut, B., Mantoura, R.F.C., 2004. Nutrient budget for the Eastern Mediterranean: Implications for phosphorus limitation. Limnology and Oceanography 49(5), 1582-1592.

Krom, M.D., Kress, N., Brenner, S., Gordon, L.I., 1991. Phosphorus limitation of primary production in the eastern Mediterranean Sea. Limnology and Oceanography 36(3), 424-432.

Los, H., 2009. Eco-hydrodynamic modelling of primary production in coastal waters and lakes using BLOOM. Ph.D. Thesis. Wageningen University.

Ludwig, W., Dumont, E., Meybeck, M., Heussner, S., 2009. River discharges of water and nutrients to the Mediterranean and Black Sea: Major drivers for ecosystem changes during past and future decades? Progress Oceanography, 80(3-4), 199-217.

Malanotte-Rizzoli, P., Manca, B.B., d'Alcala, M.R., Theocharis, A., Brenner, S., Budillon, G., Özsoy, E., 1999. The Eastern Mediterranean in the 80s and in the 90s: the big transition in the intermediate and deep circulations. Dynamics of Atmospheres and Oceans, 29, 365-395.

Nixon, S. W., 2003. Replacing the Nile: Are Anthropogenic Nutrients Providing the Fertility Once Brought to the Mediterranean by a Great River? Ambio, 32, 1.

Ovchinnikov, I.M., 1966. Circulation in the surface and intermediate layers of the mediterranean. Oceanology, 5, 48-58.

Özsoy, E., Hecht, A., Ünlüata, Ü, 1989. Circulation and hydrography of the Levantine Basin. Results of POEM coordinated experiments 1985-1986. Progress Oceanography, 22, 125-170.

Özsoy, E., Oğuz, T., Latif, M.A., Ünlüata, Ü., 1987. Kuzey Levant Denizi'nin Oşinografisi. Ulusal Deniz Ölçme ve İzleme Programı Akdeniz Alt Projesi, DEBÇAĞ 7G.

Özsoy, E. and Ünlüata, Ü., 1983. Dynamical aspects of the Cilician Basin Northeastern Mediterranean. NATO Symposium on the Atmospheric and Oceanic Circulation in the Mediterranean, La Spezia, Italy, unpublished manuscript, 46pp.

Özturgut, E., 1976. The sources and spreading of the Levantine Intermediate Water in the Eastern Mediterranean. Saclant ASW Research Centre Memorandum SM-92, La Spezia, Italy, 45pp.

Robinson, A. R., Golnaraghi, M., Leslie, W. G., Artegiani, A., Hecht, A., Michelato, A., Sansone, E., Theocharis, A., Ünlüata, Ü. , 1991. The eastern Mediterranean general circulation: features, structure and variability. Dynamics of Atmospheres and Oceans. 15, 215-240.

Shaw, H. F. and Bush, P. R., 1978. The mineralogy and geochemistry of the recent surface sediments of the Cilicia Basin, Northeast Mediterranean. Marine Geology, 27, 115-136.

Toker, M., 2003. Plio-quaternary sediments, paleo-topography of the messinian evaporites, and salt tectonism in the Cilicia Basin, Northeastern Mediterranean Sea. Ph.D. Thesis, Institute of Marine Sciences, METU, Mersin, Turkey.

Uysal, Z. and Köksalan, I., 2010. Synechococcus dynamics in the Levantine basin shelf waters (Northeastern Mediterranean). Mediterranean Marine Science.

Ünlüata, Ü., Oğuz, T., Özsoy, E., 1983. Blocking of steady circulation by coastal geometry. Journal of Physical Oceanography, 13.

Yılmaz, A. and Tuğrul, S., 1998. The effect of cold and warm core eddies on the distribution and stochiometry of dissolved nutrients in the northeastern Mediterranean. Journal of Marine Systems, 16, 253-268.